Alma Mater Studiorum – Università di Bologna

DOTTORATO DI RICERCA IN

Biologia Cellulare e Molecolare

Ciclo XXVII

Settore Concorsuale di afferenza: 05/E1

Settore Scientifico disciplinare: BIO/10

TITOLO TESI

OPA1 isoforms and protein domains in the rescue of mitochondrial dysfunctions

Presentata da: **Valentina Del Dotto**

Coordinatore Dottorato
Prof. Davide Zannoni

Relatore
Prof.ssa Michela Rugolo

Correlatore
Dott.ssa Claudia Zanna

Esame finale: Bologna, Aprile 2015

ABSTRACT

Mutations in *OPA1* gene have been identified in the majority of patients with Dominant Optic Atrophy (DOA), a blinding disease, and the syndromic form DOA-plus. OPA1 protein is a mitochondrial GTPase involved in various mitochondrial functions, present in humans in eight isoforms, resulting from alternative splicing and proteolytic processing. In this study we have investigated the specific role of each isoform through expression in OPA-/- MEFs, by evaluating their ability to improve the defective mitochondrial phenotypes. All isoforms were able to rescue the energetic efficiency, mitochondrial DNA (mtDNA) content and *cristae* integrity, but only the presence of both long and short forms could recover the mitochondrial morphology.

In order to identify the OPA1 protein domains crucial for its functions, we selected and modified the isoform 1, shown to be one of the most efficient in preserving mitochondrial phenotype, to express three specific OPA1 variants, namely: one with a different N-terminus portion, one unable to generate short form owing to deletion of S1 cleavage site and one with a defective GTPase domain. We demonstrated that the simultaneous presence of the N- and C-terminus of OPA1 was essential for the mtDNA maintenance; a cleavable isoform generating s-forms was necessary to completely rescue the energetic competence and the presence of the C-terminus was sufficient to partially recover the *cristae* ultrastructure.

Lastly, several pathogenic OPA1 mutations were inserted in MEF clones and the biochemical features investigated, to correlate the defective phenotypes with the clinical severity of patients. Our results clearly indicate that this cell model reflects very well the clinical characteristics of the patients, and therefore can be proposed as an useful tool to shed light on the pathomechanism underlying DOA.

Index

INTRODUCTION

1. MITOCHONDRIA

1.1 Structure and functions

Mitochondria are cytoplasmatic organelles present in variable amount within eukariotic cells. Mitochondria are commonly referred to as the powerhouses of the cell because they are in charge of the ATP generation through the oxidative phosphorylation (OXPHOS). In addition, these organelles are involved in other important functions, like different types of cell death, regulation of calcium homeostasis, sugar and fatty acid catabolism, aminoacid metabolism, and reactive oxygen species (ROS) production.

According to the endosymbiotic theory, mitochondria origined from an aerobic bacterium entered into a symbiotic relationship with primitive host cells, giving energy to the eukaryotic cell in exchange of a stable environment and a continuum supply of nutrients (Gray et al, 1999). Mitochondria still retain some characteristics of bacterial cells as the presence of a double membrane, the ability to synthesize ATP, an independen protein synthesis apparatus and a circular DNA (mtDNA), which codes for tRNAs, rRNAs and proteins involved in OXPHOS (Friedman and Nunnari, 2014).

In contrast to the long-accepted static image of mitochondria, the introduction of tridimensional imaging technique with high resolution allowed to identify the so-called “dynamic mitochondrial network”. These are indeed dynamic organelles that frequently move within the cell toward regions of high-energy demand and form a network where morphological changes continuously occur during cellular cycle, development or tissue differentiation and apoptosis (Ishihara et al, 2013). These modifications can happen because they undergo membrane remodelling through cycles of fusion, in which two mitochondria join to form a single mitochondrion, and fission, in which a single mitochondrion divides into two mitochondria (Chan, 2012).

Mitochondria have a double membrane system: the outer mitochondrial membrane (OMM) bounds the organelle, while the inner mitochondrial membrane (IMM) separates the matrix space from the intermembrane space (IMS). OMM is characterized by a composition similar to the endoplasmatic reticulum and can also give rise to mitochondria-associated ER-membrane (MAM) in which lipids transfer between the two organelles takes place (Hayashi, 2009). OMM contains the voltage-dependent anion channel (VDAC), a multispanning β-barrel protein also called mitochondrial porin, which confers high permeability to small molecules and ions. In contrast, the IMM is impermeable to most small molecules and ions and only the species that have a specific transporter

insert inside the membrain can pass through (Nicholls, 2002). Many of these proteins within the IMM are components of the OXPHOS system. The space between the two membranes was termed inter-membrane space (IMS) and contains hydrosoluble proteins, such as the evolutionarily conserved cytochrome c. The IMM instead includes a gel-like substance, the matrix, which contains enzymes of the tricarboxylic acid cycle and β-oxidation, and multiple copy of mtDNA (Frey, 2000; Mao and Holt, 2009). Because IMM is the active site of OXPHOS, the selective permeability is a property required for maintenance of an electrochemical proton gradient between the matrix and the IMS.

The IMM is characterized by invaginations and organized in two contiguous but distinct membranes: the inner boundary membrane, which faces the OMM, and the *cristae* membranes, which extend into the mitochondrial interior as tubules or lamellae. This particular organization confers a large surface in a small volume. According to the classic Palade's model, *cristae* were considered as simple invaginations of the IMM widely opened to the IMS (Palade, 1952), but now they are identified as a separated sub-compartment, resembling pleomorphic bags. *Cristae* can be tubular, branched or bag-shaped and are joined to the inner boundary membrane by narrow tubular structure called *cristae* junctions. These junctions are energetically favored structures, which typically have a diameter as small as 10-15 nm, may be altered by changes in matrix volume and respiratory activity. These structures are also important for mitochondrial processes involving internal diffusion of ions, metabolites and proteins (Mannella et al., 1997; Mannella et al., 2013). Also *cristae* shape is dynamic and the inner membrane topology is regulated by the cell to optimize mitochondrial function. In yeast mitochondria, *cristae* junctions are reversibly reformed within several minutes after extreme osmotic swelling and recontraction (Mannella et al, 2001), whereas in mammals, the number of *cristae* is increased upon starvation (Gomes et al, 2011; Pattern et al, 2014). Furthermore the *cristae* remodeling augment cytochrome c realease during apoptosis (Scorrano, 2002; Frezza, 2006).

1.2 OXPHOS system

OXPHOS is one of the metabolic processes that takes place inside the mitochondria and is the final step of cellular respiration. The OXPHOS provides the bulk of cellular energy in the form of ATP thanks to a flow of electrons that are transported through a series of protein complexes, which are embedded in the lipid bilayer of the mitochondrial IM (Balaban et al., 1990; Friedman and Nunnari, 2014). The OXPHOS system is composed of five enzymatic complexes (CI-V) and is constituted by 87 polypeptides. Only 13 are encoded by the mitochondrial DNA, while the remaining part is coded at the nuclear level and later imported into the mitochondria (Carelli and Chan, 2014). CI-IV, together with ubiquinone (CoQ) and cytochrome c, two mobile electron carriers, make up the electron transport chain (ETC) (Acin-Perez and Enriquez, 2014).

During the Krebs cycle or the β-oxidation of fatty acids, the electron carriers nicotinamide adenine dinucleotide (NADH) and flavin adenine dinucleotide ($FADH_2$) are reduced. Subsequently, the electrons resulting from NADH enter in the transport chain through the CI (NADH-ubiquinone oxidoreductase), while the $FADH_2$ is oxidated at the level of CII (succinate-ubiquinone oxidoreductase). CI is the largest of the respiratory complexes, comprising 45 subunits, of which seven are mitochondrially encoded (Carroll et al., 2006). CII, the only respiratory enzyme completely encoded by the nucleus, is composed of four subunits and catalyzes the oxidation of succinate to fumarate transfering the electrons to the covalently bound FAD. The electrons are further transported via a number of iron/sulphur clusters to CoQ, reducing it to $CoQH_2$ (Lancaster and Kroger, 2000). A third source transferring electrons to generate ubiquinol is the glycerol 3-phosphate dehydrogenase enzyme. CoQ after reduction can move and transport the electrons to CIII (ubiquinone-cytochrome c oxidoreductase). This complex, that couples electron transfer to the translocation of two protons across the IMM, has only one mtDNA-encoded subunit, cytochrome b; the other 10 subunits are nucleous-encoded (Berry et al., 2000, 2013). CIII is a functional dimer and transfers electrons from $CoQH_2$ to cytochorme c, that donates electrons on the cytoplasmic side of the IMM to complex IV (Darrouzet et al., 2001; Dibrova et al., 2013). CIV is the terminal enzyme of the respiratory chain, composed of 13 subunits, of which three are encoded by the mtDNA. This complex reduces dioxygen to water and harnesses the energy to translocate protons from matrix to the intermembrane space. In this step, four electrons have to be transfered from the

reduced cytochrome c pool to two molecules of oxygen, without generating any reactive oxygen species (Schultz and Chan, 2001; Ishigami et al., 2015).

During these processes, the energy released by the electrons flow through the respiratory chain allows the transport against gradient of protons from the matrix to the intermembrane space. The proton pumping occurs only at the level of CI, III and IV and creates an electrochemical gradient that is positive outside, and negative inside the IMM. The proton flux in the reverse direction provides the energy to sustain the activity of the complex V (ATP synthase) to synthesize ATP. This complex consists of two major functional domains, a large extra-membranous portion (F1) sector and a membrane-intrinsic portion (F0) sector joined together by central and peripheral stalks (Walker, 2013). CV has two subunits encoded by mtDNA (ATPase6 and ATPase8), that take part to the membrane-bound portion (F0) of the complex, and about 13 other subunits encoded by nDNA (Abrahams et al., 1994). Protons from the intermembrane space enter CV through the F0 complex leading to subunit rotation within the complex. The rotational energy of the motor is transmitted to the catalytic domain by the central stalk, which is attached directly to the rotary motor, and then used for ATP synthesis (Walker, 2012). ATP formation requires a sufficient supply of ADP and phosphate, and specific carriers transport both substrates across the mitochondrial membranes: the adenine nucleotide translocator (ANT) and the phosphate carrier (Seelert and Dencher, 2011).

Although initially the respiratory components were proposed to be closely packed to guarantee a high efficient electron transport (‘solid’ model), according another model (‘fluid’ model) the OXPHOS complexes are independent entities embedded in the inner membrane, with CoQ and cytochrome c that freely diffuse among the complexes. However, thank to development of accurate techniques to isolate and identify stable associations of two or more respiratory complexes (respiratory supercomplexes, RSC) a reformulation of the solid model, the plasticity model, has been proposed. According to this model, the mitochondrial ETC can undergo to rearrangements within the IMM to adapt to fuel availability through a dynamic distribution between free respiratory complexes and SCs. In particular, data obtained by Blue-Native gel electrophoresis (BN-PAGE) unambiguously revealed that the respiratory complexes involved in this supramolecular association are the three proton-translocating enzymes, present in various configurations and stoichiometries. The I+III_2+IV combination was denominated ‘respirasome’ because considered the minimal unit able to perform complete respiration from NADH to oxygen.

Furthermore, there are suggestions that even higher levels of organisation may exist. RSC are proposed to increase the efficiency of electron flux through substrate channeling or enhanced catalysis (Genova and Lenaz, 2014; Acin-Perez and Enriquez, 2014; Chaban et al, 2014). Although the OXPHOS process is very efficient, a small percentage of electrons may be lost prematurely by redox centers present in the respiratory complexes, leading to the reduction of oxygen with the formation of ROS. Mitochondria therefore constitute the main source of ROS production within the cell. Therefore SCs allow acceleration of electron transport concomitant with sequestration of reactive intermediates to prevent generation of ROS. In this regard, independent approaches demonstrated that ROS generation by complex I was increased in the absence of SC formation (Acin-Perez and Enriquez, 2014). Furthermore, SCs are also linked with mitochondrial ultrastructure, in fact *cristae* shape may influence the assembly and stability of RCS and hence mitochondrial respiratory efficiency (Cogliati et al., 2013).

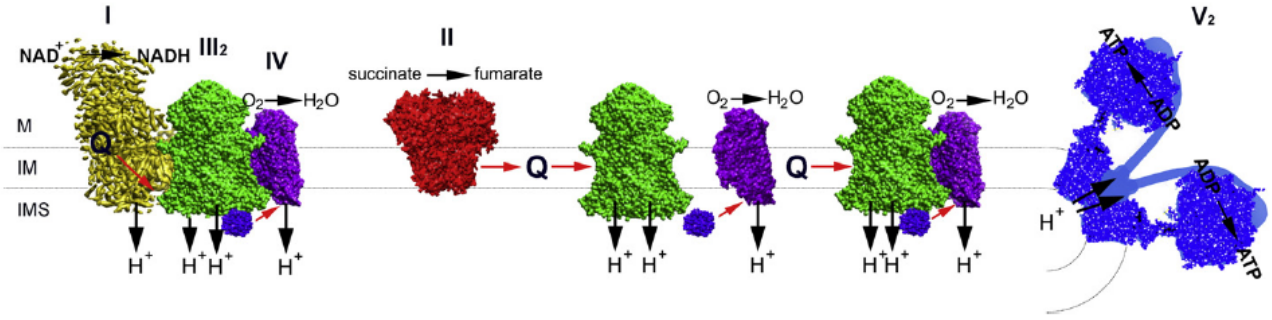

Figure 1. The plasticity model. Schematic representation of the OXPHOS system, where respiratory CI, III and IV are partly organised into supercomplexes. CII was never found associated with other complexes. Red arrows show electron pathways. CI (yellow), CII (red), $CIII_2$ (green), CIV (purple), CV (blue), cytochrome c (violet), Q, ubiquinol. The positions of the matrix (M), the intermembrane space (IMS) and inner membrane (IM) are indicated (from Chaban et al., 2014).

CV also can form various supramolecular structures, given that not only dimeric species but also higher molecular weight oligomers of the ATP synthase can be identified by BN-PAGE. Interestingly, ATP synthase dimers were found in strongly curved regions of the inner membrane (Davies et al., 2011) and they seem to be linked to *cristae* shape: in yeast mutants where the ATPase cannot dimerize, *cristae* are disorganized (Arselin et al., 2004), whereas in mammalian cells, increased *cristae* density favors ATPase dimerization during starvation (Gomes et al., 2011; Pattern et al., 2014).

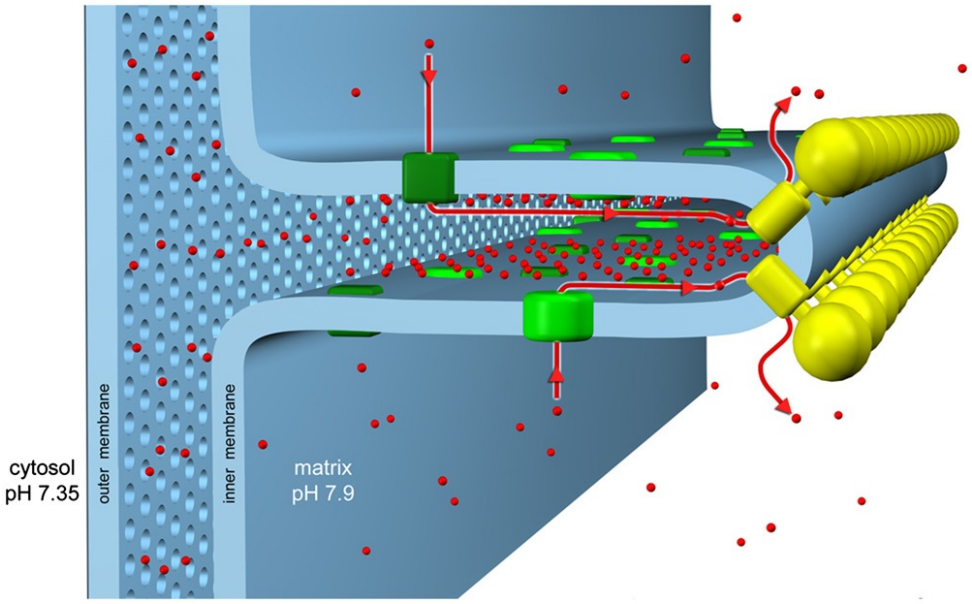

Figure 2. Schematic organization of the *cristae*. CV and CI (as well as the other respiratory chain complexes) occupy different regions of the crista membrane. CV forms dimer rows (yellow) in the strongly curved areas of the crista, ETC complexes (green), in particular CI, reside predominantly in the straight membrane regions. Protons (red), ejected into the intracristal space by the ETC, flow back into the matrix through the ATP synthase rotor, driving ATP production (from Davies et al., 2011).

1.3 Mitochondrial genome

1.3.1 Feature and structure of mtDNA

The mammalian mtDNA genome is a double-stranded, circular molecule of 16.659 base pair, localized in the mitochondrial matrix, where it is present in high copy number, ranging from tens to thousand copies per cell. The two strands of mtDNA can be distinguished into 'heavy strand' (H-strand) and 'light strand' (L- strand) strand, based on their nucleotide (GC) content (Fernandez-Silva et al., 2003). The mtDNA genome is highly compact compared to the organization of the nuclear genome, since there are no introns and intervening sequences among and between genes. Some genes overlap and certain stop codons necessary for proper mRNA translation are only generated after polyadenylation (Anderson et al., 1981).

Mitochondrial genome encodes 13 polypeptides, which are essential OXPHOS components. Of the other 24 genes, 22 are transfer RNAs and 2 ribosomal RNAs (12S e 16S), necessary for the mitochondrial synthesis of the 13 mtDNA gene products. As a result, all 37 mtDNA genes are essential for OXPHOS activity. The remaining around 1.500 genes encoding the mitochondrial proteome are scattered in the nuclear chromosomes. These proteins are translated by cytoplasmatic ribosomes and selectively imported into mitochondria through the specific translocases located in the inner and outer membrane (Harbauer et al., 2014). There are only two non-coding regions in the mtDNA. The first substantial noncoding region is the 1 kb D-loop (Displacement Loop), named because the triple-stranded structure formed by association of the nascent H-strand in this region during the replication. The D-loop contains the main regulatory elements for transcription and replication of mtDNA: the origin of H-strand DNA replication and the site of bidirectional transcription from opposing heavy and light strand promoters (Fernandez-Silva et al, 2003; Scarpulla, 2008). The second non-coding region contains the origin of L-strand replication (OL) and is located in a cluster of five tRNA genes around two thirds of the mtDNA length from the OH (Anderson et al., 1981; Fernandez-Silva et al., 2003).

Each mitochondrion contains multiple copies of mtDNA associated with specific proteins to form nucleoprotein complexes called nucleoids (Bogenhagen et al., 2008; 2012). Nucleoids are macromolecular structures, having an average mean size of about 100nm in mammals, regularly placed throughout the mitochondrial network, allowing an efficient maintenance of mtDNA in discrete segregating units (Gilkerson 2009, Kukat at al., 2011). Although is was previously reported that each nucleoid contained on average 5 to 10 copies of mtDNA, a recent study using

superesolution microscopy revealed that each nucleoid contains on average 1.4 mtDNA molecule only, meaning that the majority of the nucleoids just contain a single copy of mtDNA (Kukat at al, 2011).

A number of proteins have been identified to be part of the mitochondrial nucleoid. Mitochondrial transcription factor A (TFAM) is one of the major DNA-binding proteins associated in mammals, in particular about one thousand TFAM proteins were found for each mtDNA molecule. TFAM plays a crucial part in mtDNA transcription and its expression controls mtDNA copy number in cells, making it a central player in mtDNA maintenance and transmission (Kaufman et al. 2007, Kukat et al., 2011). Additional proteins crucial for mtDNA maintenance are the other components of nucleoids: the twinkle helicase, the mitochondrial polimerase gamma (Polγ), the single strand inding protein (mtSSB), mitochondrial transcription factors B1 and B2 (TFB1M and TFB2M) and a mitochondrial transcription termination factor (mTERF). A number of IMM proteins has been identified in purified nucleoid preparations, such as the adenine nucleotide translocase (ANT), the E2 subunit of α-ketoacid dehydrogenase, subunits of CI and CV, the SOD2 (Wang and Bogenhagen, 2006; Bogenhagen et al., 2008; Kienhöfer et al., 2009). Other types of nucleoid components identified are proteins with chaperone activity, including HSP70, HSP60, LRPPRC, prohibitin and the mAAA ATPase ATAD3A/B (Bogenhagen et al., 2008; Bogenhagen, 2012). In the model for the nucleoid structure proposed by these authors a central core, formed by proteins involved in mtDNA maintainance is surrounded by a peripheral region, composed by the metabolic proteins and chaperones (Bogenhan et al. 2008). This protein-enriched component not only protects the DNA from various insults, but also is likely to put constraints on any transactions involving the mtDNA, such as replication, repair, and transcription. In fact, mutations in genes encoding these and additional factors required for mtDNA maintenance are associated with a wide spectrum of human mitochondrial diseases (Spelbrink, 2010; Friedman and Nunnari, 2014).

In post-mitotic tissues and cells, contrary to nuclear DNA, mtDNA is continuously replicated and the mitochondrial genome copy number is maintained at relatively constant level. The segregation of mtDNA partly depends on the unbrocken occurrence of mitochondrial network fission and fusionevents, therefore the balance between these processes is crucial for proper distribution and maintenance of mtDNA (Friedman and Nunnari, 2014). The link between mitochondrial dynamics and mtDNA transmission is consistent with the primary role of dynamics in the control of mitochondrial copy number. Complementation has thus been suggested to be the consequence of

mitochondrial network dynamics allowing for rapid and extensive exchange of genetic material (Schon and Gilkerson, 2009; Carelli and Chan, 2014). One of the pecularіar features of mitochondrial genome is the uniparental inheritance of mtDNA in almost all the eukaryotes and, in the case of mammals, the maternal mtDNA is exclusively transmitted to the subsequent generations (Carelli and Chan, 2014). Because of the lack of protective histones, of an efficient DNA repair system, of intronic sequences and due to the fact that mitochondria are the main site of ROS production, mtDNA is extremely sensitive to oxidation or other genotoxic damage, and thus tends to accumulate mutations at a much higher rate than nuclear DNA (Liu and Demple, 2010). Four types of alterations of mitochondrial genome can be distinguished: partial deletions or duplications of mtDNA fragments, depletion of the mtDNA, accumulation of random mutations physiologically correlated to the ageing process and discrete point mutations (Vidoni et al., 2013). It has to ben noticed that in the same cell, tissue or individual, mutated mtDNA molecules can be present in a restricted proportion of the mtDNA population only, the condition being termed heteroplasmy. In contrast, when all copies of the mtDNA are identical (all wild-type or all mutant) the situation is referred to as homoplasmy. Therefore, the phenotype induced by a particular mutation depends not only on the type of mutation, but also on the ratio of mutated and wild-type copies, and become apparent when a percentage of mutated copies is reaches (threshold effect), which varies in different tissues (Rossignol et al., 2003). Since 1988, when a mtDNA mutation has been associated for the first time to a disease, hundreds of alteration of mtDNA causing mitochondrial pathology were discovered, showing a progressive, age-related clinical course and, because many of them involve central and peripheral nervous system and skeletal muscle, these are also known as mitochondrial encephalomyopathies (Carelli and Chan, 2014).

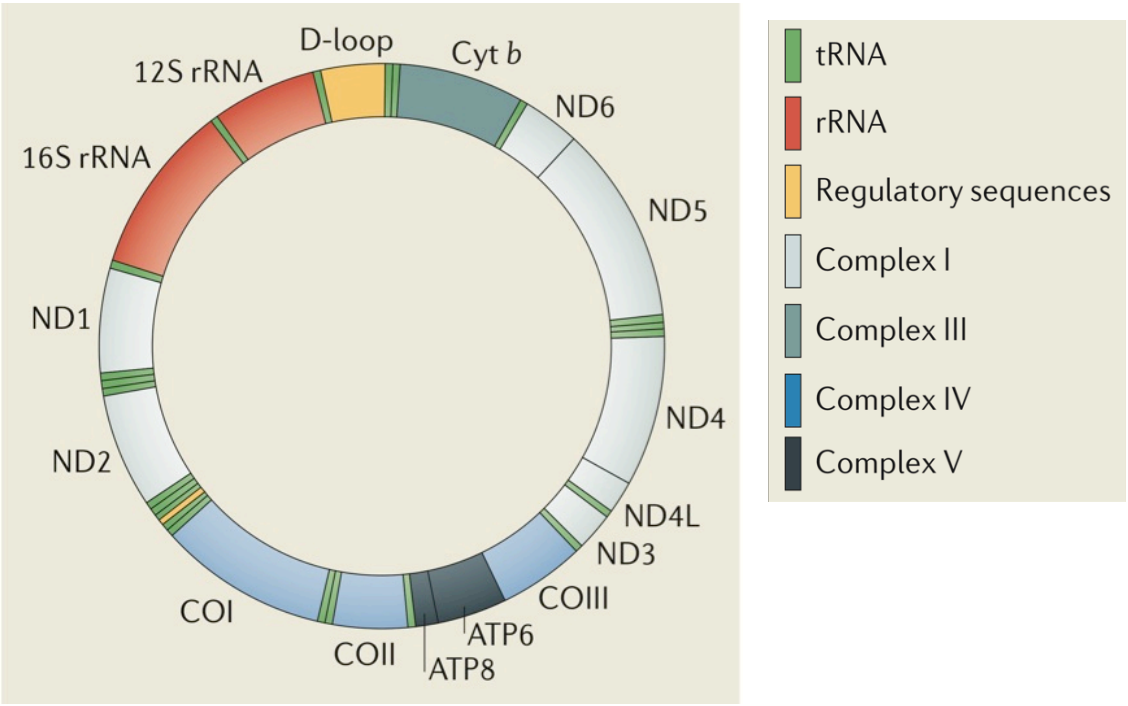

Figure 3. Schematic representation of the circular mtDNA genome, where the 13 genes encoding for the subunits of CI, III, IV and V (blue-black), the 2 rRNAs (red), the 22 tRNAs (green) and the D-loop (yellow) are indicated (from Mishra et Chan, 2014).

1.3.2 Transcription, translation and replication

The transcription of mtDNA reflects its peculiar compact and functionally economic organization. Contrary to what occurs in the nucleus, mitochondrial genes are transcribed in a polycistronic manner, specifying more than one RNA gene or mRNA, and in human mitochondria this process starts at three different sites located in the D-loop region. The transcription of the light chain starts from a single promoter (LPS) and results in the production of a transcript that is processed originating 8 mRNAs and 1 tRNA. The heavy chain promoter (HSP) contains two start sites: H1 and H2. The transcription from H1 is responsible for the synthesis of 2 ribosomal RNAs , while from the site H2 produce a long transcript polygenic, that is processed to 14 tRNA, 12 mRNA and 2 rRNA (Scarpulla, 2008).

Factors encoded by nuclear genes are involved in the transcription process: the mitochondrial RNA polymerase (POLRMT), TFAM, mitochondrial transcription factor B (TFB1M and TFB2M), and the factor termination mitochondrial mTERF (Falkenberg et al, 2007). TFAM promotes bidirectional transcription after binding its site enhancer, which is located upstream the start site of the promoter, facilitating the interaction with the other components of the transcriptional apparatus. The sequence that determines the termination of the majority of transcripts, starting from the site H1, is recognized by MTER factor, which is able to bind this sequence and simultaneously the site H1, leading to the formation of a loop which includes the transcripts of the two 12S and 16S rRNAs.

Mitochondria contain an independent protein-synthesis machinery to produce polypeptides encoded by the mitochondrial genome. The two mitochondrial rRNAs and nuclear encoded proteins compose these ribosomes that translate the mitochondrial mRNAs in the matrix. The mitochondrial genetic system utilizes genetic codes that differ slightly from the universal nuclear code, with species-specific differences (Scarpulla, 2008).

The mtDNA replication occurs at the level of the matrix and is independent from that of nuclear DNA. The mtDNA replication and transcription are closely associated phenomena because, in addition to the spatial proximity between the start points of both processes, the heavy chain needs a RNA primer to start replication. The transcript from LSP provides RNA primers, then the POLRMT is replaced by the mitochondrial DNA polymerase γ (Pol γ) and the replication starts from the origin OH of the heavy chain (Fustè et al., 2010). The gene products of nuclear origin constitute the machinery necessary for mtDNA replication, in particular DNA synthesis takes place by means of Pol γ and other factors such as the helicase TWINKLE, TFAM and a ligase (Scarpulla, 2008). Two models have been proposed: the first, asymmetric, suggests that the process beginning at the level of the OH, localized in the D-loop, proceeds throughout the parent strand H to produce the L chain until it reaches the origin OL. At this point the synthesis of the L-strand begins and proceeds in the opposite direction respect to the replication of the H-chain. The second model, proposed by Holt and defined symmetrical, differs from the previous one and supposes that in reality the mtDNA replication occurs in a symmetrical and synchronous manner (Brown et al., 2005).

1.4 Morphology

In the cytosol, mitochondria form a highly dynamic reticulum whose morphology is primarily determined by processes of fusion and fission of both OMM and IMM (Liu et al., 2009; Chan, 2012). Fusion merges the membranes of two, separate mitochondria, and results in the unification and mixing of their compartments. Fission divides a single mitochondrion into two, new mitochondria. Inhibition of fusion causes fragmentation of the network, whereas inhibition of fission induces mitochondria to become extremely elongated and overly interconnected. Therefore, the balance of these opposing forces determines the shape and length of mitochondria (Chan, 2012; Scorrano, 2013). Over the last 20 years, fusion and fission have been studied in great detail and it has become clear the importance of these processes for cellular and organismal physiology. In fact mice lacking proteins involved in mitochondrial dynamics cannot survive past midgestation and show cell type–specific defects (Chen et al., 2003; Chen et al., 2007; Ishihara et al., 2009).

Two different typologies of fusion have been described: transient and complete fusion events. Mitochondrial fusion assays showed that transient fusion is a rapid and separable merge of the outer and inner membranes and allow a partial exchange only of soluble inter-membrane space and matrix proteins. This type of fusion does not change the morphology of mitochondria and has been termed “kiss-and-run.” Instead complete fusion events permit the exchange of all mitochondrial components and affect mitochondrial morphology (Liu et al., 2009).

Because mitochondrial proteoma is encoded by both mitochondrial and nuclear DNA, during mitochondrial biogenesis the levels of these two sets of proteins must be coordinately regulated. Without mitochondrial fusion, each mitochondria of the cell could have divergent biochemical e functional profiles. The tournover of fusion and fission makes the contents of the organelles homogeneous, allowing mitochondria to act as a coherent population (Chan, 2012). The morphology is important also for the respiratory capacity, changing on the basis of cellular energetic status. IMM fusion is tuned by the levels of OXPHOS and during starvation elongated mitochondria increase levels of dimerization and activity of ATP synthase to maintain ATP production (Mishra et al, 2014; Gomes et al., 2011). Metabolically active cells have a large mitochondrial network that acts as electrically united systems able to transmit mitochondrial membrane potential, allowing an efficient dissipation of the energy in the cell (Skulakev, 2001).

Dynamic control of mitochondrial structure is performed by a set of "mitochondria-shaping" proteins that include both pro-fusion and pro-fission members. All these proteins operate in healthy cells to maintain genetic and biochemical uniformity within the mitochondrial population.

During mitochondrial fission two classes of proteins are necessary to execute this process. The first includes the dynamin protein Drp1, which is recruited from cytosol to the mitochondrial surface and oligomerizes around the circumference of the mitochondrion, promoting membrane division (Chan, 2012). It has been shown that Drp1 is essential for mitochondrial fission provoked by events like mitosis or stress, and for development of the nervous system (Wakabayashi et al., 2009; Ishihara et al., 2009). The members of second class are integral, OM proteins that recruit Drp1 to the mitochondrial surface: Fis1, Mff, MiD49 and MiD51. Although in yeast the recruitment of the dynamin omologus requires Fis1 and the two WD40-containing adaptors, in mammals it has been reported that Fis1 can directly bind Drp1 (Griffin et al., 2005; Wells et al., 2007). Importantly, in mammals there are three other receptor proteins involved in fission events: Mff, MiD49 and MiD51. Knockdown of Mff caused reduced recruitment of Drp1 to mitochondria accompanied by robust elongation and recently it has been demostrated that Mff, MiD49 or MiD51 can function independently of one another to mediate mitochondrial fission. Particularly, it seems that Fis1 and Mff promote constitutive mitochondrial fission whereas the MiDs activate recruited Drp1 only during loss of respiration (Loson et al., 2013; Otera et al., 2010).

Interestingly, mitochondrial fission plays a key role in both cell life and death. The mitochondrial fission machinery actively participates in the programmed cell death pathway (apoptosis) by inducing fragmentation of the mitochondrial network before the release of the cytochrome c and caspase activation (Youle and Karbowski, 2005). Network fragmentation is important for the proper allocation of mitochondria to daughter cells during cellular division (Kashatus et al., 2011). In fact, changes in mitochondrial morphology during the cell cycle have been shown to influence the progression of the cell from G1 to S phase, suggesting that mitochondrial morphology can regulate the cell cycle (Mitra et al., 2009). Mitochondrial fission has also been linked to mitophagy, because interruption of fission reduces the efficiency of mitophagy, suggesting that fission segregates mitochondria with loss of membrane potential, allowing their removal from the rest of the population by autophagy (Frank et al., 2012; Stotland and Gottlieb, 2015).

The mitochondrial fusion is highly dependent on the mitochondrial membrane potential, and plays a central role also in the quality control of mitochondria. Mitochondria that are moderately

dysfunctional can be rescued by mitochondrial fusion, whereas those with severe dysfunction may be separated by fission and then degraded (Twig et al., 2008). Fusion is important also for mitochondrial calcium homeostasis (Szabadkaiet al., 2006), embryonic development (Chenet al., 2003) and spermatogenesis, and mtDNA maintenance (Chen et al., 2007). Moreover mitochondrial fusion plays a protective role in certain pathological conditions, because it allows complementation of mtDNA gene products in heteroplasmic cells that have accumulated different mutations (Sato et al., 2006).

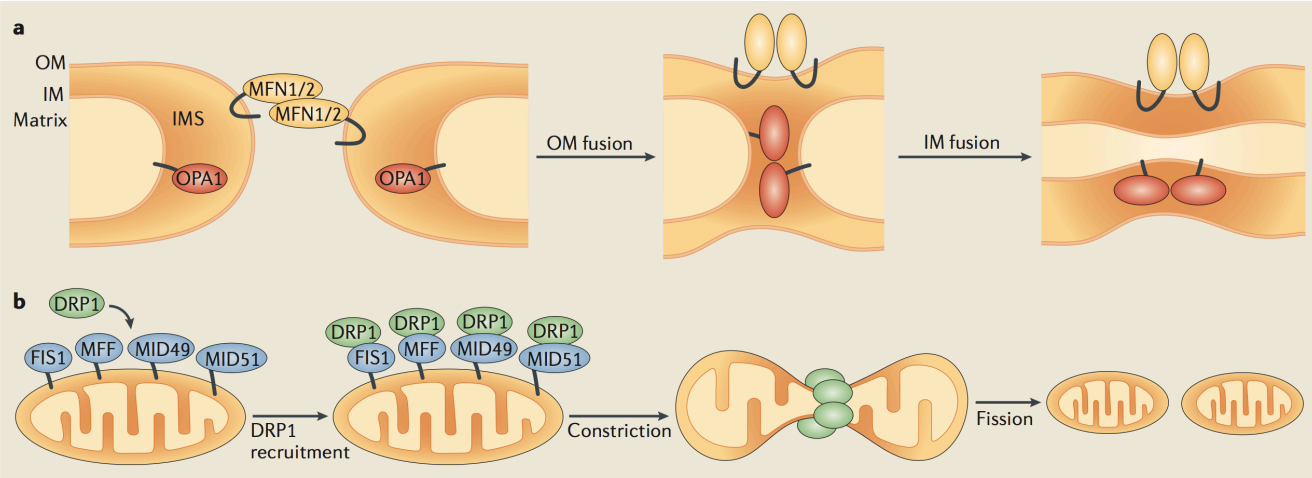

Figure 4. Schematic representation of the mitochondrial fusion and fission events. (a) OM fusion is mediated by mitofusin 1 (MFN1) and 2 (MFN2) and subsequently followed by IM fusion, mediated by the optic atrophy 1 (OPA1) protein. (b) Mitochondrial fission requires the recruitment of dynamin-related protein 1 (DRP1) from the cytosol to OMM. Four DRP1 receptors located on the OMM exist in mammals: mitochondrial fission 1 (FIS1), mitochondrial fission factor (MFF), Mitochondrial dynamics protein of49 kDa (MID49) and 51kDa (MID51) (from Mishra et Chan, 2014).

1.5 Fusion

The fusion of two mitochondria requires that the inner and outer membranes of one mitochondrion be fused with the respective membranes of another. The first step of this process occurs with the fusion of the OMM, allowing the IMM to come into proximity for the second step, the IMM fusion. In mammals, three proteins carry out this event: the mitofusins MFN1 and MFN2 for the OMM fusion and OPA1 for the IMM fusion (Chan, 2012). These proteins belong to the dynamin-like protein superfamily and contain GTPase activity essential for their functions (Praefcke and McMahon, 2004).

The first mediator of mitochondrial fusion was identified in *D. Melanogaster* as the Fuzzy onion protein (Fzo1), which has two homologues in mammals, MFN1 and MFN2 (Santel and Fuller, 2001). These proteins include a GTPase domain, two hydrophobic heptad repeat motifs (HR1 and HR2), and are anchored at the OMM by two transmembrane domains, with both N- and C-terminal facing the cytosol (Chan, 2012). *In vivo* and *in vitro* studies have shown that the MFNs act in the initial step of fusion, are essential for OMM fusion and are required on adjacent mitochondria for fusion to occur (Koshiba et al., 2004; Song et al., 2009). However, they seem to play slightly different roles. MFN1 is more active in mitochondrial fusion exhibiting a higher capacity to induce this process, whereas the role of MFN2 is less defined, but it can forms hetero-oligomers with MFN1 and is suggested to participate in later steps of mitochondrial fusion (Koshiba et al., 2004; Ishihara et al., 2004). MFN2 has been shown to be involved also in endoplasmic reticulum interactions, bridging the two organelles close at the level of MAMs, and levels of MFN2 correlate with the oxidative metabolism of skeletal muscle (de Brito et al., 2008; Bach et al., 2003).

Fusion of both mitochondrial membranes appears coordinated because of the rapid nature of the two processes, yet mitochondria do not always undergo complete fusion and the OM can fuse without the subsequent fusion of the IM (Song et al., 2009; Mishra et al., 2014). Both the mitofusins and OPA1 are required to accomplish full fusion of mitochondria (Song et al., 2009). In yeast Mgm1p/Msp1p are conserved dynamin-related GTPases essential for fusion, morphology, inheritance, and genome maintenance of mitochondria (Wong et al., 2003; Jones and Fangman, 1992). The human orthologue is OPA1, which was identified in 2000 by two European groups (Delettre et al., 2000; Alexander et al., 2000). This protein is localized in the IMS, tightly anchored in the IM, and with its C-terminus facing the inter-membrane space (Wong et al., 2003). It has been shown as OMM fusion can be readily visualized in OPA1-null mouse cells *in vivo* without progression to IM fusion, suggesting that in mammals OPA1 is the main mediator of IM fusion (Song et al., 2009).

2. OPA1

2.1 OPA1 gene and protein

OPA1 gene is located on the long arm of chromosome 3q28–q29. Human OPA1 ORF is built from 31 exons and its mRNA transcripts differ by alternate splicing in the open reading frame, including or excluding exons 4, 4b and 5b. While exon 4 is evolutionarily conserved, both exons 4b and 5b are specific to vertebrates (Delettre et al., 2001; Guillery et al., 2008; Belenguer et al., 2013). The eight OPA1 mRNA variants encode proteins of 924–1014 aminoacids, whose N-terminal includes a mitochondrial targeting sequence (MTS), followed by a predicted transmembrane domain, anchoring the protein to the IMM, and the three peptides corresponding to the alternate spliced exons 4, 4b and 5b (Olichon et al., 2007). Exon 4 domain does not present any remarkable feature, whereas exon 4b and 5b corresponding domains encode two additional hydrophobic domains, TM2a and TM2b. The latter exon encodes also a coiled coil domain (CC0), predicted to oligo-polimerize. The following part of the protein includes the conserved dynamin regions: the GTPase domain bearing the dynamin signature, the middle domain with unknown function and the C-terminal GTPase effector domain (GED) containing a coiled coil domain (CC2) (Olichon et al., 2007; Belenguer et al., 2013).

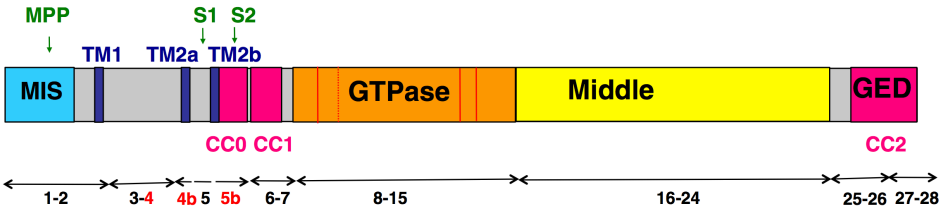

Figure 5. Schematic representation of OPA1 protein structure. The features of dynamin family are: a GTPase domain containing the three consensus GTP binding sequences (red bars) and the dynamin signature (red hatched bar), a middle domain and a GTPase effector domain (GED) containing a coiled-coil region (CCII). The mitochondrial import sequence (MIS) followed by a predicted transmembrane region (TM1), hydrophobic segments (TM2a and TM2b), and coiled-coil regions (CC0-1) are indicated. OPA1 exons numbers are schematized by double arrow and the alternative spliced exons 4, 4b and 5b are indicated in red. Matrix proteolytic cleavage sites for mitochondrial processing peptidase (MPP), paraplegin (S1) and YME1L (S2) are indicated (from Belenguer et al., 2013).

OPA1 expression is ubiquitous, but quantitatively variable according to the organ considered. High mRNA expression levels occur in retina, brain, liver, heart and pancreas. Also the relative abundance of the eight OPA1 splice forms shows great variability, although mRNAs containing ex4 are systematically abundant. In the brain, the presence of exons 4 and 4b, alone or combinated, predominate (Alexander et al., 2000; Misaka et al., 2002; Olichon, 2007).

Upon import of precursors, translated from the eight OPA1 mRNA, into the mitochondria, the MTS is cleaved by the mitochondrial processing peptidase to produce the long isoforms (l-isoforms) that are anchored to the IMM. Then the protein can also be subjected to a complex proteolytic processing that generates short isoforms (s-isoforms) lacking the transmembrane segment. These s-isoforms can be peripherally attached to the IMM, however, a fraction can diffuse in the IMS and associate to the OM (Satoh et al., 2003; Olichon et al., 2002; Song et al., 2007).

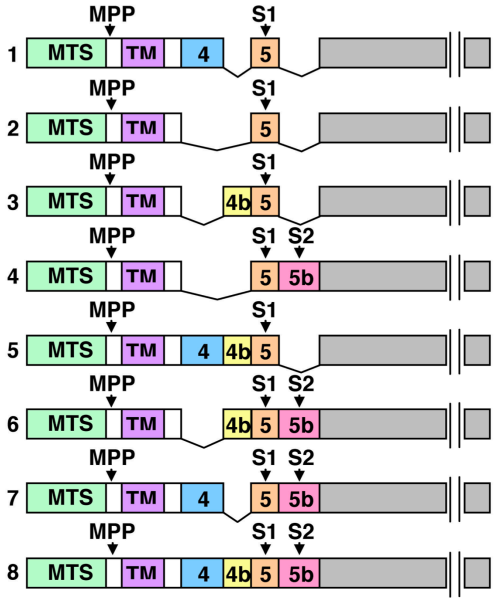

Figure 6. Schematic representation of the eight OPA1 isoforms. The mRNA splice forms differ in the presence or absence of exons 4, 4b, and 5b. Cleavage of the mitochondrial targeting sequence (MTS) by MPP leads to the long isoforms. Additional cleavage at sites S1 (exon 5) or S2 (exon 5b) leads to the short isoforms. TM, transmembrane (from Song et al., 2007).

OPA1 processing can occur because the primary sequence of OPA1 presents two cleavage sites, named S1 and S2. All the isoforms present the S1 site, located at exon 5, whereas only isoforms

containing exon 5b can be processed at S2. Accordingly, teorically four isoforms may produce two short variants (Ishihara et al., 2006; Song et al., 2007). Actually, l-OPA1 isoforms containing exon 4b are totally processed into short forms (Song et al., 2007).

Numerous and discordant studies on the generation of s-OPA1 in human cells identified several types of proteases recognizing the two cleavage sites. The presilin-associated rhomboid-like protease (PARL) seems involved in the generation of a low abundance soluble OPA1 form at the IMS (Cipolat et al., 2006). Two m-AAA proteases, paraplegin and AFG3L2 form a high molecular weight complex within the IMM (Atorino et al, 2003). Overexpression of paraplegin induces a decrease of l-isoforms and accumulation of s-isoforms by cleavage at S1 (Ishihara et al., 2006). The contribution of two other subunits of the m-AAA complex, AFG3L1 and AFG3L2, in OPA1 processing was revealed by experiments conducted in yeast (Duvezin-Caubet et al., 2007). Also in mouse embryonic fibroblasts, down-regulation of AFG3L1 and 2 or the expression of a mutated AFG3L2 variant in human cells decreased the stability of OPA1 l-isoforms (Ehses et al., 2009). However neither PARL nor paraplegin are exclusive proteases involved in OPA1 processing, in fact their knock-down/out does not affect the ratio of l- to s-isoforms (Ishihara et al., 2006; Duvezin-Caubet et al., 2007). Down-regulation of the metallopeptidase OMA1 slightly reduced the level of OPA1 s-isoforms, which are generated by S1 cleavage and accumulate at low levels in MEFs (Ehses et al., 2009; Head et al., 2009). Furthermore, the i-AAA protease YME1L is responsible for cleavage at S2 (Griparic et al., 2007; Song et al., 2007). The knockdown of YME1L, indeed, has no effect on isoform 1 processing, which occurs exclusively at site S1, whereas for isoforms 4 and 7, which contain both sites S1 and S2, reduced level of the S2- and increased level of the S1-cleaved product were reported (Song et al., 2007). The OMA1 or YME1l knockout MEFs showed an OPA1 cleavage pattern containing only l-form (Anand et al., 2014). Furthermore also prohibitins can modify the processing of OPA1, in fact their alteration results in specific loss of l-OPA1 isoforms and accumulation of s-isoforms (Merkwirth et al., 2008). The knockout of another protease, Omi/HtrA2, also induces the selective increase of mild detergent extractable OPA1 levels (Kieper et al., 2010).

To make the picture even more complex, the OPA1cleavage can occur not only under physiological conditions but can be also induced by both apoptosis and dissipation of mitochondrial membrane potential. Collapse of membrane potential destabilizes l-OPA1 and enhances the cleavage at S1 and at other sites excluding S2 (Ishihara et al., 2006; Song et al., 2007; Griparic et al., 2007; Guillery et

al., 2008). The loss of mtDNA, dissipation of ΔΨm, or decreased mitochondrial ATP levels induce OPA1 processing by OMA1 at the S1 site (Ehses et al., 2009). Recentily it has been reported that YME1L activity is regulated by mitochondrial respiration and/or ATP levels (Mishra et al., 2014). Altogether, these data reveal that OPA1 expression is highly regulated at both post-transcriptional and post-translational levels. This latter indeed comprises proteolytic processing, but probably also phosphorylation, ubiquitination, sumoylation and acetylation that have been shown to regulate other actors controlling mitochondrial dynamics. In this regard, the SIR3-dependent deacetylation of OPA1 lysines 926 and 931 has been reported, increasing OPA1 GTPase activity and recovering mitochondrial functions in OPA -/- null cells (Samant et al., 214). Further studies will certainly shed light on this complex processing mechanism.

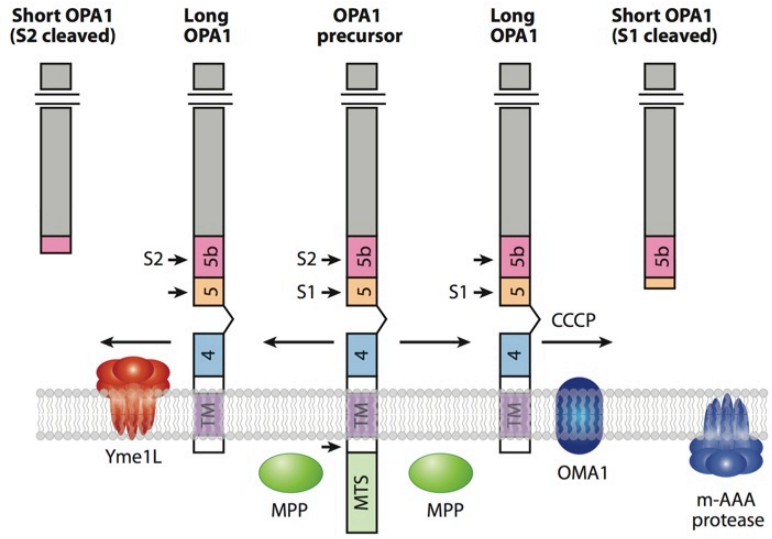

Figure 7. Processing of the precursor OPA1 splice form 7. After import of the N-terminus in the matrix, the mitochondrial targeting sequence (MTS) is cleaved by the peptidase MPP to yield the membrane-anchored, l-isoform. Further processing at the S2 site by the YME1L protease yields a s-isoform (left side). Further cleavage at the S1 site also yields a s-isoform under physiological condition or after CCCP-induced mitochondrial depolarization, activating the OMA1 protease (right side). The m-AAA protease can also regulate OPA1 processing indirectly through OMA1. Abbreviations: HR, heptad repeat; TM, transmembrane segment; CCCP (carbonyl cyanide m-chlorophenylhydrazone) (from Chan, 2012).

2.2 OPA1 and mitochondrial morphology

OPA1 orthologs in yeast were initially identified as actors involved in maintaining the mitochondrial network fused. Subsequent data obtained in mammals indicated that, in accordance to its localization, this GTPase functions primarily in the fusion process at the IMM. The profusion activity of OPA1 was confirmed by different studies showing that loss of function of OPA1, by RNAi or gene knock-out, caused fragmentation of the mitochondrial reticulum (Misaka et al., 2006; Gripatic et a., 2004, Cipolat et al., 2004; Olichon et al., 2003; Song 2007). Interestingly, the overexpression of wild-type or mutated OPA1 alleles also induces networkfragmentation, whereas in cells where mitochondria are punctuated the overproduction of this GTPase promotes elongation of the reticulum (Cipolat et al, 2004; Olichon et al., 2002). All togheter these results suggest that OPA1 protein levels are finely regulated and that its depletion or excess counteracts its physiological pro-fusion activity.

Silencing of the three alternatively spliced exons ruled out the exon 4b and exon 5b involvement in the fusion process, suggesting that the exon4-containing variants are those required to maintain the network in a fusion state (Olichon et al., 2007).

It has been initially proposed that only OPA1 l-forms, without any processing, are necessary for fusion while s-forms are unable to fuse mitochondria (Ishihara et al., 2006). Additionally, a recent paper confirmed that normal fusion is mediated by the l-forms of OPA1 and that the s-forms are important for fission (Anand et al., 2014). However, this hypothesis not been then fully confirmed and other studies showed that both l- and s-forms are necessary for fusion (Herlan et al., 2003; Song et al., 2007). Splicing variants that produce both l- and s-OPA1 have indeed the capacity to restore defective mitochondrial fusion in OPA1−/− MEFs, in contrast with those that only produce s-OPA1, containing exon 4b. Interestingly, a non-cleavable form of OPA1 was not able to rescue morphology of OPA1−/− cells but co-expression with a s-form could restore the capacity of this non-cleavable l-isoform to mediate fusion, suggesting that both l- and s-forms of OPA1 participate in a complex that governs mitochondrial fusion (Song et al., 2007). *In vitro* experiments demonstrated that a recombinant s-form of human OPA1 can assemble on liposomes containing negatively-charged phospholipids also in the absence of a transmembrane domain and this interaction dramatically activates its GTP hydrolysis activity. This short polypeptide can also promote the protrusion of lipid tubules from the surface of cardiolipin-containing liposomes, furnishing the first evidence for a possible mechanism of the OPA1 fusogenic activity. Although able to tubulate membranes, this

peptide was unable to induce membrane fusion, indicating that in such an assay the presence of l-isoforms is also needed (Ban et al., 2010). Moreover, another study supports a model where l-forms of OPA1 form complexes and their processing to s-form stimulates GTPase activity and/or triggers structural rearraggements, promoting membrane fusion. Inhibition of the proteolityc OPA1 processing, indeed, blocked the OXPHOS-induced fusion and artificial cleavage of an engineered version of Opa1 was sufficient to promote IM fusion events (Mishra et al., 2014). These *in vitro* studies, together with those in cells expressing OPA1 isoforms, support a mechanism where both l- and s- forms are necessary for IMM fusion.

This scenario is even more complicated since under some specific cellular stress conditions, the OPA1 pattern can change. OPA1 l-form alone can promote mitochondrial elongation in the presence of cycloheximide, in contrast to the requirement during normal cell growth (Tondera et al., 2009). Collapse of membrane potential by addition of uncouplers, like CCCP, causes cleavage of the l-form and complete fragmentation of the mitochondrial network.

Mitochondrial fusion is a stepwise process and it has been demonstrated that OPA1 is needed only on one mitochondrion to facilitate fusion between pairs and deletion of OPA1 does not block OM fusion. Experiments using photo-activable GFP targeted to the OMM clearly demonstrated that OM fusion can continue in the absence of IM fusion, but merge of the IMMs cannot occur without OM fusion (Song et al., 2009). Moreover, OPA1 expression can induce mitochondrial tubulation in MFN2 knock-out but not in MFN1 knock-out cells, indicating that the fusogenic activity of OPA1 requires MFN1, while MFN2 is dispensable (Cipolat et al., 2004).

OPA1 integrity is also essential its fusogenic activity, as demonstrated by the fact that different mutations in the GTPase and GED domains severely impaired this activity (Ban et al., 2010).

Since mutations in the OPA1 gene have been associated with hereditary dominant optic atrophy (DOA), tissues and cells derived from patients have been investigated to shed light on the pathophysiology of this disease. Several studies described a fragmented mitochondrial network in fibroblasts, myotubes and skeletal muscle from DOA patients bearing different OPA1 mutations (Amati-Bonneau et al., 2005, 2008; Olichon et al., 2007; Zanna et al., 2008; Chevrollier et al., 2008; Spinazzi et al., 2008). Mitochondrial morphology was also affected in OPA1 knock-out retinal ganglionic cells (RGCs), in the rodent cortical primary neurons and in mouse models with OPA1 mutations (Kamei et al., 2005; Bertholet et al., 2013; Alavi et al., 2007; Davies et al., 2007).

2.3 OPA1 and mitochondrial ultrastructure

Human OPA1 is mainly associated within the IMM (Misaka et al., 2002; Olichon et al., 2002) although a small fraction consisting of s-isoforms was found associated with the OMM (Satoh et al., 2003). As the IMM is further sub-compartimentalized in the *cristae* membrane and in the inner boundary membrane, facing the OMM, it was postulated that OPA1 function may be to provide a dynamic intra-mitochondrial skeleton (Amutha et al., 2004). This hypothesis was tested by silencing OPA1 expression in HeLa cells, showing profoundly disorganised IMM structures with misshapen baggy *cristae* and major fission of the mitochondrial network, these alterations being apparent well before those typical of apoptosis (Griparic et al., 2004; Olichon et al., 2002). Strong support to OPA1 involvement on *cristae* stability was provided by EM analysis of OPA1-/- MEFs exhibiting severe ultrastructural defects, including swollen mitochondria and defective *cristae* organization, such as concentric inner membranes (Song et al., 2009). Another study unvealed the role of the protease PARL in the generation of a low abundance s-form of OPA1, forming a complex with l-form to maintain the integrity of the *cristae* junctions. Accordingly, loss of PARL was shown to generate s-OPA1, widen the *cristae* junction and augment the sensitivity of PARL–/– MEFs to pro-apoptotic stimuli (Cipolat et al., 2006). From these observations, it was suggested that OPA1 contributes to the IMM structures, *cristae* junctions and domains of interaction with the OMM (Lenaers, et al., 2009).

Moreover Cogliati et al., 2013, by using a conditional OPA1 ablation mouse model, reported ultrastructural defects with increased *cristae* width, whereas after overexpression of this GTPase *cristae* were tighter. Interestingly, also under conditions of low substrate availability, OPA1 formed oligomers and narrowed the *cristae*, event that promoted ATP synthase assembly, thus allowing maintainance of mitochondrial activity in a fusion-indipendent manner (Patten et al., 2014). A similar behavior was observed also during starvation, where the density of *cristae* increased in wild-type and MFN2-/- mitochondria that elongate, but not in OPA1-/- mitochondria (Gomes et al., 2011).

Several studies in fibroblast reported that often the increased mitochondrial network fragmentation was associated with *cristae* ultrastructure alterations (Amati-Bonneau et al., 2005, 2008; Olichon et al., 2007; Agier et al., 2012). Particularly, our group reported that under physiological conditions fibroblasts from patients bearing different mutations causing haploinsufficency exhibited a remarkable decrease in the number and organization of *cristae*, that were even more severely

destabilized after incubation in a glucose-free medium containing galactose (Zanna et al., 2008). In several mouse models, alteration of *cristae* shape was reported, confirming the importance of this protein in maintenance of mitochondrial ultrastracture (Alavi et al., 2007; Davies et al., 2007; Sarzi et al., 2012; Williams et al., 2012).

2.4 OPA1 and apoptosis

In addition to mitochondrial fragmentation, down-regulation of OPA1, or expression of pathogenic mutants, induced also increased sensitivity of cells to spontaneous and induced apoptosis (Olichon et al., 2003: Lee YJ, 2004; Olichon A, 2007). Since OPA1 is involved in *cristae* organization, its control on the triggering of apoptosis is likely to occur through the compartimentalization of the pro-apoptogenic factor cytochrome c (Olichon et al., 2003; Frezza et al., 2006). It has been proposed that some OPA1 isoforms could form the *cristae* junction bottleneck and act as a "cork" that holds cytochrome c within the *cristae* volume.

PARL is apparently upstream of OPA1 in a pathway where s-OPA1 may be important for regulating cytochrome c release during apoptosis (Cipolat et al., 2006). Expression of wild-type, but not mutated, OPA1 protected MEFs from death induced by intrinsic apoptotic stimuli, by controling the realease of cytochrome c release from mitochondrial *cristae*. Interestingly, this effect was also observed in MFN1–/– and double MFN1–/– and MFN2–/– cells, indicating that OPA1 can protect cells from apoptosis independently of its role in mitochondrial fusion (Frezza et al., 2006). Uncoupling of fusogenic and apoptotic functions of the dynamin was also observed upon knock-down of particular OPA1 splice variants, revealing that isoforms which contain either exon 4b or exon 5b regulated cytochrome c release without activation of fission or dissipation of the membrane potential. Furthermore, studies in cells overexpressing OPA1 variants including exon 5b suggested that this domain has a specific function or conformation that might positively affect the sequestration of cytochrome c in mammalian cells (Olichon et al., 2007). A similar effect was revealed in fibroblasts of a DOA patient bearing an OPA1 mutation in exon 5b destabilizing its coiled coil structure, which induced increased susceptibility to apoptosis, some respiration uncoupling, but no mitochondrial fission (Cornille et al., 2008). Together, these observations support the model where OPA1 exon 5b could specifically shape the *cristae* junction, a structure that when deranged would allow mobilisation of cytochrome c from the *cristae* volume to the IMS (Olichon et al., 2007).

Cristae junctions are the target of pro-apoptotic BH3-only pro-apoptotic proteins, like tBid (Scorrano et al., 2002), which was shown to disassemble peculiar forms of OPA1, inducing subtle *cristae* remodelling, and complete release of cytochrome c (Frezza et al., 2006; Yamaguchi et al., 2008). Ultrastructural alterations and susceptibility to apoptosis have also been reported in fibroblasts bearing different OPA1 mutations (Zanna et al., 2008). Furthermore, the role of OPA1 disassembly in cytochrome c mobilization was evidenced in BNIP3-induced apoptosis. BNIP3 was shown to directly interact with OPA1, leading to mitochondrial fragmentation due to the inhibition of OPA1-mediated fusion. This interaction was necessary to trigger OPA1 oligomeric complex disruption leading to apoptosis, though a MFN1-dependent mechanism (see figure 8) (Landes et al., 2010; Alavi and Fuhrmann, 2013). An alternative hypothesis about the anti-apoptotic role of OPA1 derives from the evidence that OPA1 can bind more efficiently liposomes containing cardiolipin (Ban et al., 2010), a major phospholipid of the IMM, known to retain cytochrome c on the IMS face of the IM (Ott et al., 2007).

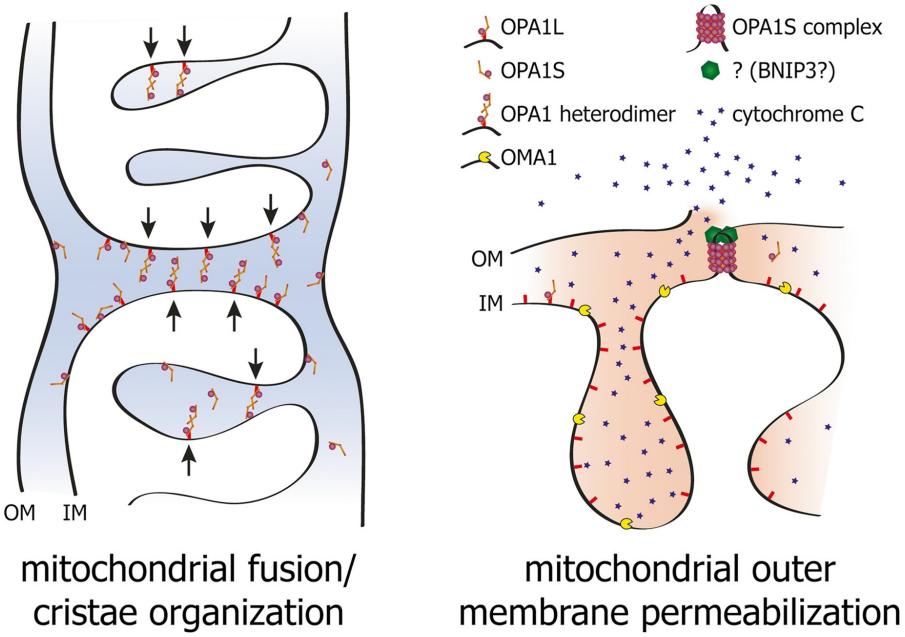

Figure 8. Model of the dual functions of OPA1 in IMM fusion, cytochrome c release and cell death. Membrane bound l- and soluble s-OPA1 form a complex that is able to attract two mitochondrial membranes to enable IM fusion (left) and *cristae* organization. Proteolytic cleavage of l-OPA1 to the soluble s-OPA1 allows formation of s-OPA1 complex, which together with BNIP3 promotes OM permeabilization, cytochrome c release, and cell death (right) by bringing the IMM in proximity to OMM, thereby facilitating membrane hemi-fusion states that are energetically favorable for membrane permeabilization (from Alavi and Fuhrmann, 2013).

2.5 OPA1 and energetic metabolism

Considering the localization of OPA1 in the IMM, the major place of OXPHOS, it is not surprising that alterations in OPA1 expression also affect mitochondrial metabolism. Specific silencing of OPA1 alternative exons showed that the presence of exon 4 was associated with the $\Delta\Psi m$ maintenance (Olichon et al., 2007). Similarly, depletion of OPA1 by RNAi in MEFs led to loss of membrane potential and to severe reduction of basal respiration, unable to be stimulated by an uncoupler (Chen et al., 2005). In mitochondria $\Delta\Psi m$ values rapidly fluctuate and these electrical events can propagate along interconnected mitochondria. Recently it has been shown that in OPA1 knockout cells the flashes were completely lost, suggesting the importantce of OPA1 in these energy conservation events (Santo-Domingo et al., 2013). Defective OXPHOS with lowered mitochondrial ATP production on muscle from DOA patients was first documented for a common micro-deletion localized in the GED domain and further extended to several other OPA1 mutations (Lodi et al., 2004; Lodi et al., 2011). Coupling defect of OXPHOS, with reduced activity of CIV and increased activity of CV, has been observed in fibroblasts from DOA patients bearing various OPA1 mutations, associated or not with reduced mitochondrial ATP synthesis respectively (Chevrollier et al., 2008). Defective mitochondrial ATP synthesis was also documented in fibroblasts and in lymphoblasts from patients carrying different OPA1 mutations (Chevrollier et al., 2008; Amati-Bonneau et al., 2005). Our group also reported in fibroblasts from patients with different OPA1 mutations causing haploinsufficiency an impaired ATP synthesis driven by CI substrates and a decreased rate of mitochondrial fusion. Furthermore, OPA1 was shown to interact with respiratory CI, II and III, providing a potential link between OPA1 mutations and the respiratory chain defect (Zanna et al., 2008). Recently, the energetic impairment has been confirmed in studies on fibroblasts (Agier et al., 2012) and lymphoblasts (Van Bergen et al., 2011) from DOA patients carrying nonsense or missense OPA1 mutations. Interestingly, in the latter case, the OXPHOS dysfunction occurs in lymphoblasts from DOA patients with poor vision only. Patients with relative preserved vision could maintain normal mitochondrial ATP synthesis rate through increased respiration, suggesting a compensatory effect (Van Bergen et al., 2011). Moreover a study in OPA1 mouse model carrying the human c.2708delTTAG mutation, revealed that in different tissues there was a increased amount of cytochrome oxidase subunits, as a possible compensatory effect to contrast the premature age-related decrease in the stability of mitochondrial supercomplexes (Sarzi et al., 2012). These contrasting results may be explained by considering that in the studies were analysed different

mutations, that may cause different phenotypes, depending on the position of aminoacidic change also in the same protein domain.

2.6 OPA1 and mtDNA maintenance

Although Mgm1 in yeast has been identified thanks to its role in mtDNA maintenance, mtDNA deletion or depletion were never reported in skeletal muscles of DOA patients (Amati- Bonneau et al., 2008; Hudson et al., 2008; Yu-Wai-Man et al., 2010), which instead present a 2- to 4-fold increase in mtDNA copy number in COX-negative fibers (Yu-Wai-Man et al., 2010b). Furthermore only a slight reduction or no change in the mtDNA copy number was observed on blood lymphocytes or fibroblasts from DOA patients (Kim et al., 2005; Zanna et al., 2008). It was only in 2008 that OPA1 has been linked to mtDNA stability. Our and another group described the occurrence of a multisystemic disorder, named DOA-plus, characterized by severe optic atrophy and sensorineural deafness, associated with accumulation of multiple mtDNA deletions in skeletal muscles (Amati- Bonneau et al., 2008; Hudson et al., 2008).

As stated above, the nucleoids anchor the mtDNA to the matrix side of the IMM and several nucleoid proteins play important role in controlling mtDNA replication and transcription, but also in protecting this genome from damaging insults (Sperlink, 2010). Our group reported that down-regulation of OPA1 variants including exon 4b reduced the mtDNA content and replication, associated with altered nucleoid distribution throughout the mitochondrial network. In particular, the 11kDa N-terminus peptide of OPA1 containing exon 4b was shown to colocalize with mtDNA, physically interacting with nucleoids and rescuing the effect due to silencing. The hypothesis is that exon 4b-containing peptide might preserve mtDNA replication and proper distribution along the network by anchoring nucleoids to the IMM (Elachouri et al., 2011). In this regard, it has to be noticed that the N-terminus MGM1 domain was also found to be associated with nucleoids (Wong et al., 2000).

The effects of OPA1 in mtDNA stability could be also related to intactness of the IMM ultrastructure. Electron microscopy analyses indeed showed that mitochondria from OPA1-depleted or knock-out cells have an altered internal structure (Griparic et al., 2004; Song et al., 2009), similar to that reported in fibroblasts bearing OPA1 mutations causing aploinsufficieny (Zanna et al., 2008). OPA1 depletion or mutation, through changes in *cristae* morphology, could thus perturb mtDNA anchoring to the IM and thus influence its maintainance and replication.

Another possibility is that impairment of mitochondrial fusion, which is thought to be important for the maintenance of the mitochondrial functions by allowing the exchange of intra-mitochondrial content, might increase mtDNA instability, preventing damaged nucleoids from being repaired or complemented by fusion (Carelli and Chan, 2014).

These hypotheses, that need to be proven, are not mutually exclusive but, on the contrary, they take into consideration the multi-faceted functions of this protein, which might influence the stability of mitochondrial genome though different mechanisms.

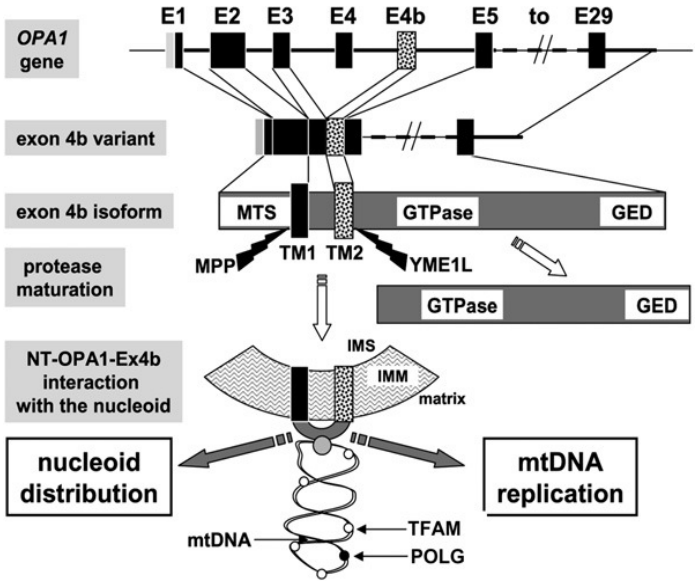

Figure 9. Schematic representation of the different steps from the OPA1 gene to generation of N-terminal peptide containing the exon 4b (NT-OPA1-Ex4b) and its interaction with the mitochondrial nucleoid. E1 to E29 are the OPA1 exons; (MTS) mitochondrial targeting sequence; (GED) GTPase effector domain; (TM) transmembrane domain; (MPP) mitochondrial processing peptidase; (YME1L) inner membrane protease cleaving OPA1-exon4b; (IMS) inner membrane space. (White spots) TFAM proteins; (black spot) POLG; (gray spot) unknown protein linking NT-OPA1-exon4b peptide to the mtDNA (from Elauchuri et al., 2010).

3. Autosomal dominant optic atrophy

3.1 Genetics of DOA

Autosomal dominant optic atrophy (ADOA, OMIM#165500), also known as Kjer's optic atrophy, first described clinically by Batten (Batten, 1896) and Kjer (Kjer, 1959), is the most common of the hereditary optic neuropathies in the general population, with an estimated disease prevalence varing from 1:10,000 to 1:30,000. In 2000, two simultaneous studies identified OPA1 mutations in patients affected by ADOA (Alexander et al., 2000, Delettre et al., 2000). Two genes (OPA1, OPA3) encoding IMM proteins and three loci (OPA4, OPA5, OPA8) are currently responsible for this genetically heterogeneous disease. Additional loci and genes (OPA2, OPA6 and OPA7) are responsible for X-linked or recessive optic atrophy (Lenaers et al., 2012). About 70% of DOA has been linked to mutations in the OPA1 gene and more than 200 pathogenic mutations have been described so far, spread throughout the protein (OPA1 LSDB http://opa1.mitodyn.org; La Morgia et al., 2014). Two major mutations categories, detected throughout the entire gene, exist in patients with DOA. Stop-codon, frame-shift and deletion-insertion (about 50% of OPA1 mutations) leading to incomplete transcription and decreased protein content, with haploinsufficiency as the genetic mechanism. The remaining are missense mutations, which cause heterozygous amino acid substitutions and are thought to act through a dominant negative mechanism. In 2008, a subgroup of missense mutations affecting the GTPase domain have been linked to a multisystemic disorder form of DOA associated with sensorineural deafness, ataxia, late chronic progressive external ophthalmoplegia (CPEO) and mitochondrial myopathy with cytochrome c oxidase negative, defined as DOA "plus" syndrome (Amati-Bonneau et al., 2008; Hudson et al., 2008; Yu-Wai-Man et al., 2010). Importantly, these patients harboured multiple deletions of mtDNA in their skeletal muscles, confirming the OPA1 function in mtDNA stability, as reported for its orthologue in Saccharomyces cerevisiae (Jones and Fangman, 1992; Guan et al., 1993). Thus OPA1 has been added to the list of genes (ANT1, Twinkle, POLG, MFN2) associated with human disorders characterized by mtDNA deletions (CPEO syndromes) (Di Mauro and Schon, 2008; Rouzier et al., 2012). Recently, other phenotypes have been reported within the frame of DOA "plus" syndrome, including MS-like features, Behr-like spastic paraparesis and cases with absent or very mild ocular phenotype, thus expanding the spectrum of "OPAopathies" (Maresca et al., 2013).

Since the majority of mutations result in protein truncation, dominant inheritance of the disease may result from OPA1 haploinsuffciency. Further evidence for this hypotesis has been provided by identification of a microdeletion that results in the complete loss of one copy of the OPA1 gene and by the decreased amount of OPA1 protein expression in fibroblasts (Marchbank et al., 2002; Zanna et al., 2008). In addition to haploinsufficiency, DOA may be caused by a dominant negative mechanism. In support of this thesis, several missense OPA1 mutations that ablate the consensus elements for GTP-binding have been reported (G300E, G401D, K468E, or D470G), and GTPase mutants of OPA1 or of the yeast ortholog Mgm1p showed a dominant negative effect in the presence of the wild-type protein. This effect was due to the capacity of mutant OPA1 to oligomerize with wild-type proteins and, in this way, interfere with GTPase activity (Amati-Bonneau P, 2008; Ferraris et al., 2008; Hudson et al., 2008). GTPase activity is critical for OPA1 function and DOA misssense mutations found in the GTPase domain adjacent to its active site (A357T, G439V, R445H) may impair GTP hydrolysis locking the protein in an 'on' or 'off ' state (Amati-Bonneau et al., 2008; Hudson et al., 2008).

3.2 Clinical features and histopathology

DOA is an hereditary neurodegenerative disorder, characterized by an extreme selectivity of its tissue expression, which is limited to the retinal ganglion cells (RGCs) and their axons forming the optic nerve, with a preferential involvement of the small fibers in the papillomacular bundle that subserve central vision. The disease causes a slowly progressive bilateral visual loss associated with centrocaecal scotomas, impairment of color vision, temporal pallor of the optic disks and relative preservation of the pupillary reflex (Delettre et al., 2002; Lenaers et al., 2012; Yu-Wai-Man et al., 2010). DOA has an insidious onset, presenting usually between ages four and six years, although in mild cases it may remain subclinical until early adult life. However, this optic atrophy has incomplete penetrance and variable expression between and within families. Visual impairment is usually moderate, but ranges from subclinical manifestations to legal blindness (Carelli et al., 2009; Yu-Wai-Man et al., 2010; Barboni et al., 2014). The visual loss is usually symmetrical, visual fields in patients with DOA characteristically show central, paracentral, or cecocentral scotomas and often appears as a large defect in individuals with severe disease. The colour vision defect is often reported as an acquired blue-yellow loss, or tritanopia, but most individuals have a generalized

nonspecific dyschromatopsia and some families have been described in which affected individuals have red-green defects (Eliott et al., 1993; Mantyjarvi et al., 1992).

Postmortem histologic studies of the two patients with DOA available to date identified similar histopathological changes, with diffuse atrophy of the RGC layer, loss of myelin and fibrillary gliosis along the anterior visual pathways extending to the lateral geniculate body (Johnston et al., 1979; Kjer et al., 1983). The optic nerve showed axonal loss and swelling, demyelination, and an increased content of collagen especially in the temporal aspect, suggesting specific vulnerability of the papillomacular bundle fibres, without signs of inflammation. Since the availability of optical coherence tomography (OCT), a non-invasive technology used to diagnose and monitor various optic neuropathies, it has been well established that eyes with DOA show a a decreased retinal nerve fiber layer (RNFL) thickness in all quadrants with a smaller average optic disk size and that this peripapillary RNFL loss occurs in consequence of axonal degeneration (Barboni et al., 2011; 2014; Milea et al., 2010). Interestingly, the OCT measurements of patients bearing different OPA1 mutation type showed that missense mutations displayed the most severe phenotype (Barboni, 2014). Although the primary site of pathology is the RGC layer, up to 20% of patients with OPA1 mutations will also develop additional neuromuscular deficits and sensorineural deafness was the most frequently observed extraocular feature, followed by chronic progressive external ophthalmoplegia, myopathy, cerebellar ataxia and peripheral neuropathy (DOA “plus” phenotype) (Yu-Wai-Man, 2010; Lenaers et al., 2012; Barboni, 2014).

Therapeutic options for DOA are very limited but preliminarily, encouraging results with idebenone (a quinone analog of coenzyme Q10) treatment have been reported in DOA, where spontaneous recovery has never been described (Barboni et al., 2013). There is also the hope that a gene therapy strategy might be straightforward and feasible in the next future (La Morgia et al., 2014).

3.3 Pathophysiological mechanism in RGCs

Mitochondria play important roles in cell physiology, therefore the threshold for mutations in genes involved in mitochondrial functions is lower in those organs that have to cope with high energy demand, such as skeletal muscle, retina, brain, and in fact these organs are mostly affected by mitochondrial diseases. The mechanism leading to degeneration of RGCs in patients with OPA1 mutations is still largely unknown, but probably the susceptibility of these cells may be due

to their particular anatomic features. RGCs show a non-uniform mitochondrial subcellular distribution. Mitochondria indeed are numerous in the unmyelinated portion of the axon, whereas they are less abundant in the myelinated portion. This particular pattern reflects the high-energy requirement in the unmyelinated section to maintain the visual signal trasmission, making these cells vulnerable to energetic impairment. Furthermore the extreme length of the RGC axons may impose stricter energetic requirements for mitochondrial functions, together to a proper mitochondrial transport along this axons. Considering the role of OPA1 in the fusion process and in the mitochondrial energetic functions, it is clear that OPA1 mutations lead, directly or indirectly, to an impairment of the cellular functions (Carelli et al., 2004; 2009; Chen and Chan, 2006). Downregulation of OPA1 in cultured RGCs led to abnormal mitochondria aggregation in both the soma and neurites (Kamei et al., 2005). Furhtermore, the RGC soma and dendrite are frequently exposed to high levels of light, condition that may aggravate the effect of mitochondrial dysfunction, due to enhanced ROS production from mitochondrial photosensitizers and reduced levels of OXPHOS. A study on light exposure of rat retinal cultures reported increased predisposition to apoptosis caused by cleavage and activation of caspase-3 by light (Lascaratos et al., 2007).

In a murine model of DOA, an increased number of autophagosomes has been observed in the RGC layer, with signs of optic nerve degeneration similar, but occurring earlier than age-related degeneration. Increased autophagy could be one of the mechanisms contributing to RGCs loss and subsequent optic atrophy (White et al., 2009).

OPA1 seems to be essential for the neuronal maturation, as shown in a *in vitro* study of cortical neurons. Downregolation of this GTPase led to an altered mitochondrial morphology and distribution, reduction of mtDNA abundance, of expression level of subunits of CI, III and IV and decreased membrane potential. Importantly, the OPA1 loss resulted in reduced dendritic growth and synaptogenesis, which could be related with impaired synaptic plasticity associated with neurodegenerative diseases, and this could contribute to the pathogenic mechanism (Bertholet et al., 2013). More recently studies of an OPA1-mutant mouse model of DOA have reported that the first morphologic evidence of the disease was damage to the dendritic process (dendropathy) of RGCs, i.e. dendritic reduction and pruning in the retinas, effect increasing with age. The RGCs showed also an aberrant mitochondrial morphology and *cristae* ultrastructure.

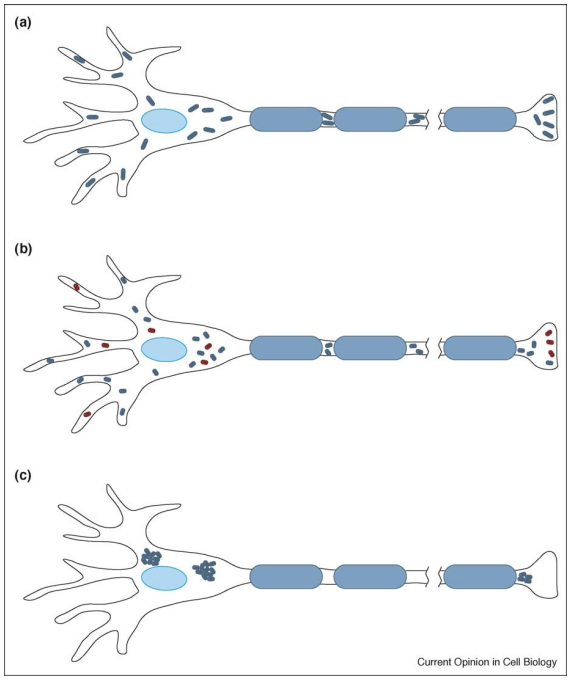

Figure 10. Proposed mechanisms of neuronal dysfunction in DOA. (a) In RGCs and motor neurons, mitochondria are actively transported and concentrated in the dendritic extensions, soma, hillock, nodes of Ranvier and synaptic regions. This pattern of mitochondria distribution may reflect greater energy requirements in these unmyelinated areas. (b) In DOA, reduced mitochondrial fusion may lead to heterogeneity in the mitochondrial population, resulting in fragmented mitochondria with impaired function (red). (c) An alternative possibility is that mitochondrial aggregation or defects in transport lead to uneven and ineffective distribution of mitochondria. A combination of these mechanisms may also occur (from Chen and Chan, 2006).

Interestingly, changes in synaptic density and structure were also apparent, suggesting that synaptic atrophy drives the dendritic atrophy and, consequently, the visual dysfunction (Williams et al., 2010; 2012).

These results are in good agreement with the crucial role played by OPA1 and mitochondrial fusion in maintaining dendrites and their synapses (Bertholet et al., 2013).

Although this huge amount of studies, relevant questions are still open regarding the pathogenesis of DOA and a deeper understanding of OPA1 biology is required to answer these and other relevant questions.

AIMS

The *OPA1* gene encodes eight isoforms of a mitochondrial GTPase and heterozygous mutations in this gene have been identified in the majority of patients with DOA, the most frequent form of hereditary optic neuropathy, and the related multisystem disorder DOA-plus. (Delettre et al., 2000; Amati-Bonneau et al., 2008). Currently there is no established treatment for these diseases, but a gene-therapy strategy, based on Adeno-Associated Virus-mediated expression of a recoded gene, may be applied to DOA patients. The fact that the protein is encoded by the nucleus and the tissue is easily accessible may make the therapy strategy more feasible, as demonstrated by the results obtained with Leber congenital amaurosis type 2, another blinding disease (Testa et al., 2013). A question to be answered is which OPA1 isoform should be used as the most efficient to recover the phenotype in RGCs, but until now the specific role of each of the eight OPA1 isoforms has not been established.

The first aim of this study is to associate specific mitochondrial functions to one or more of the eight OPA1 isoforms. This information will be useful not only to identify the best isoform for gene therapy, but also to gain further insight into the biology of this important protein. Through the use of OPA-/- MEFs, we can overcome the complexity of the OPA1 protein molecular heterogeneity. Having characterized in detail the alterations caused by the lack of OPA1 in the major mitochondrial functions, we will then selectively express each isoform in OPA-/- MEFs and then evaluate the ability to improve the defective phenotypes.

The second aim is focused to identify the OPA1 protein domains crucial for its functions. The expression of OPA1 variants at the N- terminus, at the S1 cleavage site and at the GTPase domain may help to better understand the physiology of the extreme complex OPA1 protein heterogeneity, including isoforms and their proteolytic products.

The last aim is to gain insight on the pathophysiology of different OPA1 mutations. To this purpose, the OPA1 isoform shown to be the most efficient in restoring mitochondrial phenotype will be mutagenized and expressed in MEF OPA-/-, to obtain MEF clones bearing several human pathogenic OPA1 mutations. The biochemical features of these cell models will be analyzed, trying to correlate the more or less impaired cell phenotype with the different clinical severity observed in patients.

MATERIAL AND METHODS

1. Cells culture

Mouse Embryonic Fibroblasts (MEFs) wild type and knockout for the OPA1 gene (OPA1-/-) are a kind gift of Prof. David Chan, Division of Biology, California Institute of Technology, Pasadena, CA, USA (Chen et al., 2007). Skin fibroblasts were derived, following informed consent, from one healthy donor and one DOA patients bearing the frameshift-inducing microdeletion on OPA1 gene c.2708delTTAG in exon 27.

MEFs and fibroblast cells were cultured in Dulbecco Modified Eagle Medium (DMEM Euroclone) supplemented with 10% fetal bovine serum (FBS Euroclone), 2 mmol/L L- glutamine, 100 units/mL penicillin, and 100µg/mL streptomycin, at 37°C in a 5% CO2 humidified incubator. For experiments the cells were incubated in glucose-free DMEM supplemented with 5mM galactose, 2 mM L-glutamine, 5 mM Na-pyruvate and 5% FBS or in HBSS medium (Invitrogen).

2. Molecular cloning

Plasmids expressing the eight OPA1 isoforms and the isoform1 without S1 site are from (Song et al., 2007). Open reading frames corresponding to residues 1-95 of mouse AIF and 230-960 of human OPA1 isoform 1 were cloned by PCR into the pMSCV-puro vector, with primers introducing a Xho1 site at the ATG initiation codon and a NotI site at the end of isoform 1 sequences (see list of primer sequences).

OPA1 open reading frames corresponding to NT-OPA1-Exon4 or NT-OPA1-Exon4b peptides from (Elauchouri et al., 2011) were cloned by PCR into the pMSCV-puro vector. (see list of primer sequences). Isoform 1 was further mutagenized (A166V, R290Q, I382M, D603H) and cloned into the pMSCV-puro vector, whereas the plasmids expressing isoform 1 bearing the mutations G300E, G439V, R445H, S545R, Q785R are from (Ban et al., 2010).

3. Infection of OPA1-/- MEF

To produce the virus, 293T cells were transfected. Briefly, 10^5 cells/well were seeded the day before the transfection onto a 6 wells plate. Transfections were performed according to the manufacturer's instruction by using 3µg of expression plasmid DNA (pMSCV-puro vectors), 1µg of packaging plasmid DNA (pcl-Eco) and 10µl Lipofectamine 2000 reagent (Invitrogen) per well. After overnight incubation, the media was replace with fresh media and the cells were harvested

for 48 hours. The medium, containing the virus, was filtered through 0.45 mm syringe filter and used to infect the OPA1-/- MEFs, seeded on a 12 wells plate the day before ($5x10^4$ cells/well). Puromycin (Sigma) was used at 1μg/mL for the selection

4. Mitochondrial morphology

MEFs ($1x10^4$/well) were seeded onto 8 wells glass coverslips (Nunc Lab-Tek) and after 24hr processed for immunostaining. For the starvation assay, after 24hr cells were washed twice with PBS, incubate for 6h with HBSS medium (Invitrogen) and then processed. Cells were incubated at 37°C with pre-warmed formalin for 15 minutes, washed five times with PBS and subsequently incubated with cold acetone for 10 minutes at -20°C. After five washes with PBS, MEFs were incubated for 1 hour with a blocking solution (PBS, 5%FBS, 0.1% Triton X100). Mitochondria were labelled by incubating cells for 2 hr with the anti-Tom-20 antibody, followed by five PBS washes, and 1 hour with AlexaFluor546-conjugated secondary antibody. After five PBS washes, cells were dried and mounted.

Images were captured by a confocal microscope (Zeiss LSM 710) with a 63X oil objective.

Cells were scored into three categories on the basis of mitochondrial morphology: cells with a filamentous and interconnected network (filamentous), cells with short filamentous mitochondria and balloon-like structures (intermediate) and cells with complete fragmented mitochondria (fragmented). For each experiment, 100 cells were scored for each cell lines.

5. Mitochondrial ultrastructure

MEFs cells were seeded onto two 15cm plate and cultured/grown to 70-80% confluency. The fix solution (3% parafolmaldehyde, 1.5% glutaraldehyde, 2.5% sucrose, 100mM cacodylate, pH 7.4) was added directly to the colure and cells were incubated for 15 minutes at 37°C. After removing the solution, cells were incubated with fresh fixative at room temperature for 1 hour, followed by two washes with 100mM cacodylate pH7.4, and then scraped and the pellet collected. Pellet was processed as previously described (Song et al., 2009).

Images of mitochondrial ultrastructure morphology were used to score mitochondria into three categories: more than 5 *cristae* and dense matrix (class I), between 2 and 5 *cristae* with variable density of the matrix

(class II), less than 2 *cristae* and swollen mitochondria (class III). 40-60 mitochondria per sample were analysed.

6. Mitochondrial DNA measurement

For the extraction of whole DNA, 2-4 x10^6 cells were processed. After PBS washing, the pellet was resuspended with tail buffer (1% SDS, 0.1M NaCl, 0.1M EDTA, 0.05M Tris pH8) and proteinase K. After incubation at 50°C overnight, 6M NaCl was added and phenol-chloroform extraction was performed. Total DNA extracted was precisely quantified by spectrophotometry (Nano-Drop 2000). Quantification of mtDNA relative to nuclear DNA (nDNA) was performed by a real-time PCR based method using the Brilliant III Ultra-Fast SYBER® Green QPCR Master mix (Agilent Technologies. Primers against mouse mtDNA and mouse Pecam gene (nDNA) have been previously described (Chen et al., 2010). A standard curve for mtDNA and nDNA was generated using serial dilutions of DNA of wt MEFs. For the amplification protocol we used minutes denaturation at 95°C, followed by 40 cycles of 5 seconds at 95°C and 10 seconds at 58°C. The ratios between mtDNA and nuclear DNA concentrations are used to compare the samples.

7. SRB assay

Wt-MEF and OPA1-/- MEF (1x10^4 and 2x10^4 cells/well, respectively) were seeded in 24 wells plates, then the day after washed with PBS and incubated with the different media for the times indicated. At the end of incubation the media was removed and cells were fixed with DMEM and 10% Trichloro acetic acid at 4°C for 1h, washed five times with water and dried at room temperature (RT). 0,4% Sulforhodamine (SRB) in 1% acetic acid were added in each well and colored at RT for 30 minutes in the dark. Unbound dye was removed with four washes in 1% acetic acid solution, and bound dye was solubilized by addition of 10 mM Tris pH 10.5, stirring for 10 minutes. Absorbance at 564 nm was determined with a Multilabel Plate Reader (Tecan).

8. Oxygen consumption rate (OCR)

Oxygen consumption rate was measured in a Seahorse Biosciences Extracellular Flux Analyzer (model XF96). A total of 1x10^4 cells per well were plated 18 hr prior to measurement in complete medium in a 96-well plate. Two hours prior to measurement, cells were equilibrated in media made with DMEM lacking bicarbonate (Sigma-Aldrich Catalog #D5030), using the XF96

PrepStation (Seahorse Bioscience). Oxygen levels were measured over 5 min periods, in basal condition and after injection of oligomycin (inhibitor of CV), CCCP (protonophore) and antimycin A (inhibitor of CIII).

Taking into account the different growing capability of the cell lines, the values obtained (Oxygen consumption rate, pmol O_2/min) were normalized using the SRB protocol (see above). After removing the contribution from non-mitochondrial oxygen consumption (antimycin-insensible), the ratio between maximal respiration rate (after the addition of the uncoupler CCCP) and ATP-linked respiration (basal minus respiration in presence of oligomycin) were calculated.

9. Mitochondrial ATP Synthesis

The measurements of mitochondrial ATP synthesis were done in cells grown in DMEM-glucose according to Manfredi et al. 2002 with minor modifications. After trypsinization, cells were resuspended ($1x10^7$/mL) in buffer A (150mM KCl, 25mM Tris-Cl, 2mM EDTA, 10mM KH2PO4, 0.1mM MgCl2, pH 7.4) and one aliquot of sample was used to determine the protein concentration (Bradford, 1976). Cells were permeabilized with 50µg/ml digitonin for 1 minutes and the action of digitonin was blocked by adding 2.5 times the original volume of buffer B (Buffer A added with 0.1% BSA). After verifying that the cells had been permeabilized, they were centrifuged to eliminate the digitonin and re-suspended again in buffer B at the initial concentration. 32 µl of the cell suspension was collected for CS assay (see below). Permeabilized cells were incubated with the luciferase-luciferin kit (Sigma-Aldrich) and specific substrates to determine ATP synthesis rate driven by different complexes or the glycerol-3-phosphate dehydrogenase (GPD): 1 mM pyruvate and 1 mM malate for CI; 5 mM succinate and 5 μM rotenone for CII; 5 mM malonate, 50 μM decylbenzoquinol, and 5 μM rotenone for CIII; 5 mM malonate, 20 mM glycerol-3-phosphate, and 5 μM rotenone for GPD. The reaction was started by addition of 0,1 µM ADP. At the end, 5 μM oligomycin and 11 μM ATP were added respectively to inhibit the ATP syntase activity and as an internal standard. The measurement was performed using a Bio Orbit 1250 Luminometer.

By measuring the signals emitted by the samples and by the reference standard and after taking into account the amount of protein and CS activity (see paragraph n. 10) of the sample, the cellular ATP levels in the various samples were calculated.

10. Citrate synthase activity

In order to determine the activity of citrate synthase, 10 µg of the protein was diluted in assay buffer (0,1% Triton X100, 125mM Tris-HCl, pH 8) and incubated with 0.3mM Acetyl Coenzyme A, 0.1mM DTNB and 0.5mM oxalacetate. The rate of coenzyme A production by citrate synthase was determined by recording the variations in absorbance of DTNB from the oxidised to the reduced state at 412nm at 30°C by using the spectrophotometer (V550 Jasco). The activity of citrate synthase was evaluated with a molar extinction coefficient of e= 13.6Mm-1.

11.Extraction of mitochondria from cultured cells

$15x10^6$ cells were washed once with PBS, resuspended in 0.5 ml of Sucrose-Mannitol buffer (200 mM mannitol, 70 mM sucrose, 1 mM EGTA, 10 mM Hepes, pH 7.6), with protease inhibitor cocktail and homogenized for 30 strokes with a Dounce homogenizer at 4 °C. The homogenate was centrifuged for 10 minutes at 3000 rpm, and supernatant re-centrifuged for 20 minutes at 13000 rpm. The resulting pellet (Mitochondrial franction) was resuspended in Sucrose-Mannitol buffer (OXPHOS complexes activity) or RIPA lysis buffer (SDS-page).

12. OXPHOS complexes activities

Mitochondria were extracted mechanically as described above and were stored at -80°C. Mitochondrial protein content was quantified according to Bradford. All measurements were performed with UV-Vis spectrophotometer (V550 Jasco).

For CI and CII activity, spectrophotometric assay was performed at 600 nm wavelength, at 37 °C and under constant agitation. The activity of CI was determined by following the DCIP reduction during time at the wavelength of 600 nm. 10 μg mitochondrial protein were added to a buffer containing 50 mM KPi buffer (K2HPO4/KH2PO4 solution) pH 7.8, 1 μM antimycin, 0.2 mM NADH, 70 μM DUB, 60 μM DCIP (2,6-Dichloroindophenol), 3.5 mg/ml BSA. The reaction was started by addition of 200 µM NADH. The non-specific activity measurement was conducted in a separate assay, adding 1 μM rotenone. Kinetics was calculated using the DCIP molar extinction coefficient (19,1 mM-1cm-1).

For the Complex II activity, the reaction buffer contained 100 mM KPi buffer (K2HPO4/KH2PO4 solution) pH 7.8, 0.2 mM ATP, 1 mg/ml BSA, 2 mM EDTA, 50 μM DUB, 80 μM DCIP (2,6-Dichloroindophenol), 1 μM rotenone, 300 μM KCN and 1 μM antimycin. 10 μg mitochondrial protein were added to the buffer. The reaction was started by addition of 10 mM succinate. The non-specific activity was measured in a separate assay, adding 5μM malonate at the beginning of the reaction. Kinetic was calculated using the DCIP molar extinction coefficient (19,1 mM-1cm-1). The spectrophotometric activity of both CIII and CIV was analysed at double wavelength (540nm-550 nm), at 37 °C and under constant agitation, following the reduction or oxidation of cytochrome c (molar extinction coefficient 19,1 mM-1cm-1). The reaction of CIII activity was performed using the specific buffer (50 mM KPi buffer pH 7.8, 3.5 mg/ml BSA, 300 μM KCN, 20 μM oxidized cytochrome c, 1 μM rotenone and 5 mM malonate) and was started by addition of 50 μM reduced decylbenzo quinone (DBH_2). In a separate reaction, 1μM antimycin was used to measure the non-specific activity.

For Complex IV activity, the reaction was started by addition 10 μg mitochondrial sample and 20 μM reduced cytochrome c at the specific buffer (50 mM KPi buffer pH 7.6, 1 mM EDTA, 1 μM Antimycin). The non-specific activity measurement was performed in a separate assay, adding 300μM KCN at the beginning of the reaction.

Complex V (ATPase) spectrophotometric activity was measured at 30 °C, in agitation, following NADH oxidation at 340 nm wavelength (NADH ε= 6,22 mM-1). In this assay we evaluated the hydrolytic activity of CV, which determine the production of ADP, used then by pyruvate kinase (PK) to generate pyruvate from phosphoenolpyruvate (PEP). At the end, lactate dehydrogenase (LDH) reduces this pyruvate, oxidizing NADH.

The assay buffer contained 50 mM KPi pH 8, 250 mM sucrose, 50 mM KCl, 0.96 mM PEP, 10 ug/ml AP5A (Adenosine pentaphosphate Ammonium), 0.2 mM EGTA, 5.4 mM ATP, 5 mM $MgCl_2$, 0.2 μM Ouabaine, 0.25 mM NADH, 1.25 μM Rotenone, 1.83 U/ml LDH, 2.75 U/ml PK. Samples were freezed-thawed for three times, incubated at 30°C for 10 minutes and 10 μg mitochondrial sample was used to start the reaction. The non-specific activity measurement was performed adding 2.5 μM oligomycin.

After taking into account the amount of protein and CS activity (see paragraph n. 10) of the sample, the activity of the complexes was calculated.

13. Total cellular lysates preparation

$2x10^6$ cells were seed into 10cm plate in complete medium and after 24h, pelleted and washed in PBS. The pellet was resuspended in 100 µL of RIPA lysis buffer (50 mM Tris-HCl, 0.15 M NaCl, 5 mM EDTA, 1% NP40, 0.1% SDS, 1% NaDoc, pH 7.6 and 100 µL/mL protease inhibitors). The lysate was incubated in ice for 15', frozen and thawed twice, sonicated in waterbath for 2' and centrifuged at 12000rpm for 10' at 4°C. The supernatant was then collected and protein content was assessed with Bradford assay.

14.Mitochondria from mouse tissues

Ice cold Buffer AT (0.075M sucrose, 0.22 M mannitol, 10mM Tris-HCl pH7.4, 1 mM EGTA, 0.1% fatty acid-free BSA) was added to the tissue, which was homogenized with a Dounce homogenizer for 30 strokes at 4 °C. For heart and muscle, the tissues were first homogenizer with Ika Ultraturrax in ice. The suspension was centrifuged for 5 min at 1500 g at 4°C and the supernatant was centrifuged a 9000g for 10 min a 4°C. The mitochondria pellet obtained was resuspended with buffer AT and centrifugated a 9.000g for 10 min a 4°C and the pellet stored at -80°C.

15.SDS-PAGE

30µg of proteins were solubilized in Laemmli sample buffer and boiled for 10 minutes. Samples were separated on polyacrylamide gels. 8%-10% gels were run in SDS running buffer for 1 h and 30 minutes at 100V, according to the manufacturer's intstruction. After SDS PAGE, the proteins were transferred on to a nitrocellulose membrane (0,22 BioRad) or PVDF using a semi-dry apparatus (BioRad), in transfer buffer containing 20% methanol. Transfer was performed at RT for 1h at 100V, according to manufacturer's instructions.

16.OXPHOS complexes analysis by CN/BN-PAGE

The OXPHOS complexes were separated on a Blue Native polyacrylamide gradient according to their molecular weight, while the complex I only was separated through Clear Native (Wittig et al., 2006). Cells were resuspended at 10^7 cells/ml in PBS, permeabilized with 50 µg/ml digitonin,

centrifuged at 13000 rpm for 10 minutes and the mitochondrial pellet was stored at -80°C. The day after it was resuspended in mitochondrial buffer (750 mM 6-aminocaproic acid, ACA; 50 mM BisTris, pH 7.0), the proteins quantified and DDM (n-Dodecyl β-D-maltoside) added as 2,5 times the protein quantity. Afterwards samples were incubated on ice for 10 minutes and then centrifuged at 13000 rpm for 15 minutes at 4°C. The supernatant containing the mitochondrial protein was then recovered and proteins quantified again. The supernatant collected was properly diluted in BN-Sample Buffer (0.5 mM EDTA, 5% Coomassie Brilliant Blues G250 and 750 mM ACA), whereas Clear Native samples were diluted in CN-Sample Buffer (0.1% Red Ponceaux and 50% Glycerol). 50 μg of mitochondrial protein samples were loaded onto a native gel constituted by a gradient of polyacrylamide from 4% to 12%, made with a gradient building machinery and a peristaltic pump (Delta-Pump). Running gels were prepared adding to established acrylamide concentrations 25 mM Imidazole, 0.5 M ACA, pH 7, 0.02% APS and 0.02% TEMED; 10% glycerol was added to gradient with higher concentrations. Stacking gel contained 4% acrylamide. In Blue Native were used Anode Buffer (25 mM Imidazole pH 7) and Blue Cathode buffer (50 mM Tricine, 7.5 mM Imidazole, 0.02% Coomassie Blue, pH 7), which was halfway replaced with White Cathode buffer (50 mM Tricine, 7.5 mM imidazole, pH 7). In Clear Native were used Anode buffer and Cathode buffer for CN-PAGE (50 mM Tricine, 7.5 mM Imidazole, 0.02% DDM, 0.05% NaDOC pH 7). The electrophoresis was always carried at 80V.

17.Supercomplexes analysis by BN-PAGE

The mitochondrial pellet was suspended in cold PBS and protein content quantified. Mitochondrial suspension was centrifuged for 10 minutes at 13,000 rpm. Mitochondria proteins were suspended in the supercomplex buffer (0.34 M K-acetate, 0.07 M HEPES pH 7.4, 25% glycerol, 0.047 mg/ml digitonin and 2.3 mM PMSF) and incubated for 30 minutes in ice. Suspension was centrifuged for 2 minutes at 3000 rpm, then the supernatant collected and properly diluted in Sample Buffer (5% Serva Blue G, 750 mM ACA). Native gel was prepared as previously described, with a gradient of polyacrylamide from 3% to 12%. Electrophoresis was carried at 80V and performed with Anode buffer and Blue Cathode buffer, which was halfway replaced with the White Cathode buffer.

18.ImmunoBlotting

The membrane was blocked with Tris-buffered saline (0.9% NaCl, 50 mM Tris– HCl, pH 7.6) with 0.1% Tween 20 (TBS–T) containing 5% skim milk for 1 h at room temperature, then hybridized with the primary antibody in blocking solution overnight at 4°C or 2hr at RT, washed with TBS–T, hybridized with secondary antibody in TBS–T with 0.5% milk for 1 h at RT, and then washed with TBS–T. Immunodetection was performed using the secondary horseradish-peroxidase conjugated anti-mouse/IgG and anti-rabbit/IgG (Jackson Labs) and revealed by chemiluminescence (Millipore). Membranes were probed using the following antibodies: OPA1 (1:3000, in-house monoclonal; BD Biosciences, diluted 1:500), NDUFS3 (MitoSciences, diluted 1:1000), NDUFA9 (MitoSciences, diluted 1:1000), SDHA (MitoSciences, diluted 1:10000), Core2 (MitoSciences, diluted 1:1000), COX IV (MitoSciences, diluted 1:1000), α-subunit CV (MitoSciences, diluted 1:1000), β-subunit of CV (Life Technologies, diluted 1:500), anti-porin (Alpha Diagnostics, diluted 1:1000); anti-TIM23 (BD Biosciences, diluted 1:500), β-actin (1:10000; Millipore). Secondary anti-rabbit and anti-mouse IgG-HRP (1:10,000; Jackson Labs)

19.Primers list

Mouse mtDNA:

FW: CCTATCACCCTTGCCATCAT

RW: GAGGCTGTTGCTTGTGTGAC

Mouse nDNA (Pecam):

Fw: ATGGAAAGCCTGCCATCATG

RW:TCCTTGTTGTTCAGCATCAC

AIF-230:

AIF-Fw:AAAACTCGAGGGTACCATGTTCCGGTGTGGAGGCCTGGCG GGTG

AIF-Rw:CTAATCGTTCCAAGATTCTCTGTCTTTCATTGTATCTTTTTTGGTCTTCTTT TATAG

OPA1-230-Fw:CCAAAAAAGATACAATGAAAGACAGAGAATCTTGGAACGATTAG

OPA1 into pMSCV-puro vector:

C-Terminus: AAAAGCGGCCGCCTATTTCTCCTGATGAAGAGCTTCAATGAAAGC

N-Terminus: AAAA CTCGAGGGTACCATGTGGCGACTACGTCGGGCCGCTGTGG

A166V:

Fw:CAGAAGACCTTGTAAAGTTAGTACCAGACTTTGACAAGATTGTTGAAAGC

Rw:ACAATCTTGTCAAAGTCTGGTACTAACTTTACAAGGTCTTCTGAACTAGG

R290Q:

Fw: TACGCAAGATCATCTGCCACAGGTTGTTGTGGTTGG

Rw:TACGCAAGATCATCTGCCACAGGTTGTTGTGGTTGG

I382M:

Fw:ACCGTTAGCCCTGAGACCATGTCCTTAAATGTAAAAGGC

Rw:GCCTTTTACATTTAAGGACATGGTCTCAGGGCTAACGG

D603H:

Fw:GCTAAAAATGAAATCCTTCATGAAGTTATCAGTCTGAGCCAGG

Rw:CCTGGCTCAGACTGATAACTTCATGAAGGATTTCATTTTTAGC

20.Statistics

Statistics were inferred using the Student's t-test.

RESULTS

1. Characterization of OPA1 knock-out cells

To investigate the specific role of each individual OPA1 isoform in the different mitochondrial functions, we decided to take advantage of mouse embryonic fibroblasts (MEFs) with the knockout of OPA1 gene (OPA1 -/- MEF). Accordingly, detailed biochemical characterization of OPA1 -/- MEF has been performed, starting from analysis of the mitochondrial morphology by confocal microscopy and measurement of the mtDNA copy number by qPCR. As illustrated in figure 11A, the lack of OPA1 protein caused the complete fragmentation of the mitochondrial network and a significant reduction of mtDNA content (Fig. 11B), in agreement with previous reports (Song et al., 2007; Chen et al., 2010).

We then investigated whether the lack of OPA1 impairs the energetic efficiency of cells, by determining the viability in glucose-containing DMEM and in glucose-free DMEM containing galactose (DMEM-galactose), an experimental condition known to force cells to rely on OXPHOS only for ATP production. Figure 12A shows that the growth of OPA1 -/- MEFs was much slower than wt MEFs (5- versus 15-fold increase after 3 days of incubation). In DMEM-galactose, the number of wt MEFs increased with time, although at significantly reduced rate than in DMEM, whereas OPA1 -/- MEFs were unable to grow at all (Fig. 12B), suggesting that an energetic defect is associated with OPA1 knockout.

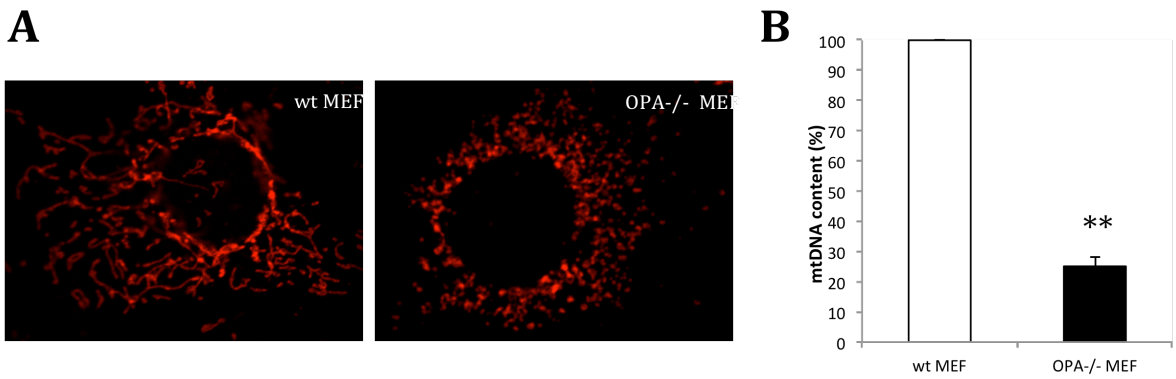

Figure 11. Mitochondrial morphology and mtDNA content of OPA1-/- MEF. (A) Immunostaining of wt and OPA-/- MEF by using anti-TOM20 antibody. Representative images out of ten similar are shown. (B) Evaluation of mtDNA content by qPCR. Data are means ± SEM of at least three experiments. Asterisks denote values significantly different ($P<0.01$).

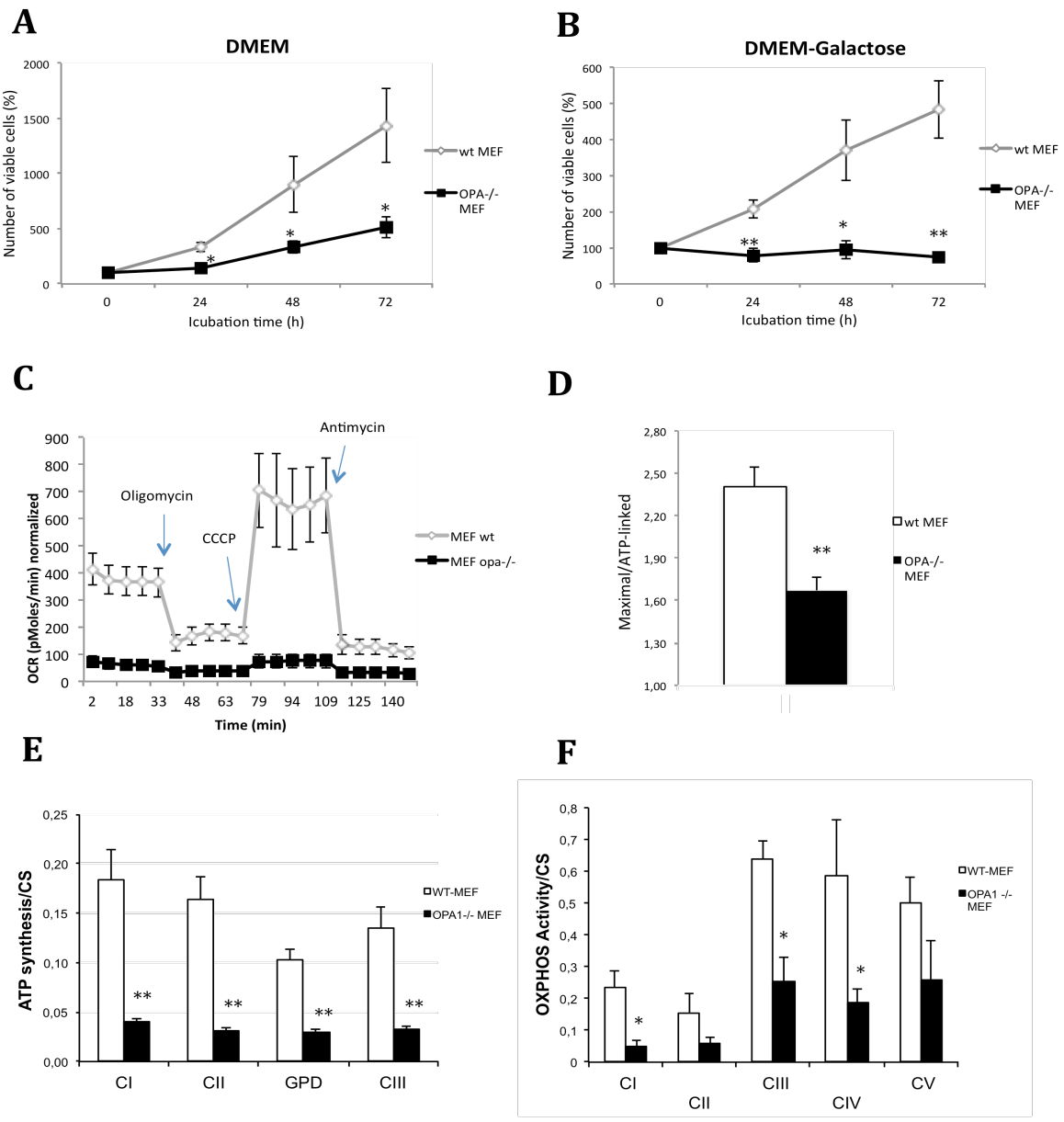

Figure 12. Energetic competence of OPA1-/- MEF. Viability of wt and OPA -/- MEFs during incubation in DMEM-glucose (A) and DMEM-galactose (B). Data are means ± SEM of six independent experiments. (C) Oxygen consumption rate (OCR) was measured with a Seahorse XF-96 analyzer. Cells were seeded on Seahorse TC plates 24hr before analysis and oligomycin, CCCP and antimycin A were injected where indicated. A representative experiment of four similar is shown. Each data point is mean ± standard deviation of 6-8 wells. (D) Data from four experiments have been normalized and expressed as a ratio of maximal respiration (after the addition of CCCP) and ATP-linked respiration (resting respiration minus respiration in presence of oligomycin). Data are means ± SEM of four determinations. (E) The ATP synthesis rate driven by complex I (pyruvate and malate) or complex II (succinate plus rotenone) or complex III (DBH_2) or glycerol 3-phosphate dehydrogenase (glycerol 3-phosphate, GPD) was determined by the luciferase assay using a luminometer. The values (nmol/min*mg protein) were normalized for CS activity. Data are means ± SEM of at least three experiments. (F) OXPHOS complexes activities in wt and OPA -/- MEFs. Activities (nmol/min*mg) were also normalized for CS activity. Data are means ± SEM of four independent experiments. * denotes P<0.05; ** P<0.01.

To more deeply define how OPA1 modulates the energetic competence of MEF cells, we assessed cellular oxygen consumption rate (OCR), ATP synthesis rate and OXPHOS complexes activities. OPA-/- MEFs showed a severe reduction of OCR (Fig. 12C). Statistically significant differences between wt and OPA1-/- MEFs were apparent in the ratio between maximal respiration rate (after the addition of the uncoupler CCCP) and ATP-linked respiration (resting minus respiration in presence of oligomycin) (Fig. 12D).

Furthermore, the rate of mitochondrial ATP synthesis in digitonin-permeabilized cells was determined, after normalization for the citrate synthase activity, an indicator of mitochondrial mass. As reported in Fig. 12E, the values of ATP synthesis rate were markedly reduced (70- 80%) in OPA1 -/- compared to wt MEFs, when driven by substrates of complex I (CI), II, III or glycerol-3-phosphate dehydrogenase. Finally, the specific activities of OXPHOS complexes were measured in isolated mitochondria. The activity of CI, CIII and CIV was significantly reduced in OPA-/- MEFs compared to wt MEFs. A tendency towards reduction, without reaching a statistical significance, was observed also for CII and CV (Fig. 12F). These data suggest a global and serious OXPHOS impairment in cells devoid of OPA1, which prompted us to investigate in detail the organization of OXPHOS complexes and supercomplexes.

SDS-PAGE analysis of protein levels of some representative subunits of OXPHOS complexes showed a significant reduction in the amount of NDUFS3, NDUFA9 and NDUFB8 subunits of CI, core II subunit of CIII, subunit IV of CIV in OPA1 -/- MEFs. In contrast the level of SDHA subunit of CII and β subunit of CV did not change (Fig. 13A). To evaluate the presence of defective assembly of OXPHOS complexes, mitochondria were isolated from both OPA-/- and wt MEFs, solubilized with dodecylmaltoside (DDM) and protein complexes were resolved by blue native gel electrophoresis (BN-PAGE), followed by western blotting analysis. Bands corresponding to CI, II, III, IV and V were consistently well resolved (Fig. 13B). The CI-in-gel activity of OPA1 -/- MEFs was lower than wt MEFs. This result was confirmed by western blot, showing that the amount of assembled CI, CIII and CIV was reduced in OPA-/-MEFs compared to wt MEFs, whereas CII, usually used as loading control, did not change. The CV, whose levels were not different compared to control by western blot analysis after SDS-PAGE (Fig. 13A), was detected as two distinct bands after BN-PAGE, the higher band corresponding to the monomeric holo-enzyme (F_1-F_0) and the lower corresponding to the F_1 portion alone, indicating the presence of catalytic-active sub-complexes, as confirmed by CV-in gel activity measurement (not shown).

It is well known that CI, III and IV are usually assembled together to form a supercomplex named "respirasome". We have therefore analyzed whether the supra-molecular organization of respiratory complexes was altered in cells lacking OPA1, by CN- and BN-PAGE of mitochondria solubilized with the mild detergent digitonin, that keeps intact interactions within supercomplexes. As reported in Fig. 13C, both the CI-in-gel activity and immunodetection with anti-NDUFA9 antibody revealed a marked reduction of the $CI+III_2$ and the high molecular weight supercomplexes ($CI+III_2+IV_n$) in OPA-/- MEFs compared to wt MEFs. This was confirmed by using the anti-core 2 antibody labeling CIII, showing that the levels of CIII dimer and $CIII_2$+IV supercomplex were not significantly changed. Analysis with anti-subunit α antibody confirmed that CV is only partially assembled in OPA-/- MEFs.

In conclusion, the detailed characterization of OPA1 -/- MEFs evidenced a drastic energetic impairment, a severe alteration of mitochondrial morphology and a consistent reduction of mtDNA content.

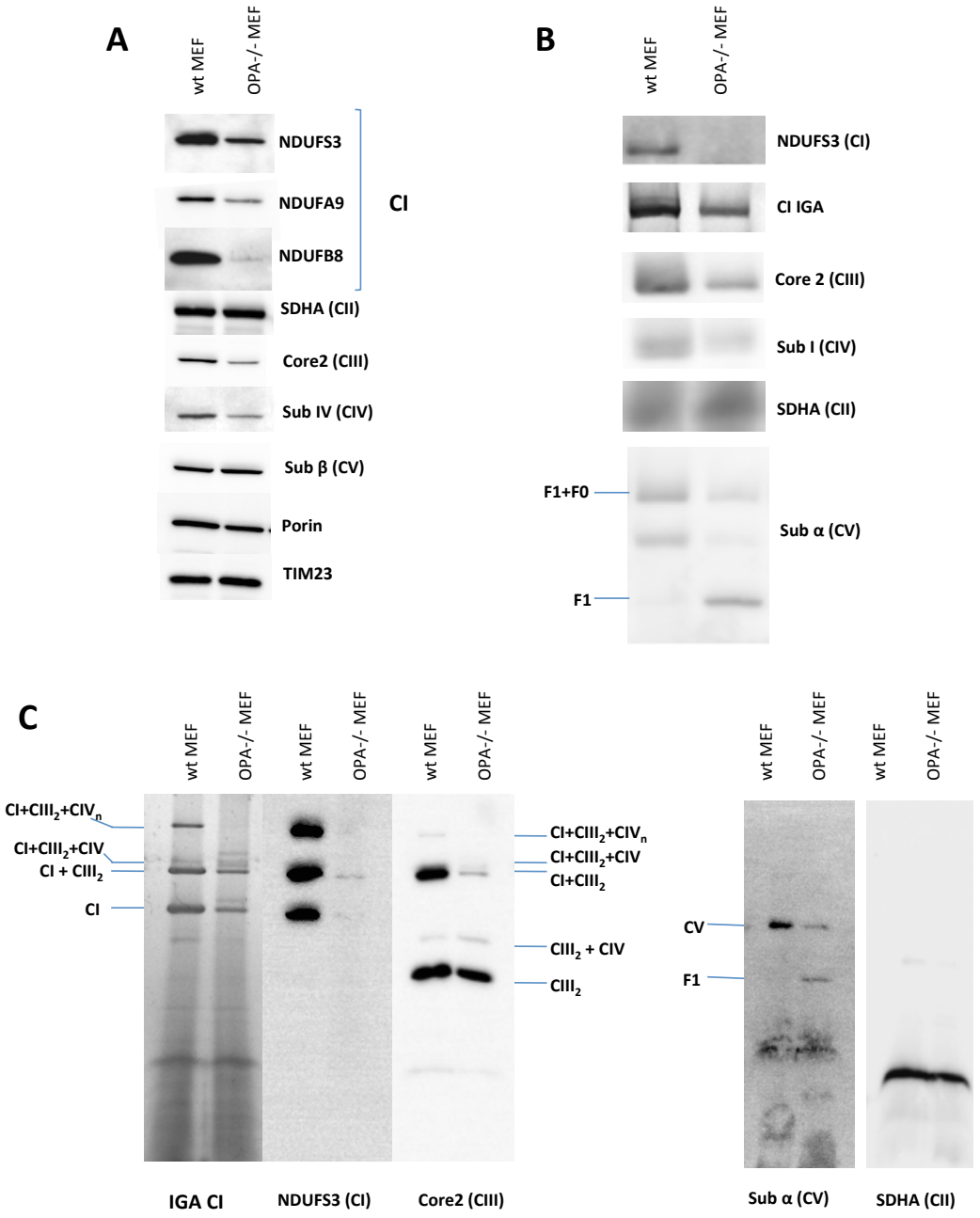

Figure 13. OXPHOS complexes assembly and supercomplexes organization in OPA1-/- MEF. (A) The expression level of NDUFS3, NDUFA9 and NDUFB8 subunits of CI, SDHA subunit of CII, CORE2 subunit of CIII, subunit IV of CIV, β subunit of CV, porin and TIM23 was determined in mitochondrial fraction from wt and OPA -/- MEFs by SDS-PAGE and western blot. (B) DDM-solubilized mitochondria were separated by CN/BN-PAGE and CI-in-gel activity (IGA) and western blot was performed using antibodies against NDUFA9 (CI), SDHA (CII), Core2 (CIII), sub α (CV). (C) Supra-molecular organization of OXPHOS complexes. Digitonin-solubilized mitochondria were separated by BN-PAGE and analyzed by western blotting. SDHA subunit of CII was used as a loading control. Supercomplexes composition and complex monomers are indicated.

2. Analysis of OPA1 isoforms

In humans OPA1 exists as a mixture of eight isoforms, as summarized in Fig. 14A, and this complexity prevents the assessment of specific function to each individual mRNA splice forms. To dissect the specific role of each isoform on the mitochondrial functions, we took advantage of OPA1 -/- MEFs to generate stable cell lines expressing one of the eight OPA1 isoforms. These cell lines were obtained through retroviral infection of OPA1 -/- MEFs using a puromycin-selectable expression vector (pMSCV-puro). After the selection, the expression of the different isoforms was evaluated by western blot (Fig. 14B). This analysis showed that the expression levels of different isoforms were slightly increased compared with the endogenous amount. Differential RNA splicing and proteolytic processing produces a variety of long (containing a transmembrane domain) and short (without transmembrane domain) forms of OPA1 (Olichon et al., 2002; Song et al., 2007). As reported in Fig. 14B, both short and long forms were present in the cell lines expressing isoforms 1, 2, 4 and 7, whereas the isoforms containing exon 4b (3, 5, 6 and 8) were totally processed and presented only the short forms.

Considering that OPA1 is primarily involved in IMM fusion, we first investigated the mitochondrial morphology of the cells expressing each isoform. Cells were immunostained with TOM20 antibody and representative images of mitochondrial morphology of each cell line were captured by confocal microscope and shown in Fig. 14C. Cells were scored into three categories on the basis of mitochondrial morphology: cells with a filamentous and interconnected network (filamentous), cells with short filamentous mitochondria and balloon-like structures (intermediate) and cells with complete fragmented mitochondria (fragmented). Quantitative analysis confirmed that cells expressing short forms of OPA1 only failed to rescue the morphology, exhibiting a completely fragmented mitochondrial network. Conversely the presence of both long and short OPA1 forms induced a significantly increased tubulation, with approximately 40-60% of cells presenting filamentous/intermediate mitochondrial reticulum (Fig. 14D) (Song et all, 2007). However, the rescue observed in cells expressing these isoforms (1, 2, 4, 7) was incomplete as compared to wt MEFs, exhibiting a much higher percentage of intermediate and filamentous mitochondria. To rule out that the infection process could someway affect mitochondrial morphology, cells infected with the empty vector were analyzed and showed a completely fragmented mitochondria network as in OPA-/- MEFs (Fig. 14C).

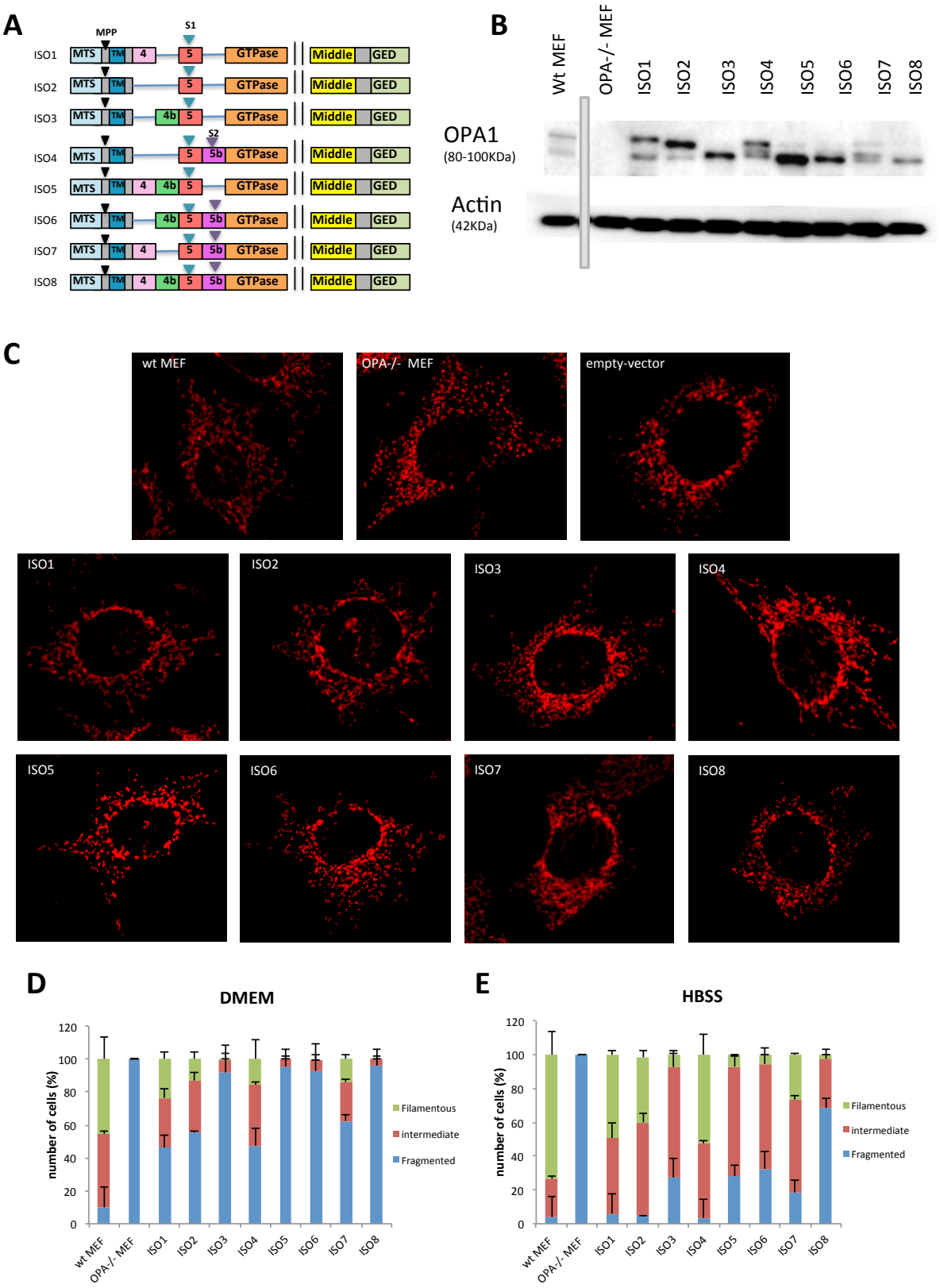

Figure 14. OPA1 expression and mitochondrial morphology of MEFs expressing the eight OPA1 isoforms.

Figure 14. (A) Schematic representation of the OPA1 isoforms showing the mitochondrial targeting sequence (MTS) cleaved by the protease MPP, the additional cleavage sites S1 (localized in the exon 5) and S2 (exon 5b), and the transmembrane domain (TM). (B) The OPA1 mRNA splice forms were expressed in OPA1 null MEFs. Representative western blot of OPA1 expression levels detected with anti-OPA1 antibody. Actin was used as a loading control. (C) Mitochondrial morphology of OPA-/- MEFs expressing each of the isoforms. Cells were immunodetected with an antibody against TOM20. Representative confocal images of mitochondrial morphology are shown. (D) Mitochondrial network was scored according to the criteria detailed in Materials and methods. 100 cells were scored for each cell lines; data are means ± SEM of three independent experiments. (E) Cells were incubated with HBSS medium for 6 hours and then analyzed for mitochondrial network. Quantification was carried out as in D.

It has been previously reported that the lack of OPA1 prevents mitochondrial fusion even in the presence of stimuli activating this process, such as nutrient deprivation (Gomes et al, 2011). Therefore, to further characterize fusion activity of individual isoforms, cells were starved with a saline solution, containing reduced amount of glucose and devoid of amino acids, vitamins and FBS (HBSS medium). After 6 hours incubation in HBSS medium, cells expressing isoforms 1, 2, 4 and 7 increased the percentage of elongated and intermediate mitochondria (Fig. 14E). In addition, after starvation, the percentage of intermediate mitochondria increased also in isoforms expressing only the short form, indicating that under these conditions the mitochondrial network can elongate in the absence of the long forms, clearly suggesting the occurrence of other mechanisms. Again, the rescue obtained in OPA-/- cells expressing the different isoforms was incomplete compared to wt MEF.

Being OPA1 involved in mtDNA replication, distribution and maintenance (Elauchouri, 2010), we investigated the effect of different OPA1 isoforms on the amount of mitochondrial genome, measured by qPCR. As reported in Fig. 15, each of the isoforms almost completely rescued the mtDNA copy number, ranging from 80% to 110%, suggesting that any isoform can restore the mtDNA content.

The severe energetic impairment observed in OPA-/- MEFs is likely to be due to the significant decrease of mtDNA content and the consequent inhibition of mtDNA-encoded proteins synthesis.

Given that the OPA1-/- MEFs stably expressing the eight OPA1 isoforms completely recover the mtDNA content, we decided to evaluate which isoform could be mostly relevant for the bioenergetic competence, without the interference of mtDNA decrease.

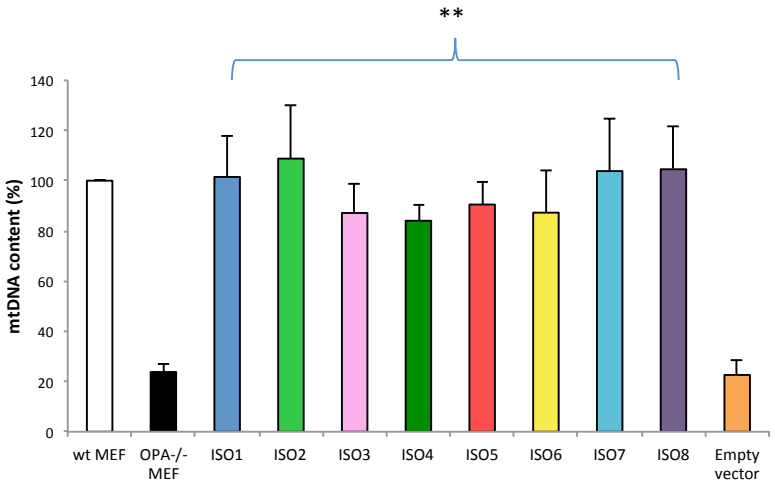

Figure 15. mtDNA maintenance in MEFs expressing the 8 OPA1 isoforms. Relative mtDNA copy number (normalized with the nuclear DNA content) in the different cell lines, as measured by qPCR. Data are expressed as means ± SEM of at least three different experiments. Asterisks denote values significantly different ($P<0.01$).

First, we analyzed the cell viability by using the colorimetric sulforhodamine B assay. Cells expressing the eight OPA1 isoforms grew faster than OPA-/- MEFs in DMEM, although not as fast as wt MEFs (Fig. 16A). In DMEM-galactose, again all the isoforms rescued the growth of OPA1 -/- MEFs, reaching values similar to wt MEFs after 72 hours.

These results suggest that the expression of any isoform can recover the energetic defect of OPA-/- MEFs. To test this hypothesis, we assessed cellular OCR and ATP synthesis rate. The expression of the different isoforms robustly increased mitochondrial respiratory activity, as compared with OPA-/- MEFs (Fig. 16 C-F). In particular, the ratio between maximal respiration and ATP-linked was completely recovered by the expression of OPA1 isoforms (Fig. 16G).

As reported in Fig. 16H, the values of ATP synthesis rate, driven by substrates of CI, II, III or GPD-DH were increased in MEFs expressing the eight isoforms, compared to OPA-/- MEFs, reaching values similar to control cells. The MEFs expressing OPA1 isoforms 2 and 8 seem less efficient in rescuing the energetic impairment, however the large variations in the SEM values make insignificant these differences.

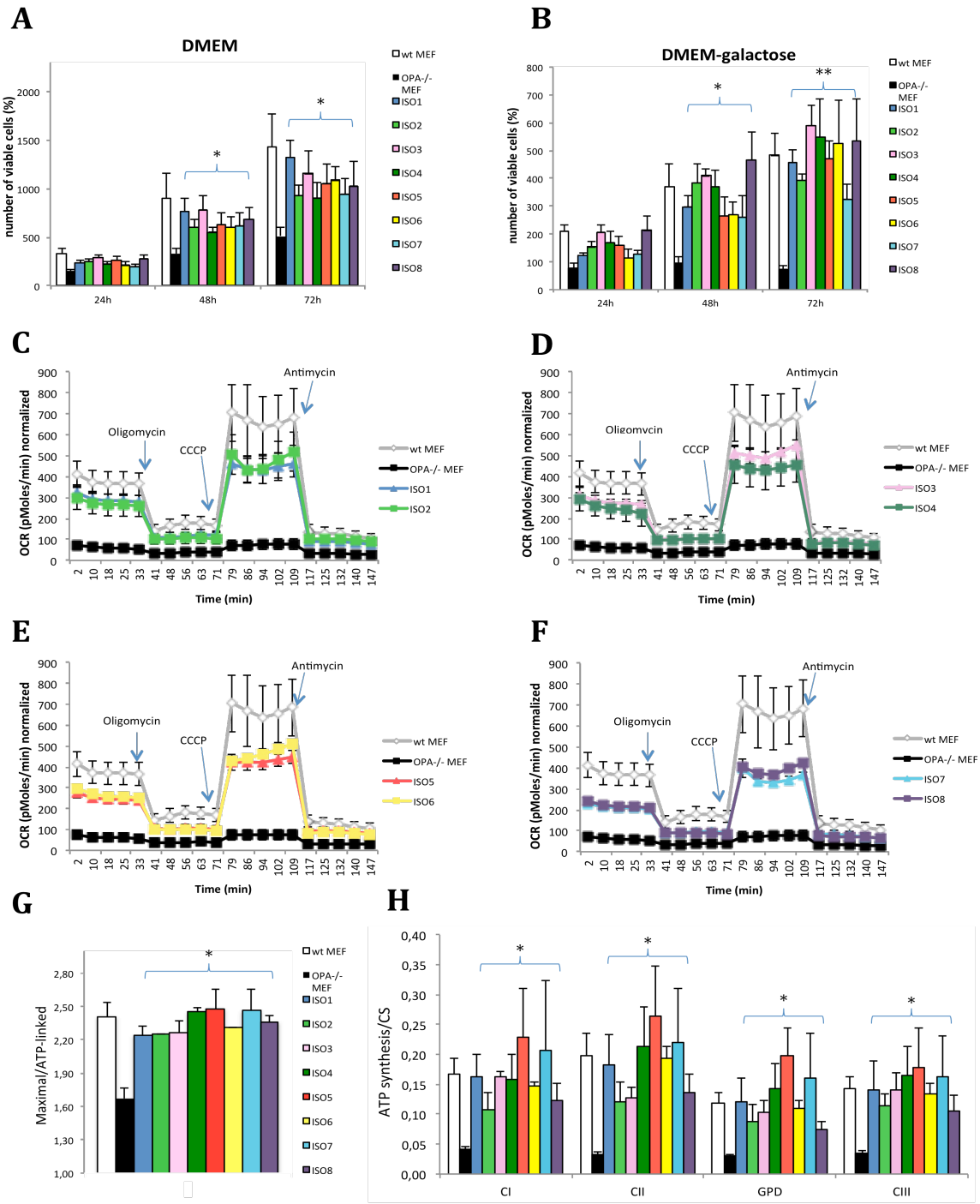

Figure 16. Energetic profile of MEFs expressing the 8 OPA1 isoforms. Viability of different cell lines during incubation in DMEM (A) and DMEM-galactose (B) at the indicated times of incubation. Data are mean ± SEM of three independent experiments. (C-F). OCR profile by Seahorse XF-96 Analyzer of OPA-/- and wt MEFs and MEFs expressing the eight isoforms. Where indicated, oligomycin, CCCP and antimycin A were added. A representative experiment of four similar is shown. Each data point is mean ± standard deviation of 6-8 wells. (G) Data from two experiments have been normalized and expressed as a ratio between maximal respiration and ATP-linked. Data are means ± SEM of two determinations. (H) ATP synthesis rates were determined by luminometric luciferase assay and normalized for CS activity. Data are the means ± SEM of at least three determinations. * denotes P<0.05; ** P<0.01.

Given that both the mtDNA content and the energetic competence were similarly recovered by expression of different isoforms, we investigated whether the assembly of OXPHOS complexes and supercomplexes was also improved. CN-PAGE analysis with DDM-solubilized mitochondria followed by western blotting with the anti-NDUFA9 antibody showed an almost complete recovery of CI content in MEFs expressing the isoforms 1, 2, 3, 4 and 7, whereas a weak increase was apparent in MEFs expressing the isoforms 5, 6 or 8 (Fig. 17A). Although the intensities of bands corresponding to CII, used as loading control, were slightly different, this cannot explain the different amounts of CI observed. The difference in CI band is likely dependent on the difficulty to transfer from gel to PVDF membrane CI for immunodetection. Determination of the CI in-gel activity however revealed that the intensity of bands was similar for all the isoforms to that of wt MEFs. It is also apparent that the amount of CIII was even higher that in wt MEFs. In this blot the band corresponding to CIII could not be detected in OPA-/- MEFs, probably because of the strong signal of CIII in the other lanes. CV was still detected as two bands, however, all isoforms induced its almost complete assembly, evidenced by the stronger intensity of the high molecular weight band, corresponding to CV holo-enzyme, compared with the low weight band present in OPA-/- MEFs.

The supra-molecular organization of respiratory complexes was also evaluated, showing significant changes (Fig. 17B). Band intensities immunodetected by anti-NDUFA9 corresponding to the CI and $I+III_2$ were markedly higher in all the cells expressing the eight isoforms compared to OPA-/-MEF. We also noticed supercomplexes at higher molecular weight (likely $CI+III_2+IV_n$) except for isoforms 2 and 7, where the amount of CII however seems slightly reduced. This is confirmed by the results of the CI-in-gel activity, where the intensity of different bands was similar in MEFs expressing any isoform. The amount of dimeric CIII and supercomplex III_2+IV, were both restored after reintroduction of the eight OPA1 isoforms. Blotting with subunit α antibody confirmed the correct assembly of CV. In summary, these results suggest that the presence of any of the eight isoforms increases the amount of both respiratory complexes and supercomplexes to levels similar or even higher than wt MEFs.

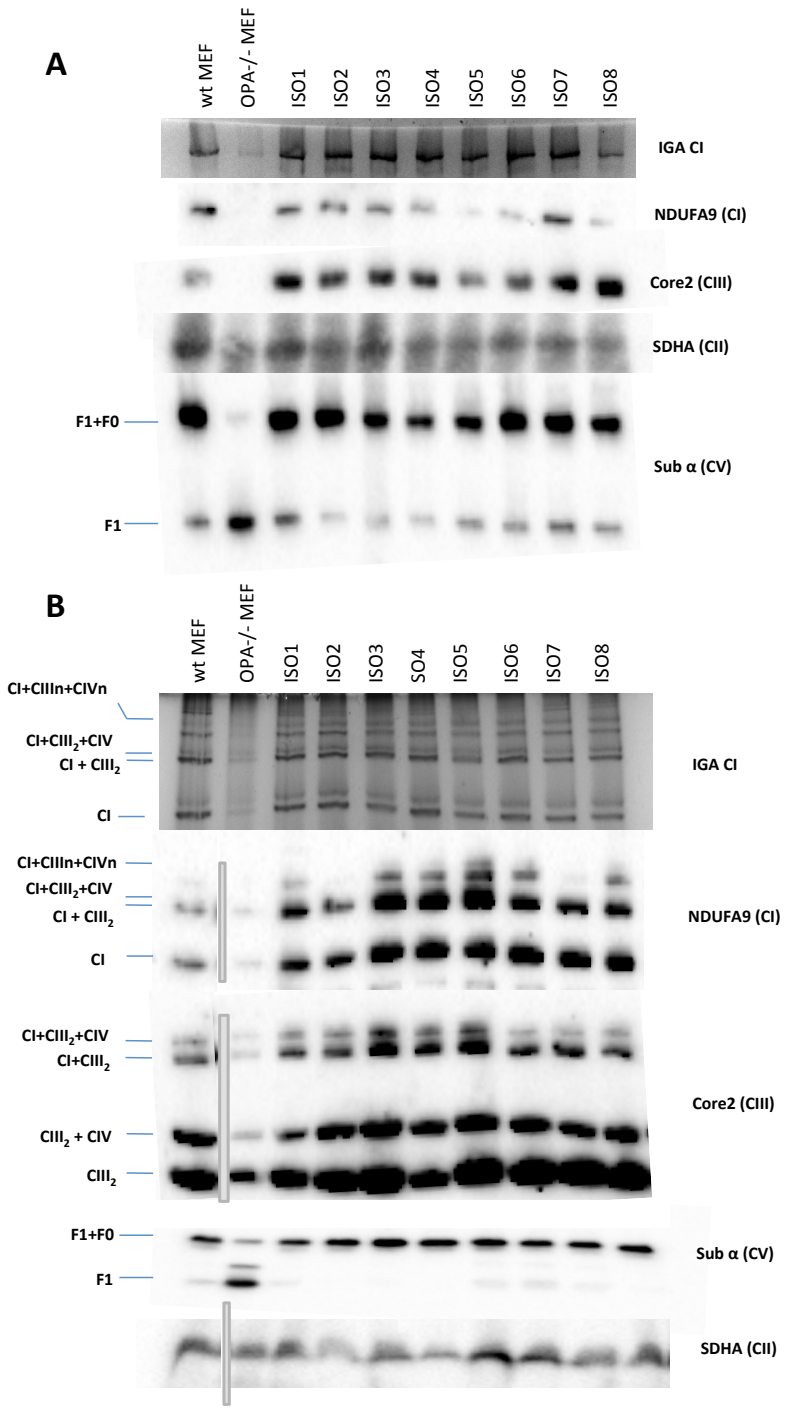

Figure 17. OXPHOS complexes and respiratory supercomplexes in MEFs expressing the OPA1 isoforms. After CN/BN-PAGE of DDM (A) or digitonin-solubilized mitochondria (B), the CI in-gel activity (IGA) was measured. Western blot analysis was carried out using antibodies against NDUFA9 (CI), SDHA (CII), Core2 (CIII), sub α (CV). CII was used as a loading control. In (B) supercomplex composition is indicated on the left. A representative experiment of three similar is shown.

Recently Cogliati et al., 2013, provided experimental evidence of a direct link between OPA1, IMM organization and respiratory supercomplexes arrangement, showing that intact *cristae* shape is essential for supercomplexes assembly and stability, respiratory efficiency and cell growth. To assess if the recovery of supercomplexes assembly is associated with mitochondrial ultrastructure, cells were fixed and processed for electron microscopy (EM). The images captured from the same cell sample, showed mitochondria with quite different *cristae* structures. To quantify the changes in mitochondrial ultrastructure, we decided to score mitochondria into three categories: more than 5 *cristae* and dense matrix (class I), between 2 and 5 *cristae* with variable density of the matrix (class II), less than 2 *cristae* and swollen mitochondria (class III). Representative EM images of each cell line are shown in Fig. 18A. As already reported (Song et al., 2009), OPA1-/- cells exhibited severe ultrastructural defects, including swollen mitochondria and reduced *cristae* number, and quantification resulted in the presence of approximately 50% of class II and III mitochondria (Fig. 18B). Conversely, in wt MEFs more than 80% of mitochondria belonged to class I. Interestingly, we observed a marked increase of class I mitochondria, ranging between approximately from 20 to 40% of organelles analyzed in MEFs expressing the eight OPA1 isoforms. However, the percentage of class III mitochondria was always relevant (25-50%), suggesting that the expression of one isoform alone, although able to fully recover the supercomplexes organization, cannot completely rescue the organelle ultrastructure.

To more clearly define the relationship between OPA1, *cristae* structure and supercomplexes organization, we performed some experiments by using different tissues obtained from the OPA1 mouse strain carrying the most frequent mutation associated with DOA patients, the c.2708_2711delTTAG deletion in exon 27, as well as fibroblasts derived from DOA patients bearing the same mutation.

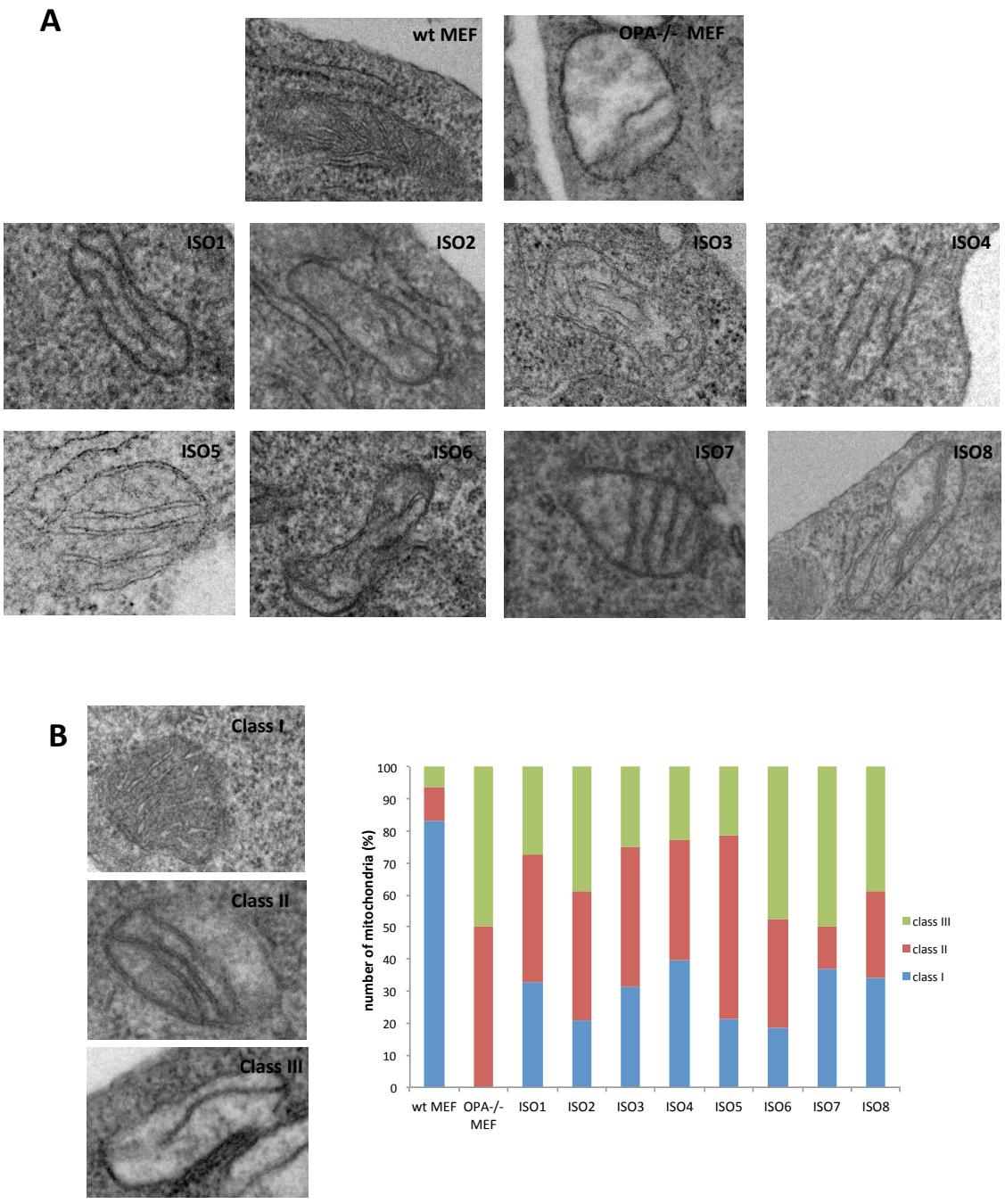

Figure 18. Mitochondrial ultrastructural analysis of MEFs expressing the eight OPA1 isoforms. (A) Representative EM images of mitochondria of MEFs expressing the eight isoforms. (B) Cells were scored according to *cristae* content (see Materials and methods) into three classes: representative images of mitochondria belonging to class I, II and III, respectively are shown, 40-60 mitochondria per sample were analyzed.

Mitochondria were isolated from brain, heart and glycolytic muscles of both control (OPA1+/+) and Opa1^{delTTAG} mutated (OPA1+/-) mouse. The expression level of OPA1 protein was reduced of approximately 25% in brain and glycolytic fibers and of 50% in heart of OPA1+/- mouse (Fig. 19A), as previously reported (Sarzi et al., 2012). According to these authors, in glycolytic fibers mitochondria appeared swollen, with vacuolated shape, loss of *cristae* organization; the cardiac muscle of Opa1+/- mice also displayed evidences of structural anomalies (Sarzi et al., 2012). Although the reduced level of OPA1 protein and altered ultrastructure, the organization of respiratory supercomplexes did not reveal changes in their amount or assembly in heart and glycolytic muscles. The bands in brain were very faint, likely because the amount of mitochondria in the extracts is low, being heavily contaminated by intact synaptosomes (Fig. 19B).

Figure 19C illustrates the results obtained in skin fibroblasts derived from a patient bearing the very same c.2708_2711delTTAG microdeletion. The fibroblasts were previously shown to exhibit a remarkable decrease (50%) in the number and organization of *cristae* under basal conditions (DMEM) and an even more severe *cristae* ultrastructure destabilization was observed after incubation in DMEM-galactose (Zanna et al., 2008). The CI in-gel-activity after BN-PAGE unveiled the presence in mutant cells of three bands, one corresponding to supercomplex CI+III_2+IV, present also in control fibroblasts, the second very close, corresponding to supercomplexes CI+III_2, absent in controls, and the third at very high molecular weights, corresponding to CI+III_n+IV_n, barely detectable in controls. This pattern was not changed by incubation in DMEM-galactose (Fig. 19C). This result needs to be confirmed by further analysis in other fibroblast cell lines bearing the same and different OPA1 mutations, however it suggests that, although a certain reshuffle in supercomplexes might occur, no dramatic change in their content nor supramolecular organization is apparent. Therefore, these data do not seem to support the strict link between *cristae* ultrastructure and supercomplexes organization.

To conclude, the exhaustive analysis of the biochemical features of MEFs expressing each of the eight OPA1 isoforms allows us to disclose that each isoform is able to completely recover the mtDNA content but can only incompletely rescue the energetic profile and *cristae* ultrastructure. Furthermore, our data also confirm that only the presence of both long and short forms can re-establish the mitochondrial morphology.

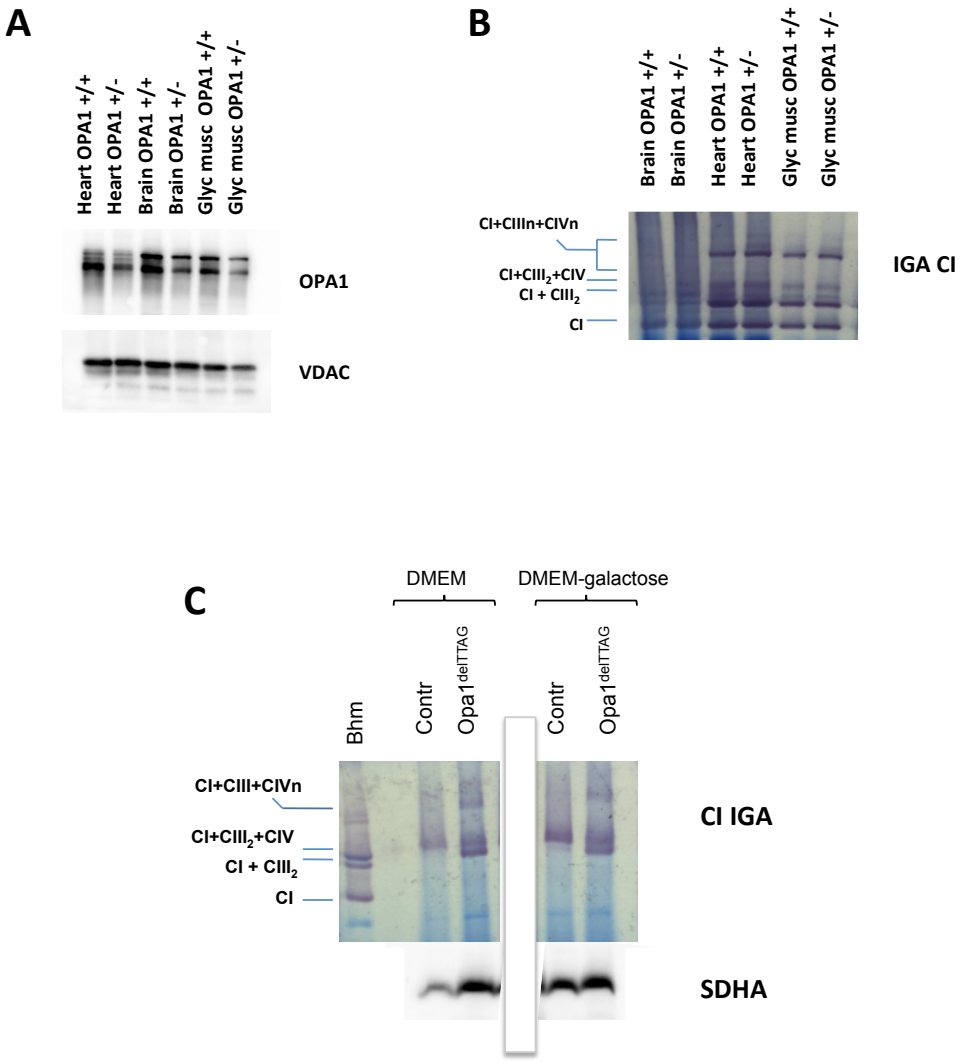

Figure 19. Supercomplexes assembly in Opa1^{delTTAG} mutant mouse tissues and patients' fibroblasts. (A) Western blot analysis of OPA1 expression in Opa1+/- versus Opa1+/+ mice tissues. VDAC was used as a loading control. (B) Supercomplexes analysis by BN-PAGE. CI in-gel activity (IGA) and western blot of CV using antibody against α subunit. Supercomplex composition and complex monomers are indicated on the right. (C) Control and Opa1^{delTTAG} fibroblasts were incubated in DMEM or DMEM-galactose. After BN-PAGE, CI IGA was determined. Bovine heart mitochondria (BHM) were run as a marker; CII (SDHA subunit) was used as a loading control.

3. OPA1 domains

The results described above lead us to conclude rather surprisingly that there is no established specific function associated with each of the eight OPA1 forms, except for the fusion process that has previously shown to require the presence of both long and short forms and has been associated with isoforms 1, 2, 4, 7 (Song et al. 2007). Thus, we thought to investigate the role of specific domains of OPA1 protein and whether the balance of short and long forms has any implication in mitochondrial functions.

To this purpose, we generated cell lines expressing variant polypeptides of OPA1. As reported in Fig. 20A, an isoform 1 construct in which the S1 site in exon 5 was removed by deletion of 10 residues surrounding alanine 195 (ΔS1 mutation) was constructed, to abolish the short form. In fact, isoform 1 lacking this cleavage site did not undergo the proteolytic processing, resulting in expression of the long form (ISO1 Long) only. Another construct encoded the OPA1 isoform 1 bearing the G300E mutation in the GTPase domain, which is associated with classical DOA, to investigate the role of GTPase activity on mitochondrial functions. The third construct was generated by using the cDNA in which residues 1–229 of OPA1 variant 1 were replaced by the MTS-targeting signal of apoptosis-inducing factor (AIF) (Ishihara, 2006), a mitochondrial intermembrane flavoprotein that translocates to the nucleus in response to proapoptotic stimuli (AIF-230). Because AIF has a membrane-anchoring domain (TM) similar to OPA1, we believe that this polypeptide is similar to the ISO1 Long. Our group previously reported that OPA1 isoforms containing the exon 4b, that are completely processed in short forms, are important for mtDNA maintenance (Elauchouri et al., 2010), probably by anchoring the mtDNA associated within nucleoids to the IMM through the N-terminus. The AIF-230 construct, having the N-terminus of another protein, allows us to test the role of this portion in mtDNA content and other mitochondrial functions (Ishihara, 2006; Otera, 2005). Lastly, we generated two constructs with the N-terminus of OPA1 only, starting from exon 1 to exon 4 (OPA1-ex4) or from exon 1 to exon 4b (OPA1-ex4b), respectively, both fused with a mCherry protein. All these constructs were introduced into OPA-/- MEFs by retroviral infection, as previously described.

As expected, western blotting confirmed that ISO1 Long produced only the long form whereas G300E produced two bands (long and short forms) (Fig. 20B). AIF-230 presented only one band, confirming that the protein did not undergo proteolytic cleavage. The mobility of this band was

similar to the short isoforms, as expected from the predicted molecular weight, but, considering its structure, it has to remembered that AIF-230 is a OPA1 variant inserted in the IMM without its own N-terminus, cleaved by MPP during mitochondrial import.

We first analyzed the morphology of the mitochondrial reticulum in cells incubated in DMEM. As reported in Fig. 20C, the expression of all these variants markedly increased the network fragmentation in comparison to isoform 1. Quantification on the basis of the type of mitochondrial network, as previously described, is reported in Fig. 20D. Cells were then starved with HBSS and mitochondrial morphology analyzed. Figure 20E shows that under these conditions the percentage of filamentous /intermediate mitochondria network was similar in MEFs expressing isoform 1, ISO1 Long and slightly reduced in AIF-230. Conversely G300E-expressing cells exhibited a completely fragmented network similar to OPA-/- MEFs, clearly indicating that the functional GTPase domain is essential for recovery of mitochondrial morphology. Being the GTPase activity required for the fusion process, the morphology of cells expressing OPA1-ex4 and OPA1-ex4b, lacking the entire GTPase domain, was not analyzed.

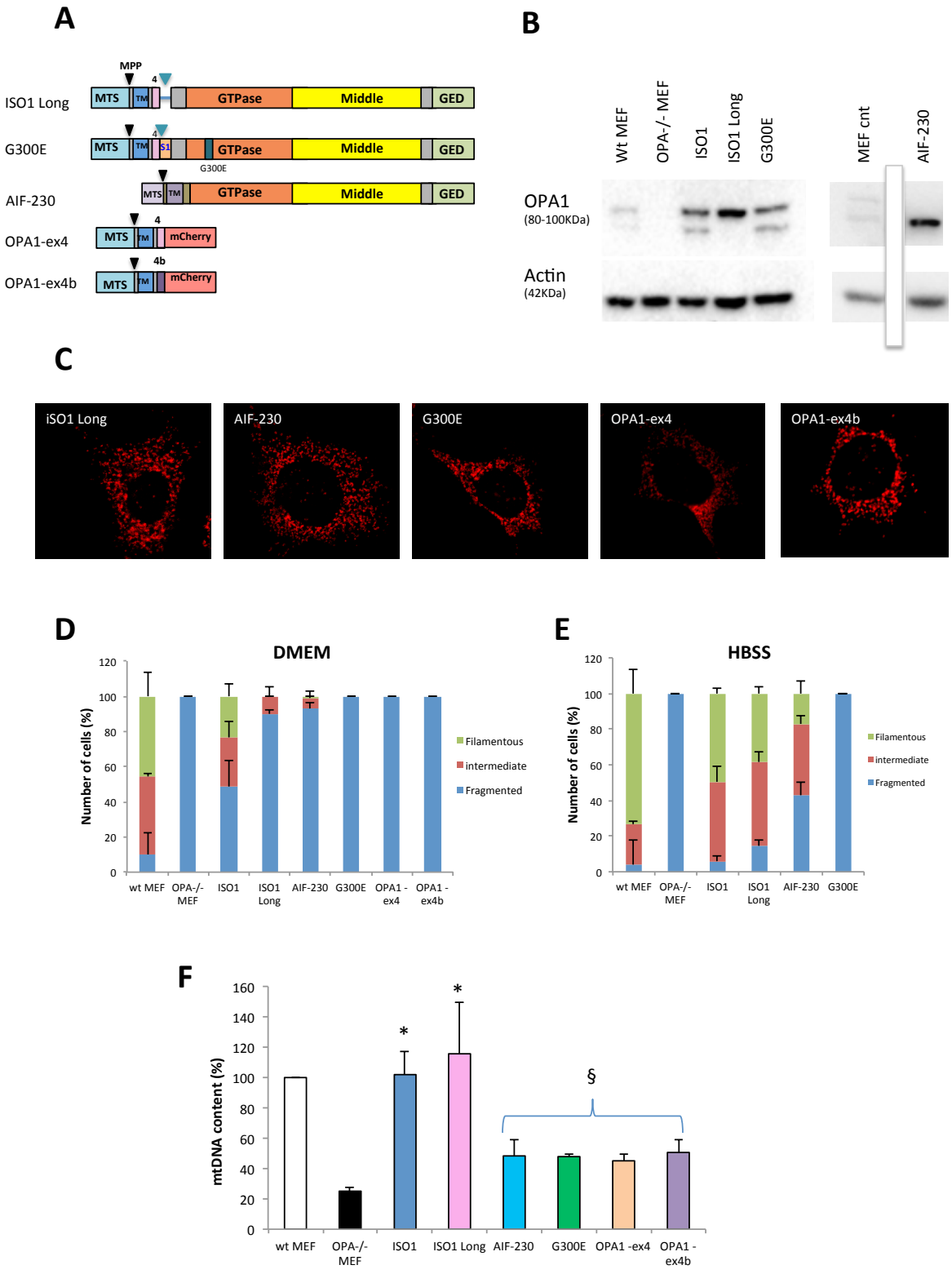

Figure 20. Mitochondrial morphology and mtDNA content of MEFs expressing the different variants of OPA1.

Figure 20. (A) Schematic representation of the OPA1 constructs; their processing sites (MTS and S1, respectively) are indicated by black and blue arrowheads. (B) Representative western blot of OPA1 variants expression detected with anti-OPA1 antibody. Actin was used as a loading control. (C) Mitochondrial morphology of MEFs expressing the different variants. Cells were labeled with anti-TOM20 antibody. Representative confocal images of mitochondrial morphology are shown. (D) Mitochondrial network was scored as detailed in Materials and methods. 100 cells were scored for each cell lines; error bars indicate SEM of three independent experiments. (E) Cells were starved with HBSS for 6 h and then mitochondrial network was analyzed. Quantification was carried out as in D. (F) Relative mtDNA copy number in the different cell lines, as measured by qPCR. Data are expressed as means ± SEM of at least three independent experiments. * denotes values significantly different from the OPA-/- MEF ($P<0.05$); § denotes values significantly different from wt MEF ($P<0.05$).

Next, we analyzed the mitochondrial genome content. Interestingly, the presence of the ISO1 Long completely recovered the mtDNA copy number, whereas all the other variants induced only a slight increase (Fig. 20F). These results suggest that the mtDNA content depends on the presence of functional N- and C-terminus of OPA1 rather than correct equilibrium between long and short forms.

The viability and the OCR profile of different MEF lines were then determined. During incubation in DMEM or DMEM-galactose, the growth of cells expressing ISO1 Long was similar to the isoform 1, whereas that of AIF-230 was lower and that of G300E was very low, similar to the OPA-/- cells (Fig. 21A and B). In agreement, cells expressing the G300E mutant protein failed to increase the OCR, similarly to OPA-/- MEFs (Fig. 21C and D). The respiration of ISO1 Long and AIF-230 expressing cells was improved, showing a significant increase in the OCR reserve capacity compared with OPA-/- MEFs. Therefore, although these two cell lines have different mtDNA content, their energetic efficiency is similar.

The amount and assembly of OXPHOS complexes and supercomplexes was then evaluated. As shown in Fig. 22A, expression of either ISO1 Long or AIF-230 could partially recover CI, CIII, supercomplexes I+III_2 and III_2+IV, although the higher molecular weight bands corresponding to CI+III_2+IV_n supercomplex were hardly detectable. The CI in-gel activity exhibited a similar behavior. The assembly of CV was almost completely recovered in the ISO1 Long cell line, whereas only partially in cells expressing AIF-230. Interestingly, the introduction of the G300E mutated isoform 1 was unable to recover the defective phenotype of OPA1-/- MEF, both at the level of supercomplexes and of CV, indicating that the GTPase activity is essential for the maintenance of OXPHOS complexes and supercomplexes integrity.

The mitochondrial ultrastructure of cells expressing these three variants were also analyzed by electron microscopy and some representative images are shown in Fig. 22B. The *cristae* structure of the G300E mutant was similar to OPA1-/- MEF, whereas the presence of ISO1 long form or AIF-230 induced an marked increase of class I mitochondria, although lower than in presence of isoform 1, and a significant percentage also of class II and III mitochondria (Fig. 22C).

All together these data suggest that, in addition to the obvious importance of a functional GTPase domain, the presence of a proper N-terminal portion and of a cleavage site generating short forms seems to be essential to completely recover the energetic function, both in term of OCR and OXPHOS complexes/supercomplexes organization.

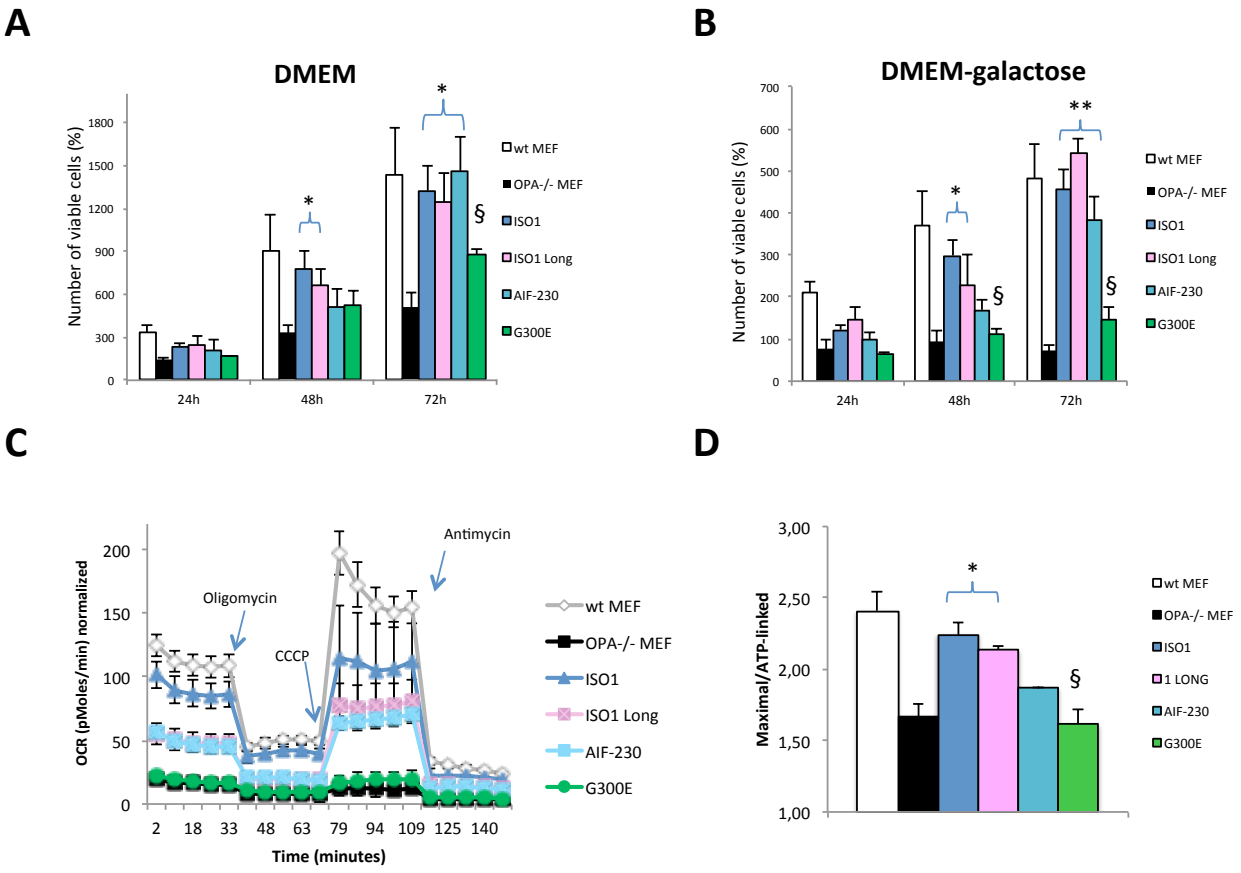

Figure 21. Energetic profile of MEFs expressing the different OPA1 variants. Viability of different cell lines during incubation in DMEM (A) and DMEM-galactose (B). Data are expressed as mean ± SEM of at least three indipendent experiments. *denotes values significantly different from the OPA-/- MEF ($P<0.05$); § denotes values significantly different from the wt MEF ($P<0.05$). (C) OCR profile by Seahorse XF-96 analyzer. In graphic is reported OCR of one measurement, representative of two experiments. A representative experiment of four similar is shown. Each data point is mean ± standard deviation of 6-8 wells. (D). Data from two experiments have been normalized and expressed as a ratio between maximal respiration and ATP-linked. Data are means ± SEM of two determinations.

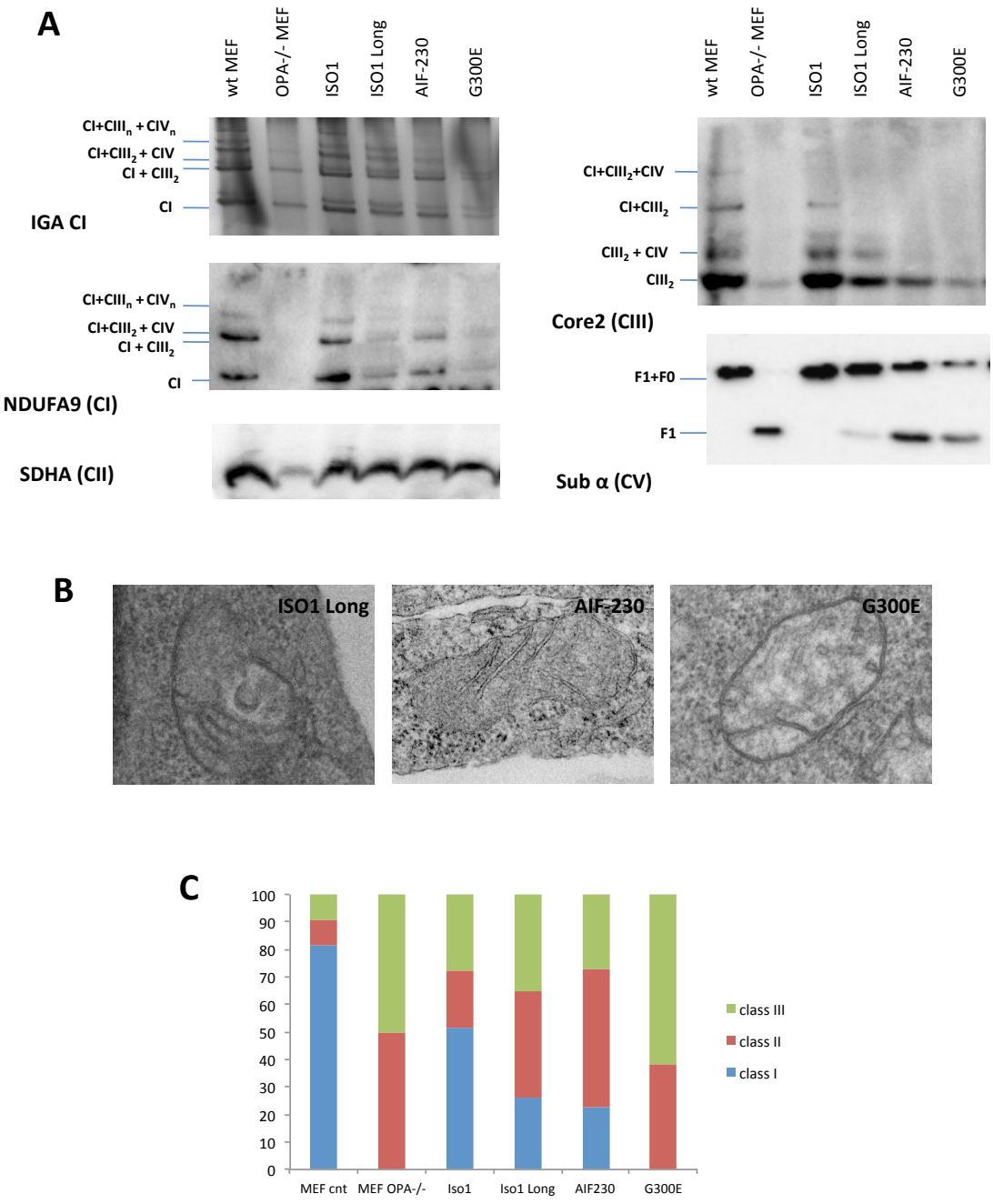

Figure 22. OXPHOS complexes, supercomplexes and mitochondrial ultrastructure of MEFs expressing the different OPA1 variants. (A) BN-PAGE, CI in-gel-activity (IGA) and western blot of the indicated respiratory supercomplexes. SDHA subunit of complex II was used as a loading control. (B) Representative EM images of mitochondria of the MEFs cell lines are shown. (C) Mitochondrial ultrastructure was scored according to the criteria detailed in Materials and methods. Approximately 40-60 mitochondria per sample were analyzed.

4. OPA1 mutations

The results obtained in cells expressing the *OPA1* G300E mutation suggest that the GTPase activity of OPA1 is essential for the mitochondrial functions. These observations prompted us to analyze other pathogenic mutations localized in the same GTPase domain, together with mutations present in other OPA1 domains, to evaluate their biochemical phenotype.

Accordingly, we expressed in OPA-/- MEFs the OPA1 isoform 1 bearing different mutations, selected on the basis of their clinical phenotypes, ranging from very mild associated with pure optic atrophy to more severe causing severe syndromic forms. In particular, those associated with classical DOA are A166V, I382M, D603H, Q785R, while the R290Q, G439V, R445H, S545R are associated with the multisystemic syndrome named DOA-plus (Fig. 23A), which includes mitochondrial myopathy with mtDNA deletions in addition to the classical optic atrophy (Amati-Bonneau et al., 2008).

The protein expression of each mutant was determined by western blot, showing a normal pattern of OPA1 long and short forms (Fig. 23B). Fig. 23C illustrated representative images of the mitochondrial morphology of these cells. The expression of A166V, D603H, Q785R and I382M reduced the percentage of tubular and intermediate mitochondria compared to wt isoform 1. Conversely, the other four mutations caused the complete fragmentation of the mitochondrial network in DMEM and even after incubation with HBSS (Fig. 23D, E). It is noteworthy that, except S554R, all these mutations with a phenotype similar to OPA-/- MEF are localized within the GTPase domain, similarly to the G300E.The measurement of mtDNA copy number revealed a large variability in the genome copy number (Fig. 24A). The G439V and R445H mutations only presented a very low mtDNA content, similar to OPA1-/- MEFs. In cells bearing the other mutations the mtDNA copy number was quite different, ranging from 50 (G300E) to 130% (A166V). A preliminary analysis of the energetic competence has been carried out (Fig. 24B). G439V and R445H mutations in the GTPase domain presented a rather severe phenotype, with OCR values similar to OPA1-/- MEFs. Mutations S545R, R290Q and Q785R showed a cellular respiratory capacity close to MEFs expressing wt isoform 1. Finally, mutations A166V, I382M and D603H had an OCR profile equivalent to wt MEFs. Additional experiments are necessary to confirm these results.

In summary, mutations within the GTPase domain seem to affect the OPA1 function more critically than those in the other protein domains, although with different degree of severity, reflecting the clinical phenotypes of the patients. The I382M mutation, even if localized in the GTPase domain, doesn't compromise the cellular mitochondrial functions, in agreement with the really mild phenotype observed in the patient.

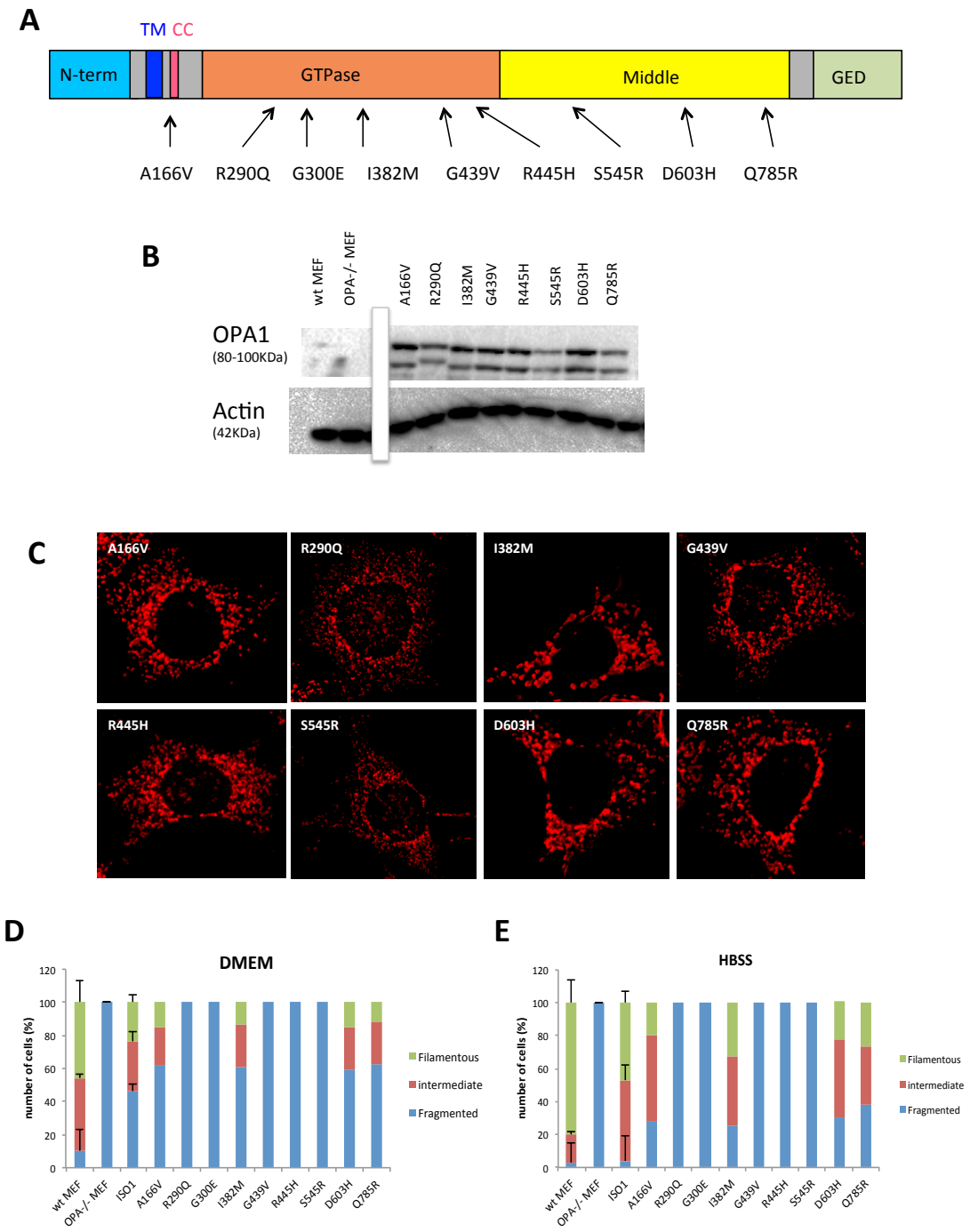

Figure 23. OPA1 expression and mitochondrial morphology of MEFs expressing different OPA1 mutations. (A) Schematic representation of OPA1 and localization of the mutations, indicated by arrows. (B) Mutations were inserted in isoforms 1 and expressed in OPA1 -/- MEFs; OPA1 expression level was detected by western blot. Actin was used as a loading control. (C) Mitochondrial morphology of MEF expressing the eight mutated isoforms 1. Cells were labeled with anti-TOM20 antibody. Representative confocal images of mitochondrial morphology are shown. (D) Mitochondrial network was scored according to the criteria detailed in Materials and methods. 100 cells were scored for each cell lines. (E) Cells were incubated with HBSS medium for 6h and then analyzed for mitochondrial network morphology. Quantification was carried out as in D.

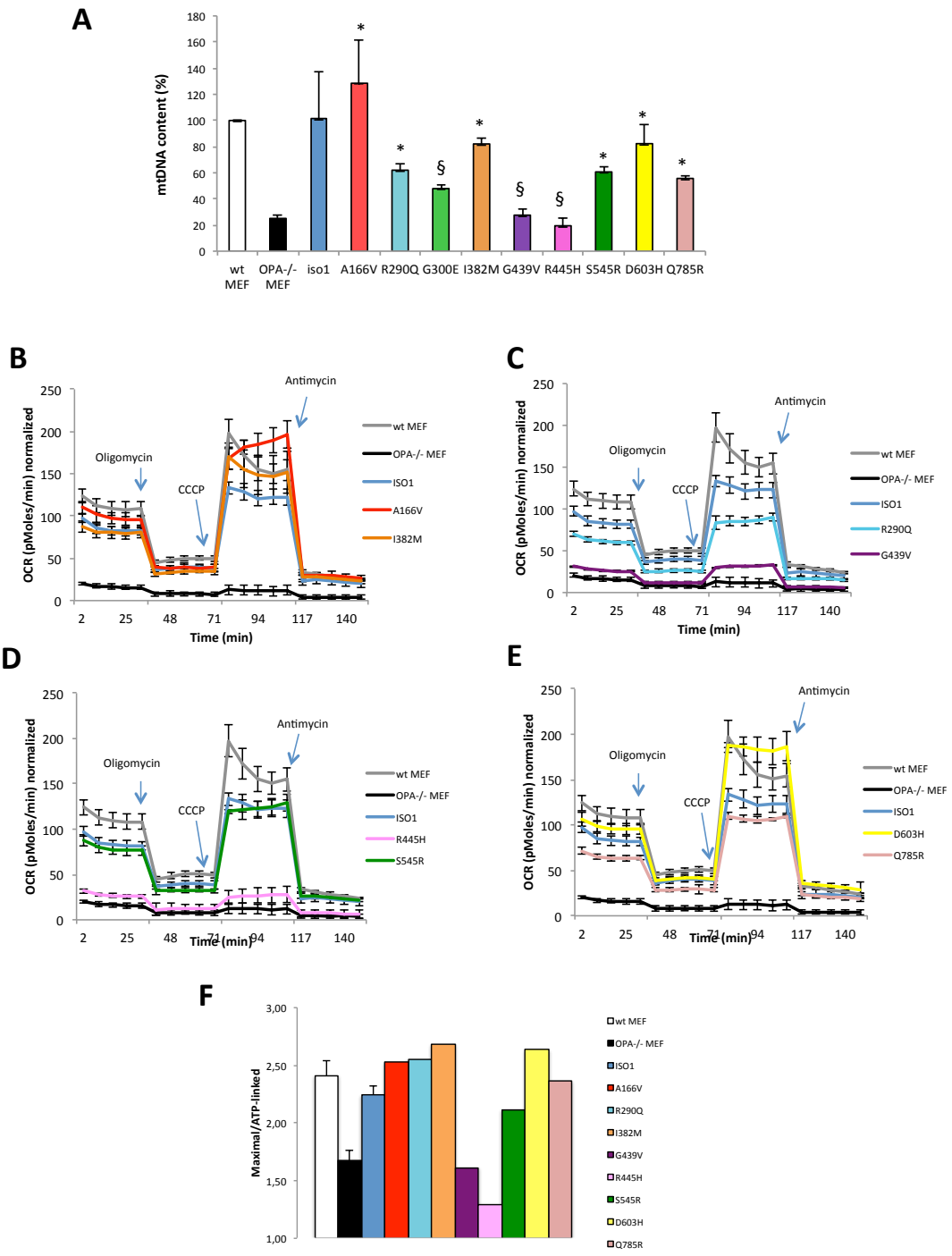

Figure 24. mtDNA content and energetic profile of MEFs expressing the nine OPA1 mutations. (A) Relative mtDNA copy number in each cell line measured by qPCR. Data are expressed as mean ± SEM of at least three experiments. * denotes values significantly different from the OPA-/- MEF ($P<0.05$); § denotes values significantly different from the wt MEF ($P<0.05$). (B-E) OCR profile comparing OPA-/-, wt and isoforms 1 MEFs with cells expressing the different mutants. The experiment was performed only one time. Each data point is mean ± standard deviation of 6-8 wells. (D) Ratio between maximal respiration and ATP-linked from data reported in Fig. B-E.

DISCUSSION AND CONCLUSIONS

A growing body of evidence associates OPA1 protein to several mitochondrial functions, such as morphology, OXPHOS efficiency, mtDNA content and *cristae* shape maintenance (Belenguer and Pellegrini, 2013). In this study we confirm that the lack of this GTPase severely impaired all the above described functions. Furthermore, through a detailed biochemical analysis we show that the presence of any of the eight isoforms can rescue the majority of the mitochondrial dysfunctions, with variable degree of efficiency. In addition, by generating specific OPA1 variants, we have been able to assign a specific role to some protein domains. Finally, we have evaluated the impact of different pathogenic OPA1 mutation associated with DOA on the cellular phenotype.

The complex molecular heterogeneity of OPA1 protein, due to the existence of eight isoforms undergoing proteolytic processing, makes it difficult to establish the specific function(s) to each individual mRNA splice form. Having characterized in detail the biochemical dysfunctions of OPA1 -/- MEFs, we used these cells as a model system to selectively express each individual isoform in order to reveal their ability to recover specific mitochondrial functions.

In agreement with previous reports (Song et al., 2007), only expression of the four isoforms (1, 2, 4, 7) generating one l-form in addition to one or more s-forms, induced a significant elongation of the mitochondrial network confirming the hypothesis that, under physiological conditions, a mixture of both s- and l-forms is required to preserve a proper morphology. Notably, it was previously shown that s-form can assemble on liposomes containing negatively-charged phospholipids and, although it could tubulate membranes, it was unable to cause membrane fusion (Ban et al., 2010). The finding that mitochondrial network morphology was only partially rescued in comparison with wt MEFs is difficult to explain. One possible reason is that at least two or even more isoforms must be simultaneously present for complete recovery of the morphology. During nutrient starvation, expression of isoforms 1, 2, 4, 7, generating both l- and s- forms, further increased the percentage of filamentous mitochondria, but also cells expressing only s-forms (isoforms 3, 5, 6, 8) increased the percentage of the mitochondria with intermediate network. Under these stress conditions, the fission process is inhibited and fusion, becoming an unopposed event, induces elongation, but in cells completely lacking the pro-fusion proteins, this effect cannot occur (Gomes et al., 2011). These results suggest that, under these stress conditions, all isoforms are able to sustain some fusion activity.

The role of OPA1 in mitochondrial genome maintenance has been evidenced from analysis of muscle biopsies of patients (Amati-Bonneau et al., 2008; Hudson et al., 2008) and from studies carried out in cellular systems (Elachouri et al., 2011). Interestingly, here we demonstrate that the expression of each of the eight isoforms could fully recover the mtDNA content. Therefore, the mtDNA maintenance is not strictly linked to recovery of network morphology, in contrast with the close association reported previously by others (Chen et al., 2010; Pattern et al., 2014). This result is quite unexpected because it shows that mtDNA recovery can occur also in the absence of fusion activity.

That reduced amount of OPA1 induces an energetic impairment has been previously documented in fibroblasts, lymphoblasts and skeletal muscles from DOA patients (Zanna et al., 2008; Agier et al., 2012; Van Bergen et al., 2011; Lodi et al, 2011). As expected, OPA1-/- MEFs, completely devoid of this protein, exhibited a severe energetic impairment. The expression of each isoform completely recovered all these dysfunctions, i.e. growth capability, the mitochondrial ATP synthesis rate and the mitochondrial respiration. Furthermore, the reduced OXPHOS complexes amount and supercomplexes assembly were restored. This set of experiments clearly indicates that all the isoforms, individually expressed, can recover the energetic impairment due to the lack of OPA1.

OPA1-null cells also present severe defects in the mitochondrial ultrastructure and recently a direct link between *cristae* structure and respiratory chain supercomplexes assembly has been suggested (Song et al., 2009; Cogliati et al., 2013). When the ultra-structural analysis of MEFs expressing the eight isoforms, which completely recovered the supercomplexes assembly, was carried out, it was apparent that rescue was only partial, given that mitochondria with reduced number of *cristae* and altered matrix density were still present. This is in agreement with data reported in mouse tissues (Sarzi et al., 2012) and DOA patients' fibroblasts (Zanna et al., 2008) bearing the same c.2708_2711delTTAG OPA1 mutation and presenting mitochondrial ultrastructural defects, where no significant alterations of supercomplexes containing CI were apparent. In both cases, the *cristae* shape was one of the most affected features associated with reduced amount of OPA1 protein. Similarly, in MEF-derived cell lines, none of the isoforms was able to completely rescue the mitochondrial ultrastructure. It can be concluded that the small changes of OPA1 protein level or of isoforms profile primarily influence the mitochondrial ultrastructure, whereas only a very drastic reduction of OPA1 is required to weaken the interactions underlying supercomplexes

organization. Notably, in the mouse tissues and patients' fibroblasts, the mutation c.2708_2711delTTAG, although not affecting supercomplexes pattern, caused a reduction of CIV activity (Sarzi et al., 2012) and ATP synthesis driven by CI (Zanna et al., 2008), suggesting that partial reduction of OPA1 protein can impact the energetic efficiency without influencing the supercomplexes assembly.

It has also to be noticed that no significant difference was apparent among OPA1 isoforms in the ability to rescue the energetic efficiency, mtDNA content and *cristae* integrity, again indicating that these effects occur either in the presence or absence of membrane fusion activity.

This detailed study does not allow us to assign a specific mitochondrial function to the eight OPA1 isoforms, with the exception of the mitochondrial fusion. However our results identified isoform 1 as one of the most efficient in recovering the phenotype of OPA-/- MEF. Moreover, it has to be taken into consideration that isoform 1 is one of the most highly expressed isoforms in human tissues, together with isoform 5, 7 and 8, and the most expressed in HeLa cells (Olichon et al 2007; Delettre et al., 2000). It follows that isoform 1 is the best candidate for the study of the function of specific domains of OPA1 protein. Furthermore, we propose also its use, in the next future, for development of a gene therapy strategy for DOA based on viral transduction.

Being all isoforms effective in restoring more or less the mitochondrial phenotype of OPA1-/- cells, it was important to shed light on the role of specific protein domains, by analyzing ad hoc generated peptides. Expression of ISO1 Long, in which the S1 cleavage has been deleted, of AIF-OPA1 variant, in which the 1-229 residues of OPA1 were replaced by the N-terminus of AIF, and of isoform 1 with an inactive GTPase domain failed to recover the mitochondrial morphology in OPA-/-MEFs, in agreement with previously reports (Song et al., 2007; Olichon et al., 2007; Ban et al., 2010), further suggesting that a balance between short and long forms and an active GTPase activity are required (Fig. 25A). The need of a cleavable l-form to promote IM fusion event was also observed in *in vitro* studies of OXPHOS induced-fusion (Mishra et al., 2014). In disagreement with a previous report showing that expression of different AIF-OPA1 variants increases fragmentation in Oma1-/- Yme1l-/- MEFs (Anand et al., 2014), we demonstrate that the presence of AIF-230 variant did not modify the mitochondrial network in OPA-/- cells, in accord with results obtained in other cell lines (Ishiara et al., 2006; Merkwirth et al., 2008). Furthermore, the mitochondrial network became more elongated after starvation in the presence of ISO-Long and also of AIF-230, but not when the GTPase activity was abolished (Fig 20D). These latter results

clearly indicate that the fusion process activated by these stress condition is also mediated by OPA1.

Our group previously demonstrated that alteration of OPA1 isoforms pattern by silencing of the exon 4b-containing isoforms reduced the mtDNA copy number of HeLa cells, that could be reestablished by the expression of a 10 kDa peptide containing the OPA1 N-terminus, from exon 1 to exon 4b (Elauchouri et al., 2011). In OPA-/- MEFs, the presence of this N-terminus not associated with other isoforms or of an isoform lacking of the N-terminus domain (AIF-230) was unable to significantly increase the mtDNA content. The inefficacy of the N-terminus peptide OPA1 containing exon 1-4b is not in contrast with previous data, since in that case the peptide was expressed in cells exhibiting the OPA1 protein pattern (Elauchouri et al., 2011). Also isoform 1 with mutated GTPase domain was ineffective to rescue the mitochondrial genome content. It follows that the simultaneous presence of a N-terminus and of a C-terminus of OPA1 is essential for the mtDNA maintenance (Fig. 25B).

The bioenergetics characterization revealed that both the cell lines expressing ISO1 Long and AIF-230 were less efficient in mitochondrial respiration and presented a reduced amount of supercomplexes assembled, suggesting that l-form can only partially rescue this phenotype. As these two cell lines have different mtDNA content but similar energetic behavior, it follows that the role of OPA1 in the mitochondrial energetic is independent of its function in mtDNA maintenance, in agreement with data previously reported in fibroblasts (Zanna et al., 2008). Moreover, these results suggest that a cleavable isoform generating s-forms and containing a functional GTPase domain is necessary to completely rescue the energetic competence (Fig 25C).

The partial rescue in *cristae* shape observed in cell expressing isoform 1 was abolished only by inactivation of the GTPase domain (Fig 25D). Our results of bioenergetic and ultrastructural analyses are different from those reported with the OPA1 Q297V mutation, which provoked defective GTPase activity but still allowed OPA1 oligomerization (Pattern et al., 2014). It is apparent that the effect of these two mutations is different, the G300E reflecting a more severe impairment of OPA1 functions. Indeed G300E substitution was shown to cause the complete loss of GTP hydrolysis activity in vitro (Ban et al., 2010), in agreement with fact that this is a very conserved aminoacid in the G1 domain / P-loop, that coordinates the nucleotide phosphate groups in the GTP-binding domain. It is also to be considered this is a pathogenic mutation associated to DOA (Delettre et al., 2000), whereas the mutation Q297V has never been found in patients.

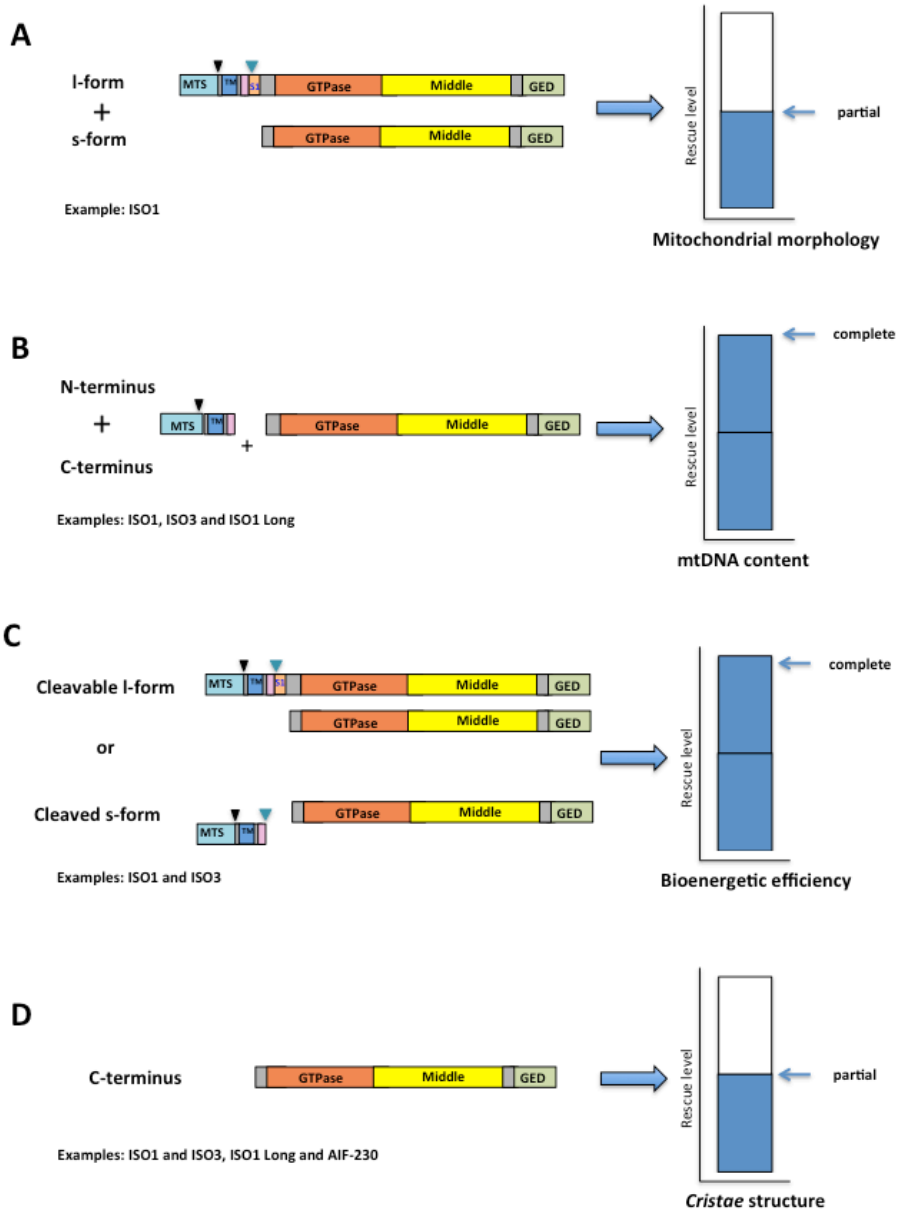

Figure 25. Schematic representation of the OPA1 forms/domains and different mitochondrial functions. (A) Expression of isoforms with both s- and l- forms only partially rescued mitochondrial morphology. (B) Expression of both N-terminus and C-terminus domains completely recovered mtDNA copy number. (C) Expression of either cleavable or totally cleaved isoforms completely rescued the energetic efficiency. (D) Expression of either cleavable or not cleavable isoform, containing or not the N-terminus, only partially recovered the *cristae* shape.

Our findings suggest that the roles of OPA1 in mitochondrial fusion, OXPHOS efficiency, *cristae* and mtDNA maintenance can be separated. This happens because the different OPA1 functions rely on the s-/l-forms equilibrium, the presence and cleavability of N-terminus, and a functional C-terminus (Fig 25).

The other important finding of this study concerns the pathophysiology of OPA1 mutations. To this purpose, we have also analyzed a set of other OPA1 mutations, selected on the basis of their different clinical phenotypes, to study how they could impact on protein functions.

The deleterious effects associated with mutations were variable. The more severe phenotypes were observed in cells expressing the mutations G439V, R445H, whereas the other two DOA-plus mutations, S545R and R290Q, although partially recovered the mtDNA content and OCR, completely affected the mitochondrial network. A similar profile, though less severe, was observed for the cells expressing Q785R. These results agree with data obtained *in vitro,* showing that the G439V, R445H, S545R mutations presented a reduced GTPase activity, whereas this activity was less affected in Q785R (Ban et al., 2010). The remaining three mutations showed a slight reduction of mitochondrial network tubulation only, in accord with the mild clinical phenotype observed in the patients. Noticeably, the effect of OPA1 mutations depends on their localization or on the severity of GTPase activity impairment.

Although these results are preliminary, and additional experiments and other OPA1 mutations need to be studied to better understand their pathological features, we believe that our model system is very valuable to analyze the effect of OPA1 missense mutations and to investigate the mechanism underlying DOA and the related DOA-plus. The main advantage of MEF bearing OPA1 missense mutations is the rather strong phenotype allowing identifications of defects barely detectable in fibroblast from patients, where the contribution of wt protein can mitigate the damaging effects of mutations. Finally, we are confident that this model might be also useful for evaluation of the efficacy of compounds able to ameliorate the defective phenotype, hopefully leading to a therapy improving the conditions of the patients.

REFERENCES

Abrahams JP, Leslie AG, Lutter R, Walker JE. Structure at 2.8 A resolution of F1-ATPase from bovine heart mitochondria. Nature. 1994; 370:621-628.

Acin-Perez R, Enriquez JA. The function of the respiratory supercomplexes: The plasticity model. Biochim Biophys Acta. 2014; 1837:444-50.

Agier V, Oliviero P, Lainé J, L'Hermitte-Stead C et al. 2012. Defective mitochondrial fusion, altered respiratory function, and distorted cristae structure in skin fibroblasts with heterozygous OPA1 mutations. Biochim Biophys Acta 1822: 1570-80.

Alavi MV, Bette S, Schimpf S, Schuettauf F, et al. A splice site mutation in the murine Opa1 gene features pathology of autosomal dominant optic atrophy. Brain. 2007; 130:1029-42.

Alavi MV, Fuhrmann N. Dominant optic atrophy, OPA1, and mitochondrial quality control: understanding mitochondrial network dynamics. Mol Neurodegener. 2013; 8:32.

Alexander C, Votruba M, Pesch UE, Thiselton DL, et al. OPA1, encoding a dynamin-related GTPase, is mutated in autosomal dominant optic atrophy linked to chromosome 3q28. Nat Genet. 2000; 26:211-5.

Amati-Bonneau P, Guichet A, Olichon A, Chevrollier A, et al. OPA1 R445H mutation in optic atrophy associated with sensorineural deafness. Ann Neurol. 2005; 58:958-63.

Amati-Bonneau P, Valentino ML, Reynier P, Gallardo ME, et al. OPA1 mutations induce mitochondrial DNA instability and optic atrophy plus phenotypes. Brain. 2008; 131:338-51.

Amutha B, Gordon DM, Gu Y, Pain D. A novel role of Mgm1p, a dynamin-related GTPase, in ATP synthase assembly and cristae formation/maintenance. Biochem J. 2004; 381:19-23.

Anand R, Wai T, Baker MJ, Kladt N, et al. The i-AAA protease YME1L and OMA1 cleave OPA1 to balance mitochondrial fusion and fission. J Cell Biol. 2014; 204:919-29.

Anderson S, Bankier, AT, De Bruijn MHL, Coulson AR, et al. Sequence and organization of the human mitochondrial genome. Nature. 1981; 290, 457–465.

Arselin G, Vaillier J, Salin B, Schaeffer J et al. The modulation in subunits e and g amounts of yeast ATP synthase modifies mitochondrial cristae morphology. J Biol Chem. 2004; 279:40392-9.

Bach D, Pich S, Soriano FX, Vega N et al. Mitofusin-2 determines mitochondrial network architecture and mitochondrial metabolism. A novel regulatory mechanism altered in obesity. J Biol Chem. 2003; 278:17190-7.

Balaban RS. Regulation of oxidative phosphorylation in the mammalian cell. Am J Physiol. 1990; 258:C377-89.

Ban T, Heymann JA, Song Z, Hinshaw JE, Chan DC. OPA1 disease alleles causing dominant optic atrophy have defects in cardiolipin-stimulated GTP hydrolysis and membrane tubulation, Hum Mol Genet. 2010; 2113–2122.

Barboni P, Savini G, Parisi V, Carbonelli M et al. Retinal nerve fiber layer thickness in dominant optic atrophy measurements by optical coherence tomography and correlation with age. Ophthalmology. 2011; 118:2076–2080.

Barboni P, Valentino ML, La Morgia C, Carbonelli M et al. Idebenone treatment in patients with OPA1-mutant dominant optic atrophy. Brain. 2013; 136:e231

Barboni P, Savini G, Cascavilla ML, Caporali L et al. Early macular retinal ganglion cell loss in dominant optic atrophy: genotype-phenotype correlation. Am J Ophthalmol. 2014; 158:628-36 e3

Batten B. A family suffering from hereditary optic atrophy Trans Ophthalmol Soc UK, 1896

Berry EA, Guergova-Kuras M, Huang LS, Crofts AR. Structure and function of cytochrome bc complexes. Annu Rev Biochem. 2000; 69:1005-75.

Berry EA, De Bari H, Huang LS. Unanswered questions about the structure of cytochrome bc1 complexes. Biochim Biophys Acta. 2013; 1827:1258-77.

Bertholet AM, Millet AM, Guillermin O, Doloyau M et al. OPA1 loss of function affects in vitro neuronal maturation. Brain; 2013; 136:1518–1533.

Bogenhagen DF, Rousseau D, Burke S. The layered structure of human mitochondrial DNA nucleoids. J Biol Chem. 2008; 283:3665-75.

Bogenhagen DF. Mitochondrial DNA nucleoid structure. Biochim Biophys Acta. 2012; 1819:914-20.

Brown TA, Cecconi C, Tkachuk AN, Bustamante C, Clayton DA. Replication of mitochondrial DNA occurs by strand displacement with alternative light-strand origins, not via a strand-coupled mechanism. Genes Dev. 2005; 19:2466-76.

Carelli V, Ross-Cisneros FN, Sadun AA. Mitochondrial dysfunction as a cause of optic neuropathies. Prog Retin Eye Res. 2004; 23:53-89.

Carelli V, La Morgia C, Iommarini L, Carroccia R, et al. Mitochondrial optic neuropathies: how two genomes may kill the same cell type? Biosci Rep. 2007; 27:173-84.

Carelli V and Chan DC. Mitochondrial DNA: Impacting Central and Peripheral Nervous Systems. Neuron. 2014; 84:1126-42.

Carroll J, Fearnley IM, Skehel JM, Shannon RJ, Hirst J, Walker JE. Bovine complex I is a complex of 45 different subunits. J Biol Chem. 2006; 281:32724-7.

Chaban Y, Boekema EJ, Dudkina NV. Structures of mitochondrial oxidative phosphorylation supercomplexes and mechanisms for their stabilisation. Biochim Biophys Acta. 2014; 1837:418-26.

Chan DC. Fusion and fission: interlinked processes critical for mitochondrial health. Annu Rev Genet. 2012; 46:265–287

Chen H, Detmer SA, Ewald AJ, Griffin EE, Fraser SE, Chan DC. Mitofusins Mfn1 and Mfn2 coordinately regulate mitochondrial fusion and are essential for embryonic development. J Cell Biol. 2003;160:189-200.

Chen H, Chomyn A, Chan DC. Disruption of fusion results in mitochondrial heterogeneity and dysfunction. J Biol Chem. 2005; 280:26185-92.

Chen H, Chan DC. Critical dependence of neurons on mitochondrial dynamics. Curr Opin Cell Biol. 2006; 18:453-9.

Chen H, McCaffery JM, Chan DC. Mitochondrial fusion protects against neurodegeneration in the cerebellum. Cell. 2007; 130:548-62.

Chen H, Vermulst M, Wang YE, Chomyn A, et al. Mitochondrial fusion is required for mtDNA stability in skeletal muscle and tolerance of mtDNA mutations. Cell. 2010; 141:280-9.

Chevrollier A, Guillet V, Loiseau D, Gueguen N, et al. Hereditary optic neuropathies share a common mitochondrial coupling defect. Ann Neurol. 2008; 63: 794-8.

Cipolat S, Martins de Brito O, Dal Zilio B, Scorrano L. OPA1 requires mitofusin 1 to promote mitochondrial fusion. Proc Natl Acad Sci USA. 2004; 101:15927-32.

Cipolat S, Rudka T, Hartmann D, Costa V et al. Mitochondrial rhomboid PARL regulates cytochrome c release during apoptosis via OPA1-dependent cristae remodeling. Cell. 2006; 126:163-75.

Cogliati S, Frezza C, Soriano ME, Varanita T, et al. Mitochondrial Cristae Shape Determines Respiratory Chain Supercomplexes Assembly and Respiratory Efficiency. 2013; 155:160-71

Cornille K, Milea D, Amati-Bonneau P, Procaccio V, et al. Reversible optic neuropathy with OPA1 exon 5b mutation. Ann Neurol. 2008; 63:667-71.

Darrouzet E, Moser CC, Dutton PL, Daldal F. Large scale domain movement in cytochrome bc(1): a new device for electron transfer in proteins.Trends Biochem Sci. 2001; 26:445-51.

Davies VJ, Hollins AJ, Piechota MJ, Yip W, et al. Opa1 deficiency in a mouse model of autosomal dominant optic atrophy impairs mitochondrial morphology, optic nerve structure and visual function. Hum Mol Genet. 2007; 16:1307-18.

Davies KM1, Strauss M, Daum B, Kief JH, et al. Macromolecular organization of ATP synthase and complex I in whole mitochondria. Proc Natl Acad Sci U S A. 2011; 108:14121-6.

de Brito OM and Scorrano L. Mitofusin 2 tethers endoplasmic reticulum to mitochondria. Nature. 2008; 456: 605-10.

Delettre C, Lenaers G, Griffoin JM, Gigarel N et al. Nuclear gene OPA1, encoding a mitochondrial dynamin-related protein, is mutated in dominant optic atrophy. Nat Genet. 2000; 26:207-10.

Delettre C, Griffoin JM, Kaplan J, Dollfus H et al. Mutation spectrum and splicing variants in the OPA1 gene. Hum Genet. 2001; 109:584-91.

Delettre C, Lenaers G, Pelloquin L, Belenguer P, Hamel CP. OPA1 (Kjer type) dominant optic atrophy: a novel mitochondrial disease, Mol. Genet. Metab. 2002; 75:97–107.

Di Mauro S, Schon EA. Mitochondrial disorders in the nervous system. Annu Rev Neurosci. 2008; 31: 91- 123.

Dibrova DV, Cherepanov DA, Galperin MY, Skulachev VP, Mulkidjanian AY, Evolution of cytochrome bc complexes: from membrane- anchored dehydrogenases of ancient bacteria to triggers of apoptosis in vertebrates. Biochim Biophys Acta. 2013; 1827:1407-27.

Duvezin-Caubet S, Koppen M, Wagener J, Zick M et al. OPA1 processing reconstituted in yeast depends on the subunit composition of the m-AAA protease in mitochondria. Mol Biol Cell. 2007; 18:3582-90.

Ehses S, Raschke I, Mancuso G, Bernacchia A et al. Regulation of OPA1 processing and mitochondrial fusion by m-AAA protease isoenzymes and OMA1. J Cell Biol. 2009; 187:1023-36.

Elachouri G, Vidoni S, Zanna C, Pattyn A, et al. OPA1 links human mitochondrial genome maintenance to mtDNA replication and distribution. Genome Res. 2011; 21:12-20

Eliott D, Traboulsi EI, Maumenee IH. Visual prognosis in autosomal dominant optic atrophy (Kjer type). Am J Ophthalmol. 1993; 115:360-7.

Falkenberg M, Larsson NG, Gustafsson CM. DNA replication and transcription in mammalian mitochondria. Annu Rev Biochem 2007; 76:679-99.

Fernandez-Silva P, Enriquez JA, Montoya J. Replication and transcription of mammalian mitochondrial DNA.Exp Physiol. 2003; 88:41-56

Ferraris S, Clark S, Garelli E, Davidzon G et al. Progressive external ophthalmoplegia and vision and hearing loss in a patient with mutations in POLG2 and OPA1. Arch Neurol. 2008; 65:125-31.

Frank M, Duvezin-Caubet S, Koob S, Occhipinti A et al. Mitophagy is triggered by mild oxidative stress in a mitochondrial fission dependent manner. Biochim Biophys Acta. 2012;

1823:2297-310.

Frey TG and Mannella CA. The internal structure of mitochondria. Trends. Biochem. Sci. 2000; 25:319-324.

Friedman JR, Nunnari J. Mitochondrial form and function. Nature. 2014; 505:335-43.

Fusté JM, Wanrooij S, Jemt E, Granycome CE, et al. Mitochondrial RNA polymerase is needed for activation of the origin of light-strand DNA replication. Mol Cell. 2010; 37:67-78.

Genova ML, Lenaz G. Functional role of mitochondrial respiratory supercomplexes 2014; 1837:427-43.

Gilkerson RW. Mitochondrial DNA nucleoids determine mitochondrial genetics and dysfunction. Int J Biochem Cell Biol. 2009; 41:1899-906.

Gomes LC, Di Benedetto G, Scorrano L. During autophagy mitochondria elongate, are spared from degradation and sustain cell viability. Nat Cell Biol. 2011; 13:589-98.

Gray, MW, Burger G, Lang BF. Mitochondrial evolution. Science. 1999; 1476–1481

Griffin EE, Graumann J, Chan DC. The WD40 protein Caf4p is a component of the mitochondrial fission machinery and recruits Dnm1p to mitochondria. J Cell Biol. 2005; 170: 237-48.

Griparic L, van der Wel NN, Orozco IJ, Peters PJ, van der Bliek AM. Loss of the intermembrane space protein Mgm1/OPA1 induces swelling and localized constrictions along the lengths of mitochondria. J Biol Chem. 2004; 279:18792-8.

Griparic L, Kanazawa T, van der Bliek AM. Regulation of the mitochondrial dynamin-like protein Opa1 by proteolytic cleavage. J Cell Biol. 2007; 178:757-64.

Guillery O, Malka F, Landes T, Guillou E, et al. Metalloprotease-mediated OPA1 processing is modulated by the mitochondrial membrane potential. Biol Cell. 2008; 100:315-25.

Harbauer AB, Zahedi RP, Sickmann A, Pfanner N, Meisinger C.The protein import machinery of mitochondria-a regulatory hub in metabolism, stress, and disease. Cell Metab. 2014; 19:357-72.

Hayashi T, Rizzuto R, Hajnoczky G, Su TP. MAM: more than just a housekeeper. Trends Cell Biol. 2009; 19:81-8.

Herlan M, Vogel F, Bornhovd C, Neupert W, Reichert AS. Processing of Mgm1 by the rhomboid-type protease Pcp1 is required for maintenance of mitochondrial morphology and of mitochondrial DNA. J Biol Chem. 2003; 278:27781-8.

Hudson G, Amati-Bonneau P, Blakely EL, Stewart JD, et al. Mutation of OPA1 causes dominant optic atrophy with external ophthalmoplegia, ataxia, deafness and multiple mitochondrial DNA deletions: a novel disorder of mtDNA maintenance. Brain 2008; 131:329-37.

Ishigami I, Hikita M, Egawa T, Yeh SR, Rousseau DL. Proton translocation in cytochrome c oxidase: Insights from proton exchange kinetics and vibrational spectroscopy. Biochim Biophys Acta. 2015; 1847:98-108

Ishihara N, Eura Y, Mihara K. Mitofusin 1 and 2 play distinct roles in mitochondrial fusion reactions via GTPase activity. J Cell Sci. 2004; 117:6535-46.

Ishihara N, Fujita Y, Oka T, Mihara K. Regulation of mitochondrial morphology through proteolytic cleavage of OPA1. EMBO J. 2006; 25:2966-77.

Ishihara N, Nomura M, Jofuku A, Kato H, et al. Mitochondrial fission factor Drp1is essential for embryonic development and synapse formation in mice. Nature Cell Biol. 2009; 11, 958–966.

Ishihara N, Otera H, Oka T, Mihara K. Regulation and physiologic functions of GTPases in

mitochondrial fusion and fission in mammals. Antioxid Redox Signal. 2013; 19:389-99

Johnston PB, Gaster RN, Smith VC, Tripathi RC. A clinicopathologic study of autosomal dominant optic atrophy. Am J Ophthalmol. 1979; 88:868-875

Jones BA, Fangman WL. Mitochondrial DNA maintenance in yeast requires a protein containing a region related to the GTP-binding domain of dynamin. Genes Dev. 1992; 6:380- 9.

Kamei S, Chen-Kuo-Chang M, Cazevieille C, Lenaers G et al. Expression of the opa1 mitochondrial protein in retinal ganglion cells: its downregulation causes aggregation of the mitochondrial network. Invest Ophthalmol Vis Sci. 2005; 46:4288-94.

Kashatus, DF, Lim KH, Brady DC, Pershing NL, Cox AD and Counter CM. RALA and RALBP1 regulate mitochondrial fission at mitosis. Nature cell biology. 2011; 13:1108-1115.

Kaufman BA, Durisic N, Mativetsky JM, Costantino S et al. The mitochondrial transcription factor TFAM coordinates the assembly of multiple DNA molecules into nucleoid-like structures. Mol Biol Cell. 2007; 18:3225-36.

Kienhöfer J, Haussler DJ, Ruckelshausen F, Muessig E et al. Association of mitochondrial antioxidant enzymes with mitochondrial DNA as integral nucleoid constituents. The FASEB Journal 2009; 23:2034-44.

Kieper N, Holmström KM, Ciceri D, Fiesel FC et al. Modulation of mitochondrial function and morphology by interaction of Omi/HtrA2 with the mitochondrial fusion factor OPA1. Exp Cell Res. 2010; 316:1213-24

Kjer P, Jensen OA, Klinken L. Histopathology of eye, optic nerve and brain in a case of dominant optic atrophy. Acta Ophthalmol. 1983; 61:300-312.

Kjer P. Infantile optic atrophy with dominant mode of inheritance: a clinical and genetic study of 19 Danish families. Acta Ophthalmol Suppl. 1959; 164:1-147.

Koshiba T, Detmer SA, Kaiser JT, Chen H, McCaffery JM, Chan DC. Structural basis of mitochondrial tethering by mitofusin complexes. Science. 2004; 305:858-62.

Kukat C, Wurm CA, Spåhr H, Falkenberg M, Larsson NG, Jakobs S. Super-resolution microscopy reveals that mammalian mitochondrial nucleoids have a uniform size and frequently contain a single copy of mtDNA. Proc Natl Acad Sci USA. 2011; 108:13534-9.

La Morgia C, Carbonelli M, Barboni P, Sadun AA, Carelli V. Medical management of hereditary optic neuropathies. Front Neurol. 2014; 5:141.

Lancaster CR, Kröger A. Succinate: quinone oxidoreductases: new insights from X-ray crystal structures.Biochim Biophys Acta. 2000; 1459:422-31.

Landes T, Emorine LJ, Courilleau D, Rojo M, Belenguer P, Arnauné-Pelloquin L. The BH3-only Bnip3 binds to the dynamin Opa1 to promote mitochondrial frag- mentation and apoptosis by distinct mechanisms. EMBO Rep. 2010; 11:459–465.

Lascaratos G, Ji D, Wood JPM, Osborne NN. Visible light affects mitocondrial function and induces neuronal death in retinal cell cultures. Vis Res 2007; 47: 1191–201.

Lenaers G, Reynier P, Elachouri G, Soukkarieh C, et al. OPA1 functions in mitochondria and dysfunctions in optic nerve. Int J Biochem Cell Biol. 2009; 41:1866-74.

Lenaers G, Hamel C, Delettre C, Amati-Bonneau P et al. Dominant optic atrophy. 2012; Orphanet J Rare Dis. 9;7:46.

Liu X, Weaver D, Shirihai O, Hajnóczky G. Mitochondrial 'kiss-and-run': interplay between mitochondrial motility and fusion-fission dynamics. EMBO J. 2009; 28:3074-89.

Liu P, Demple B. DNA repair in mammalian mitochondria: much more than we thought? DNA repair in mammalian mitochondria: Much more than we thought? Environ Mol Mutagen.

2010; 51:417-26.

Lodi R, Tonon C, Valentino ML, Iotti S, et al. Deficit of in vivo mitochondrial ATP production in OPA1-related dominant optic atrophy. Ann Neurol. 2004; 56:719-23.

Lodi R, Tonon C, Valentino ML, Manners D et al. Defective mitochondrial adenosine triphosphate production in skeletal muscle from patients with dominant optic atrophy due to OPA1 mutations, Arch Neurol. 2011; 68:67-73.

Lóson OC, Song Z, Chen H, Chan DC. Fis1, Mff, MiD49, and MiD51 mediate Drp1 recruitment in mitochondrial fission. Mol Biol Cell. 2013; 24;659-667.

Manfredi G, Yang L, Gajewski CD, Mattiazzi M. Measurements of ATP in mammalian cells. Methods. 2002; 26:317-26.

Mannella CA, Marko M, Buttle K. Reconsidering mitochondrial structure: new views of an old organelle. Trends Biochem Sci. 1997; 22:37-8.

Mannella CA, Pfeiffer DR, Bradshaw PC, Moraru II et al. Topology of the mitochondrial inner membrane: dynamics and bioenergetic implications. IUBMB Life. 2001; 52:93–100.

Mannella CA, Lederer WJ, Jafri MS. The connection between inner membrane topology and mitochondrial function. J Mol Cell Cardiol. 2013; 62:51-7.

Mäntyjärvi MI, Nerdrum K, Tuppurainen K. Color vision in dominant optic atrophy. J Clin Neuroophthalmol. 1992; 12:98-103.

Mao CC and Holt IJ. Clinical and molecular aspects of diseases of mitochondrial DNA instability. Chang Gung Med J. 2009; 32:354-69.

Marchbank NJ, Craig JE, Leek JP, Toohey M et al. Deletion of the OPA1 gene in a dominant optic atrophy family: evidence that haploinsufficiency is the cause of disease. J Med Genet. 2002; 8:39-47.

Merkwirth C, Dargazanli S, Tatsuta T, Geimer S et al. Prohibitins control cell proliferation and apoptosis by regulating OPA1-dependent cristae morphogenesis in mitochondria. Genes Dev. 2008; 22:476-88.

Milea D, Sander B, Wegener M, Jensen H et al. Axonal loss occurs early in dominant optic atrophy. Acta Ophthalmol. 2010; 88:342–346.

Mishra P, Carelli V, Manfredi G, Chan DC. Proteolytic cleavage of Opa1 stimulates mitochondrial inner membrane fusion and couples fusion to oxidative phosphorylation. Cell Metab. 2014; 19:630-41.

Misaka T, Miyashita T, Kubo Y. Primary structure of a dynamin-related mouse mitochondrial GTPase and its distribution in brain, subcellular localization, and effect on mitochondrial morphology. J Biol Chem. 2002; 277:15834-42

Misaka T, Murate M, Fujimoto K, Kubo Y. The dynamin-related mouse mitochondrial GTPase OPA1 alters the structure of the mitochondrial inner membrane when exogenously introduced into COS-7 cells. Neurosci Res 2006; 55:123-33.

Mitra K, Wunder C, Wunder C, Roysam B, Lin G, Lippincott-Schwartz J. A hyperfused mitochondrial state achieved at G1-S regulates cyclin E buildup and entry into S phase. Proceedings of the National Academy of Sciences of the United States of America. 2009; 106:1960-11965.

Nicholls DG. Mitochondrial function and dysfunction in the cell: its relevance to aging and aging-related disease. Int J Biochem Cell Biol. 2002; 34:1372-81.

Olichon A, Emorine LJ, Descoins E, Pelloquin L et al. The human dynamin-related protein OPA1 is anchored to the mitochondrial inner membrane facing the inter-membrane space. FEBS

Lett. 2002; 523:171-6.

Olichon A, Baricault L, Gas N, Guillou E et al. Loss of OPA1 perturbates the mitochondrial inner membrane structure and integrity, leading to cytochrome c release and apoptosis. J Biol Chem. 2003; 278:7743-6.

Olichon A, Elachouri G, Baricault L, Delettre C, Belenguer P, Lenaers G.. OPA1 alternate splicing uncouples an evolutionary conserved function in mitochondrial fusion from a vertebrate restricted function in apoptosis. Cell Death Differ. 2007; 14:682-92.

Olichon A, Landes T, Arnauné-Pelloquin L, Emorine LJ et al. Effects of OPA1 mutations on mitochondrial morphology and apoptosis: relevance to ADOA pathogenesis. J Cell Physiol. 2007; 211:423-30.

Otera H, Ohsakaya S, Nagaura Z, Ishihara N, Mihara K. Export of mitochondrial AIF in response to proapoptotic stimuli depends on processing at the intermembrane space. EMBO J. 2005; 24:1375-86

Otera H, Wang C, Cleland MM, Setoguchi K et al. Mff is an essential factor for mitochondrial recruitment of Drp1 during mitochondrial fission in mammalian cells. The Journal of cell biology. 2010; 191:1141-1158.

Ott M, Zhivotovsky B, Orrenius S. Role of cardiolipin in cytochrome c release from mitochondria, Cell Death Differ. 2007; 14:1243–1247.

Palade GE. The fine structure of mitochondria. Anat Rec. 1952; 114:427–51

Patten DA, Wong J, Khacho M, Soubannier V, et al. OPA1-dependent cristae modulation is essential for cellular adaptation to metabolic demand. EMBO J. 2014; 33:2676-91.

Praefcke GJ, McMahon HT. The dynamin superfamily: universal membrane tubulation and fission molecules? Nat Rev Mol Cell Biol. 2004; 5:133-47

Rossignol R, Faustin B, Rocher C, Malgat M, Mazat JP, Letellier T. Mitochondrial threshold effects. Biochem. J. 2003; 370, 751–762.

Samant SA, Zhang HJ, Hong Z, Pillai VB, et al. SIRT3 deacetylates and activates OPA1 to regulate mitochondrial dynamics during stress. Mol Cell Biol. 2014; 34:807-19.

Santel A and Fuller MT. Control of mitochondrial morphology by a human mitofusin. J Cell Sci. 2001; 114: 867-74.

Santo-Domingo J, Giacomello M, Poburko D, Scorrano L, Demaurex N. OPA1 promotes pH flashes that spread between contiguous mitochondria without matrix protein exchange. EMBO J. 2013; 32:1927-40.

Sarzi E, Angebault C, Seveno M, Gueguen N et al. The human OPA1delTTAG mutation induces premature age-related systemic neurodegeneration in mouse. Brain. 2012; 135:3599–3613.

Sato A, Nakada K, Hayashi J. Mitochondrial dynamics and aging: Mitochondrial interaction preventing individuals from expression of respiratory deficiency caused by mutant mtDNA. Biochim Biophys Acta. 2006 May-Jun; 1763:473-81.

Satoh M, Hamamoto T, Seo N, Kagawa Y, Endo H. Differential sublocalization of the dynamin-related protein OPA1 isoforms in mitochondria. Biochem Biophys Res Commun. 2003; 300:482-93.

Scarpulla RC. Transcriptional paradigms in mammalian mitochondrial biogenesis and function. Physiol Rev. 2008; 88:611-638.

Schultz BE, Chan SI. Structures and proton-pumping strategies of mitochondrial respiratory enzymes. Annu Rev Biophys Biomol Struct. 2001; 30:23-65.

Schon EA and Gilkerson RW. Functional complementation of mitochondrial DNAs: mobilizing

mitochondrial genetics against dysfunction. Biochim. Biophys. Acta, 2010; 1800:245-9

Scorrano L, Ashiya M, Buttle K, Weiler S, et al. A distinct pathway remodels mitochondrial cristae and mobilizes cytochrome c during apoptosis.Dev Cell. 2002; 2:55-67.

Scorrano L. Keeping mitochondria in shape: a matter of life and death. Eur J Clin Invest. 2013; 43:886-93.

Seelert H and Dencher NA. ATP synthase superassemblies in animals and plants: Two or more are better. 2011; 1807:1185-97 Abrahams

Skulachev VP. Mitochondrial filaments and clusters as intracellular power-transmitting cables. Trends Biochem Sci. 2001; 26: 23-9.

Song Z, Chen H, Fiket M, Alexander C, Chan DC. OPA1 processing controls mitochondrial fusion and is regulated by mRNA splicing, membrane potential, and Yme1L. J Cell Biol. 2007; 178:749-55.

Song Z, Ghochani M, McCaffery JM, Frey TG, Chan DC. Mitofusins and OPA1 mediate sequential steps in mitochondrial membrane fusion. Mol Biol Cell. 2009; 20: 3525-32.

Spelbrink JN. Functional organization of mammalian mitochondrial DNA in nucleoids: history, recent developments, and future challenges. IUBMB Life. 2010; 62:19-32.

Spinazzi M, Cazzola S, Bortolozzi M, Baracca A et al. A novel deletion in the GTPase domain of OPA1 causes defects in mitochondrial morphology and distribution, but not in function. Hum Mol Genet. 2008; 17:3291-302.

Stotland A, Gottlieb RA. Mitochondrial quality control: Easy come, easy go. Biochim Biophys Acta. 2015; S0167-4889(15)00010-5.

Szabadkai G, Simoni AM, Bianchi K, De Stefani D, et al. Mitochondrial dynamics and Ca2+ signaling. Biochim Biophys Acta. 2006; 1763:442-9.

Tondera D, Grandemange S, Jourdain A, Karbowski M, et al. SLP-2 is required for stress-induced mitochondrial hyperfusion. EMBO J. 2009; 28:1589-600.

Twig G, Hyde B, Shirihai OS. Mitochondrial fusion, fission and autophagy as a quality control axis: the bioenergetic view. Biochim Biophys Acta. 2008; 1777:1092-7.

Van Bergen NJ, Crowston JG, Kearns LS, Staffieri SE et al. Mitochondrial oxidative phosphorylation compensation may preserve vision in patients with OPA1- linked autosomal dominant optic atrophy. PLoS One. 2011; 6:e21347

Vidoni S, Zanna C, Rugolo M, Sarzi E, Lenaers G. Why mitochondria must fuse to maintain their genome integrity. Antioxid Redox Signal. 2013; 19:379-88

Walker JE. The ATP synthase: the understood, the uncertain and the unknown. Biochem Soc Trans. 2013; 41:1-16.

Wakabayashi J, Zhang Z, Wakabayashi N, Tamura Y et al. The dynamin-related. GTPase Drp1 is required for embryonic and brain development in mice. 2009; J. Cell Biol. 186:805–16

Wells RC, Picton LK, Williams SC, Tan FJ, Hill RB. Direct binding of the dynamin-like GTPase, Dnm1, to mitochondrial dynamics protein Fis1 is negatively regulated by the Fis1 N-terminal arm. J Biol Chem. 2007; 282:33769–75

White KE, Davies VJ, Hogan VE, Piechota MJ et al. OPA1 deficiency associated with increased autophagy in retinal ganglion cells in a murine model of dominant optic atrophy. Invest Ophthalmol Vis Sci. 2009; 50:2567-71.

Williams PA, Morgan JE, Votruba M. Opa1 deficiency in a mouse model of dominant optic atrophy leads to retinal ganglion cell dendropathy. Brain. 2010;133:2942–2951.

Williams PA, Piechota M, von Ruhland C, Taylor E, Morgan JE, Votruba M. Opa1 is essential for retinal ganglion cell synaptic architecture and connectivity. Brain. 2012; 135:493–505.

Wittig I, Braun HP, Schägger H. Blue native PAGE. Nat Protoc. 2006; 1:418-28.

Wong ED, Wagner JA, Scott SV, Okreglak V et al. The intramitochondrial dynamin-related GTPase, Mgm1p, is a component of a protein complex that mediates mitochondrial fusion. J Cell Biol. 2003; 160:303-11.

Yamaguchi R, Lartigue L, Perkins G, Scott RT et al. Opa1-mediated cristae opening is Bax/Bak and BH3 dependent, required for apoptosis, and independent of Bak oligomerization. Mol Cell. 2008; 31:557-69.

Youle RJ and Karbowski M. Mitochondrial fission in apoptosis. Nat Rev Mol Cell Biol. 2005; 6:657-663.

Yu-Wai-Man P, Griffiths PG, Gorman GS, Lourenco CM, et al. Multi-system neurological disease is common in patients with OPA1 mutations, Brain. 2010; 133:771–786.

Yu-Wai-Man P, Griffiths PG, Burke A, , Sellar PW et al. The prevalence and natural history of dominant optic atrophy due to OPA1 mutations. Ophthalmology. 2010; 117:1538–1546.

Zanna C, Ghelli A, Porcelli AM, Karbowski M et al., OPA1 mutations associated with dominant optic atrophy impair oxidative phosphorylation and mitochondrial fusion. Brain 2008; 131:352–67.

Züchner S, Vance JM. Mechanisms of disease: a molecular genetic update on hereditary axonal neuropathies. Nat Clin Pract Neurol. 2006; 2:45-53.